An efficient data protection architecture based on fragmentation and encryption

Han Qiu

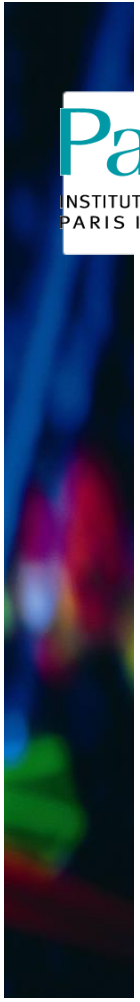

ParisTech
INSTITUT DES SCIENCES ET TECHNOLOGIES
PARIS INSTITUTE OF TECHNOLOGY

TELECOM ParisTech

2017-ENST-0049

EDITE ED 130

Doctorat ParisTech

T H È S E

pour obtenir le grade de docteur délivré par

Télécom ParisTech

Spécialité “ Informatique et Réseaux”

présentée et soutenue publiquement par

Han QIU

Le 20 Octobre 2017

An Efficient Data Protection Architecture Based on Fragmentation and Encryption

Directeur de thèse : **Gérard MEMMI**

Jury

M. Jean-Jacques QUISQUATER, Prof., Université catholique de Louvain	Rapporteur
M. Gildas AVOINE, Prof., INSA Rennes/IRISA	Rapporteur
M. Henri MAÎTRE, Prof., Télécom ParisTech	Examinateur
M. Frédéric CUPPENS, Prof., IMT Atlantique	Examinateur
M. Olivier BETTAN, Thales Solutions de Securité & Services	Examinateur
Mme. Houda LABIOD, Prof., Télécom ParisTech	Examinateur
M. Jean LENEUTRE, Maître de conférences, Télécom ParisTech	Examinateur

T H È S E

Télécom ParisTech
école de l’Institut Mines Télécom – membre de ParisTech
46, rue Barrault – 75634 Paris Cedex 13 – Tél. + 33 (0)1 45 81 77 77 – www.telecom-paristech.fr

Acknowledgements

Firstly, I would like to express my most sincere gratitude to my supervisor Prof. Gérard Memmi for the tremendous support of my PhD study and research, for his patience, motivation, immense knowledge, and dedication to students. Thank you for leading me through such a splendid journey. With your leading, the past four years has been a fantastic adventure that will be unique and important in my life.

Besides my advisor, I would like to specially thank my jury member Prof. Henri Maître who contributed to the most important discussions that helped to improve this work and encourage me to widen my research from various perspectives.

I am grateful to all the other jury members: Prof. Frédéric Cuppens, Prof. Houda Labiod, Mr. Olivier Bettan, and Mr. Jean Leneutre for attending my dissertation, and, in particular, the reviewers of the manuscript: Prof. Jean-Jacques Quisquater and Prof. Gildas Avoine, for their important suggestions and comments.

Thanks also to all the colleagues and staffs in Télécom ParisTech for all help and collaboration in technical knowledge and administrative tasks.

Last but not least, I would like to express my gratitude to my family for encouraging and supporting me so many years, and I hope this work will be the pride of you. I also want to thank my girlfriend for being with me and sharing with me for every piece joy and upset in these years. Thanks to my friends I met in France for the memorable moments we shared.

This thesis is funded by ITEA CAP2 project.

Abstract

In this thesis, a completely revisited data protection scheme based on selective encryption is presented. First, this new scheme is agnostic in term of data format, second it has a parallel architecture using GPGPU allowing performance to be at least comparable to full encryption algorithms.

Bitmap, as a special uncompressed multimedia format, is addressed as a first use case. Discrete Cosine Transform (DCT) is the first transformation for splitting fragments, getting data protection, and storing data separately on local device and cloud servers. This work has largely improved the previous published ones for bitmap protection by providing new designs and practical experimentations. General purpose graphic processing unit (GPGPU) is exploited as an accelerator to guarantee the efficiency of the calculation compared with traditional full encryption algorithms. Then, an agnostic selective encryption based on lossless Discrete Wavelet Transform (DWT) is presented. This design, with practical experimentations on different hardware configurations, provides strong level of protection and good performance at the same time plus flexible storage dispersion schemes. Therefore, our agnostic data protection and transmission solution combining fragmentation, encryption, and dispersion is made available for a wide range of end-user applications. Also a complete set of security analysis are deployed to test the level of provided protection.

Abstract

Une architecture logicielle de protection de données entièrement revisité basé sur le chiffrement sélectif est présentée. Tout d'abord, ce nouveau schéma est agnostique en terme de format de données (multimedia ou textuel). Deuxièmement, son implementation repose sur une architecture parallèle utilisant un GPGPU de puissance moyenne permettant aux performances d'être comparable aux algorithmes de chiffrement utilisant l'architecture NI proposée par Intel particulièrement adaptée.

Le format bitmap, en tant que format multimédia non compressé, est abordé comme un premier cas d'étude puis sera utilisé comme format pivot pour traiter tout autre format. La transformée en cosinus discrète (DCT) est la première transformation considérée pour fragmenter les données, les protéger et les stocker séparément sur des serveurs locaux et sur un cloud public. Ce travail a contribué à largement améliorer les précédents résultats publiés pour la protection sélective d'image bitmap en proposant une nouvelle architecture et en forunissant des expérimentations pratiques. L'unité de traitement graphique à usage général (GPGPU) est exploitée pour optimiser l'efficacité du calcul par rapport aux algorithmes traditionnels de chiffrement (tel que AES). Puis, un chiffrement sélectif agnostique basé sur la transformée en ondelettes discrètes sans perte (DWT) est présenté. Cette conception, avec des expérimentations pratiques sur différentes configurations matérielles, offre à la fois un fort niveau de protection et de bonnes performances en même temps que des possibilités de dispersion de stockage flexibles. Notre solution agnostique de protection de données combinant fragmentation, chiffrement et dispersion est applicable à une large gamme d'applications par un utilisateur final. Enfin, un ensemble complet d'analyses de sécurité est déployé pour s'assurer du bon niveau de protection fourni meme pour les fragments les moins bien protégés.

Table of contents

List of figures

List of tables

Chapter 1

Introduction

1.1 Background

In the last two decades, digital data has increased in a very large scale in many fields. In 2008, International Data Corporation (IDC) estimated 2.25×10^{21} bits of digital information had been created [12]. This amount would surpass 6×10^{23} bits by 2023. More importantly, for the personal users, the latest advances of information technology (IT) including computers, smart phones and tablets make it very easy to generate data to distribute. For example, nowadays 72 hours of videos are uploaded to YouTube in every minute on average [103]. Therefore, the data being generated, processed, transmitted and distributed is massive through the Internet.

Both large scale parallel multi-core machines and more efficient and affordable PCs were built to serve generating, transmitting, storing and computing digital data. One of the most important advance in distributed systems is to link smaller, more affordable servers together to build a large scale computer cluster for data service. The main advantage of Cloud is to offer more scalable, fault-tolerant services with high performance at a low cost compared with one super computer. Moreover, Cloud computing technology can basically provide almost infinite computing and storage resources on demand that can fits both individual users and companies by renting hardware resources remotely on a short-term basis (most commonly, a number of processors by the hour and storage space by the day). Therefore, cloud users enjoy the variety of cloud services (e.g. Data as a Service (Daas), Software as a Service (SaaS), Platform as a Service (PaaS), Infrastructure as a service (IaaS), etc).

With both the development of digital data and computer technology, the trends in recent years is to outsource information storage and processing to cloud-based services. Especially the cloud-based data storage services for individual users are gaining popularity. Relying on large free storage space and reliable communication channel, cloud-based service providers

like Dropbox, Google Drive are providing individual users almost infinite and low cost storage space.

However, this situation raises a question of the trustworthiness of cloud-based service providers. In fact, many security and privacy incidents are observed in today's Cloud-based systems. Some of these incidents are listed in [188]:

• Steven Warshak stops the government's repeated secret searches and seizures of his stored email using the federal Stored Communications Act (SCA) in July, 2007.

• A Salesforce.com employee fell victim to a phishing attack and leaked a customer list, which generated further targeted phishing attacks in October 2007.

• Google Docs found a flaw that inadvertently shares users docs in March 2009.

• Epic.com lodged a formal complaint to the FTC against Google for its privacy practices in March 2009. EPIC was successful in an action against Microsoft Passport.

• Yahoo confirmed that at least 500 million user accounts has been stolen from the company's network in late 2014.

• Equifax announced that 143 million US-based users had their credit history information compromised in 2017.

Most of these incidents are due to human errors. Moreover, the cloud providers themselves cannot be trusted either. In 2013, the PRISM surveillance program [54] was exposed. In this program, the NSA has obtained direct access to the systems of Google, Facebook, Apple and other US Internet giants which made privacy of individual users' data vulnerable. This is due to the data that transmitted to the cloud will be handled by the Cloud itself. The situation could be even worse in some specific use cases like outsourcing encryption shown in Xiang et al. [176] (the client need to outsource protected images to other users through an insecure channel but does not have sufficiently computational power or energy supply to perform the encryption). Thus, it becomes increasingly important for users to efficiently protect their personal data(texts, images, or videos) independently from the storage or any other application or service providers.

So, in this work, one basic assumption is that Cloud service providers cannot be entirely trusted. We have to assume that one 'curious' or 'malicious' program sits on at least one Cloud server and is able to observe all the data stored in the Cloud and transmitted through the Cloud. In a worse case, all data stored on the Cloud server can be used by this program to sniff the user's privacy by any means of analysis or attack for even a small piece of data. More importantly, the data transmission channel is also not perfectly protected and more threats like crackers could compromise the data on it. And the only trustworthy area is the local machine one end-user has. In this thesis, the design for the data stored in local machines includes encryption algorithms applied so even stealing data from local machine is not a

threat. And another basic assumption is there is no such situation that a malicious program stays on end-user's computer and can observe all data in the process.

One reasonable solution is to protect the data locally on an end-user's machine before it is sent to Cloud servers. And this makes encryption naturally become promising. Traditional encryption systems like the standard cipher symmetric key encryption systems (e.g. 3DES, or its successor AES, etc.) work with the assumption that data are sequence of symbols relatively independent (i.i.d.) and of even importance and indeed, that the data must be decrypted with accuracy. This typically does not apply to most of the personal data that are photos and videos: pixels are known to be highly correlated with theirs neighbors and there is well-known strong inter-frame correlation as well. The spatial or temporal redundancies of these multimedia data are not sufficiently exploited by historical encryption methods, as when they are designed, multimedia data with special formats are still rare. For example, users may even tolerate some small level of distortion in some cases when deciphering an image with a moderate requirement on its rendition [80]. Another problem is that the traditional encryption methods are not enough to protect: for instance, an image has been encrypted rowwise by means of AES can let element of the structure of an image still understandable (see Fig. 1 of [64]).

Some other data protection methods like Selective Encryption (SE) have been published in recent decades. The aim at exploiting special redundancies of multimedia data and are based on compression algorithms. SE usually dedicated to image or video protection where they support to automatically separate the image or video into two fragments: a 'private' fragment which contains most of the information such that this fragment is sufficient to understand the original image or at least process some exploitation, a second fragment that we call 'public' which is supposed to contain a much smaller amount of information such that this fragment is not exploitable. These two fragments are protected using different approaches depending on their respective levels of importance or confidentiality. The state of the art in Selective Encryption methods is showing that all these methods propose to encrypt the private fragment as a small subset of the original content [101] which in some cases constitutes a lightweight and fast encryption compared with a full encryption. This raises a first issue consisting in determining the optimal private fragment which first, deserves strong protection and secondly, is as small as possible. Then we face a second issue consisting in making sure that the weak level of protection we apply to the public fragment will prevent leaks of useful information.

Not every SE used image compression transforms, for instance, one very simple answer would be to encrypt the center of the image, leaving the border in clear (see Figure 4 in [138] for instance). This simple solution can be considered for lightweight protection, however,

it does not address our two issues since the border of the image may leak valuable key information. A more interesting one is to use transformations used in image compression algorithms such as the Discrete Cosine Transform (DCT) (see [80] or our own work in [126] for instance) to separate the information in the frequency domain.

Although the SE methods are more suitable for multimedia data in some cases, there are limitations , for instance, most SE methods are specifically related to the format of data (bitmap, jpeg) they are dealing with. Once SE method is designed based on the compression methods or coding technology used, it is dedicated for a specific multimedia content only. More importantly, there are some large volume data transmitted today that are not compressed or cannot be compressed to save storage spaces like an operating system image. It is not efficient to exploit many SE methods according to many different multimedia data formats. Thus, a challenge comes up that if it is possible to design an efficient SE method that can generally fits all kinds of data formats and guarantee not only security but also data integrity.

1.2 Motivation

As pointed before, outsourcing information storage and processing, cloud-based services for data storage have gained in popularity and today can be considered as mainstream. They attract organizations or enterprises especially individual users who do not want or cannot cope with the cost of a private cloud. Beside the economic factor, both groups of customers subordinate their choice of an adequate cloud provider to other factors, particularly resilience, security, and privacy.

Hardening data protection using multiple methods rather than 'just' encryption is becoming of paramount importance when considering continuous and powerful attacks to spy, alter, or even destroy information. Even if encryption is a great technology rapidly progressing, encryption is 'just' not enough to progress with this unsolvable question not mentioning its high computational complexity. In [2], the authors showed how to compromise https sites with 512-bit group; the authors even suggested that 1024-bit encryption could be crypt-analyzed with enough computational power. Cryptograph never like the idea that a cipher can be broken and information can be read given sufficient computational resources [106], this is nevertheless one of the central design tenets of a number of projects like the Potshards system [147]. Moreover, there remains the difficult question of the management of the encryption key that over time, can be known by too many people, and stolen or lost.

One ultimate purpose and ambition is to look at data protection and privacy from end to end by way of combining fragmentation, encryption, and then dispersion [105, 104]. This means to derive general schemes and architecture to protect data during their entire life

cycle everywhere they go throughout a network of machines where they are being processed, transmitted, and stored. Moreover, it is to offer users choices among various well understood cost effective levels of privacy and security which would come with predictable levels of performance in terms of memory occupation, energy consumption, and processing time. However, in order to provide a practical method for protecting data during their storage, we will set a series of assumptions for the hardware and software environment that is the end-users have a resource limited personal environment like laptops or desktops. Moreover, the execution time has to be comparable to the traditional full encryption algorithms. To verify this point, we will need to setup a benchmark.

Also, the concept of 'Fragmentation' is introduced with a different usage. Normally fragmentation is vastly used for resilience purposes. In [128], one of the first results about fragmenting for both fault-tolerance and data protection is found. In [75], the authors address this question by using a Reed Solomon error correcting code [130] to avoid mere duplication. In summary, fragmentation means separating with a more or less complex algorithm data into pieces or fragments for resilience purposes. In this thesis, we redefine the fragmentation as separating a piece of data by considering difference in confidentiality, data nature and space usage, in order to protect the fragments differently according to their level of confidentiality or criticality. For instance, the uncompressed image is containing a lot of redundancy that encryption only a small part of the low frequency coefficients can effectively reduce the image quality. Then these fragments should in turn be stored in different physical locations in a more or less sophisticated manner in order to increase the level of protection for the whole information.

Defining different levels of data importance is based on the thesis that massive amount of data have a non-uniform level of criticality or confidentiality (therefore, a non-uniform need for protection). In fact, non-uniform distribution of data is the basis of compression and only pure white noise is uniformly distributed. Also, as data has not been produced at the same time, they are aging at a non-uniform pace which again relate to the non-uniform level of criticality and a need for a multilevel security system. This makes the idea of combining fragmentation with encryption possible by letting some critical data be separated and strongly encrypted, while some other data less critical be only fragmented and possibly more rapidly encrypted with a weaker encryption algorithm or even in some use cases, let clear.

Last but not least, by definition, fragmentation enables the parallelization of transforming or encrypting pieces of information which lets us expect strong gain in efficiency compared with a full encryption sequentially executed, addressing scalability requirements. Defragmentation could then have to follow a reverse parallel pattern.

Then the other basic assumption is the need for a trusted area. Whatever is the software solution used for protecting data, it is our belief that a complete solution will have to use hardened hardware (a trusted area of one or several machines) at one critical moment or another during the data life cycle. In particular, places where information is being fragmented or defragmented, encrypted or decrypted are particularly critical since the information is gathered in clear during a period of time. Also, places where information is being created, printed out, or visualized by a human end-user have to be trusted and protected from any uninvited observer. A last, reason for considering a trusted area would be to use it as a safe and store ultra-confidential information even as this information is strongly encrypted. This point is widely recognized since a long time and in many publications [51] or [3] for instance) or by many industry experts. In fact, most of the trusted area are just relatively more secure than the others while there is a race between the crackers and protection technology. In order to save the endless challenges about whether a storage space is a trusted area, we define in this thesis that the local area is trustworthy compared with the cloud storage space while all data stored locally are still encrypted at application layer by default.

Use cases are important since a specific architecture can comply with a set of use cases but at the same time may very well fail at addressing needs for another group of use cases. Use cases can be defined according to the number of desired authorized participants (one, two, or many), their roles as users or end-users (owner, author (who may not be the owner), read-only user, service provider,...) (aka Alice and Bob), the number and type of attackers (from honest but curious, eavesdropper (aka Eve), to malicious (aka Mallory), insider, man in the middle, coalition of attackers, powerful rogue enterprise,...), the type and location of attacks (at storage, transmission, processing time, ...), the size, nature, and format of the data (image, video, text, database, unstructured data,...), the kind of distributed machine environments (one machine to another machine, one personal machine (from a laptop to a mobile device like smart phone or a tablet) to one cloud, a general distributed environment involving several providers,..). We can see by combining these various possibilities that use cases can be very contrasted and their number can be relatively large.

We consider the use case with relatively simplified situation: an end-user (Alice) wants to save her multimedia data in a public cloud in order to save memory in her private resource-limited environment (be a desktop, a laptop, or even a smart phone), however, for privacy reasons, she does not want putting her entire data either in plain-text or encrypted in the hands one storage provider. The solution is quite straight forward that is to protect the data on the private resource-limited environment that end-users have with all the possible calculation resources to achieve a reasonable performance.

In this thesis, we first present the related work mainly around the notion of Selective Encryption (SE) methods which are designed for specific multimedia contents in Chapter 2. The performance issue and the limitations are given to illustrate weakness of most SE methods. Then in Chapter 3, we introduce the hardware level discussion, mainly the idea of using General Purpose Graphic Unit (GPGPU) which is original for SE methods. Of course GPGPU behave as an accelerator for the methods designed in subsequent chapters but they also have an issue of portability that we will discuss. In Chapter 4, a special use case of bitmap image is considered as the data need to be protected. All design and implementation details are given with benchmark evaluations. In Chapter 5, we upgrade methods of Chapter 4 to fit with agnostic fashion of data by not only design with practical concerns but also parallel implementations partly on a CPU, partly on a GPU. We analyze in details of performance, security, and integrity issues, and describe how our SE methods can be used to safely store public fragments in public storage systems. Then we conclude in Chapter 6 with future works.

1.2.1 Benchmark problem

Benchmark is critical and is a key rationale [121] for developing protection methods. There are very little research that thoroughly investigate performance of existing specific SE methods in a practical way [77]. One main reason is that some SE works are integrated within the compression or encoding algorithms which authorize authors to simply ignore possible delay caused by the first step of SE methods since they are shared. This unpractical issue is explained in Chapter 2.4.3 within a real end user environment. Moreover, most of the SE methods are not comparable with traditional full encryption algorithms like AES implemented with state of the art hardware or software, or are not considering the huge progression in performance caused by constantly evolving hardware.

In fact, it is easy to assume that encrypting a small part of the data ought to be faster than doing it in full based on the syntax 'selective' encryption. However, the gain in performance is not that obvious, as this approach may adds a pre-processing phase of data analysis and splitting that could lead to overall worse performance than full encryption. We propose to benchmark these methods from an end-user viewpoint: from the moment he is starting the operation of protection to the moment his data is protected (this is an end to end consideration) and compare the method with a full encryption (today, AES)–Of course, this comparison must use similar hardware.

The need for regularly performing benchmarking is enforced by the fast pace progression of various hardware architecture (particularly GPU architectures) and software implementations of full encryption methods (for instance, there is a clear acceleration from AES to

AES-NI [17]). These changes of hardware architecture and software algorithms may very well change the ranking of the various methods and ultimately, change the end-user decision. This is why we pay attention to the implementation of these methods and test on different hardware environment. For example, even with the GPU acceleration, we have to recognize that performance for GPU implementation is still not just a simple software coding but, in fact, a particular implementation could reach best in class performance on a given platform but not on another one [37].

It is important to consider performance as a key factor to determine whether the SE method is practical. Also the possible changes caused by hardware upgrade and software optimization still need to be considered and discussed as they may change the whole design. In summary, we are showing the possibility of using the SE methods in a practical way rather than giving an ultimate solution for end-user data protection use case.

1.2.2 Security analysis

Attack resistance is, in our opinion, another key rationale even if a number of authors accept to present SE as a compromise between security and performance and categorize SE as a lightweight security process. Most of the state of the art papers we have seen in [101] or later are mostly looking at visual degradation. It is fair to consider only the visual degradation for the image case as it it the most important standard. Just like in Chapter 4 we show the protection for bitmap format is analyzed with mainly the traditional visual degradation. However, for an agnostic SE methods, more requirements are needed including statistical analysis based on frequency analysis, correlation analysis, entropy analysis, differential analysis and whether subject to a possible avalanche effect (resisting to error propagation). This is done in Chapter 5 where we use different file formats to test the design.

In fact, as the design in this thesis is based on the fragmentation for the data, there will be fragments with different security levels and dispersed on different locations. For the most important fragment, the protection method is the traditional full encryption (can be easily replaced with any other protection methods) and the storage place is considered as secure so the security analysis is omitted. The fragments that are transmitted and stored on the Cloud servers are the part that needs security analysis.

In Chapter 5, we present figures for the security analysis for one case and some statistical results in tables for many times repeated tests. As long as different file formats are used, some criteria like PSNR and SSIM just suit for images are not used for other file formats like texts. And some compressed multimedia data is also used for test but just with a general statistical analysis.

In summary, all core purposes of security analysis is to prove no matter what kind of plain texts are the input, the output cipher texts ought to be as close as possible to the ideal random data. And as the encryption key is introduced in Chapter 5 for the protection of the data stored locally, the sensitivity analysis of the key is also needed to prove the resistance for attacks like chosen plain text attack.

Chapter 2

Data protection methods

In this chapter, firstly, basic introduction of secure storage and secure computation is given. A small test for FHE accelerated by GPGPU is also presented. Then, selective encryption, a special data protection method normally for multimedia data, is introduced and discussed. At last, our selective encryption approach is given.

2.1 Secure storage and secure computation

Three main functions are required to protect digital data during its life cycle: secure storage, secure computing and secure sharing. One of the most promising method for securing computing is Fully Homomorphic Encryption (FHE) which provides full privacy during the whole computing process for the encrypted data. And the most popular technology for data storage and sharing is Cloud computing, which offers several benefits like fast development, pay-for-use and lower costs, scalability, rapid provisioning, greater resiliency, low-cost disaster recovery, and data storage solutions. With over three decades long, outsourcing information storage and processing, cloud-based services for data storage have gained in popularity and today can be considered as mainstream. They attract organizations or enterprises as well as end users who do not want or cannot cope with the cost of a private cloud.

The cloud offers all these advantages, however, this is not without taking cloud computing needs to move the application data or databases to large data centers, where the operation and management of the data and services are not trustworthy [122].

Hardening data protection using multiple methods rather than 'just' encryption is becoming of paramount importance when considering continuous and powerful attacks to spy, alter, or even destroy private and confidential information. Even if encryption is a great technology rapidly progressing, encryption is 'just' not enough to progress with this unsolvable

question not mentioning its high computational complexity. In [2], the author shows how to compromise Diffie-Hellman key exchange (used in https sites) with 512-bit group. It is also shown that 1024-bit encryption could be cryptanalyzed with enough computational power. Cryptographs never like the idea that a cipher can be broken and information can be read given sufficient computational resources [106], this is nevertheless one of the central design tenets of a number of projects like the Potshards system [147]. Moreover, there remains the difficult question of the management of the encryption key that over time, can be known by too many people, and stolen or lost.

Our purpose and ultimate ambition is to look at data protection and privacy from end to end by way of combining fragmentation, encryption, and then dispersion. This means to derive general schemes and architecture to protect data during their entire life cycle everywhere they go throughout a network of machines where they are being processed, transmitted, and stored. Moreover, it is to offer end users choices among various well understood cost effective levels of privacy and security which would come with predictable levels of performance in terms of memory occupation and processing time. For this thesis, we aim to provide secure data storage scheme for end users with reasonable assumptions that end users will have a resource limited personal environment and will look at a honest but curious third party cloud storage provider with a cost effectiveness additional constraint.

2.2 Fully homomorphic encryption

2.2.1 What is FHE

Fully Homomorphic Encryption (FHE) is a concept asked in 1978 by Rivest et al. [135] and answered by Gentry [55]. This concept can be described as “is there a way that delegates processing of your data, without giving away access to it”.We immediately understand the value proposition of such encryption algorithms even before considering outsourcing or public cloud computing since it is about performing computation with encrypted data in perfect security. The trustworthiness question in cloud computing has been discussed for years and today, there is still no perfect solution. FHE could very well be this ‘perfect solution’ only once proven efficient from a performance point of view which depends upon the use case under consideration.

Fig. 2.1 shows how FHE can be used with a cloud server to compute the value of a function f for a data *Data* : the user Alice sends the encrypted *Data* (encrypted with Key) and the function f (the calculation Alice wants) to the cloud and the cloud will receive only the encrypted *Data* and the function f. The property of FHE allows the cloud to perform the

computation on encrypted *Data* with the *Evaluate* function (shown in Fig 2.1, compute on ciphertext) without knowing or accessing to *Data*. Alice will be able to decrypt 'evaluated' *Data* with the corresponding Key' and get the result *f(Data)*. This process is basically shown as the equation below:

$$Evaluate(f, Encrypt(Data)) = Encrypt(Evaluate(f, Data)) \tag{2.1}$$

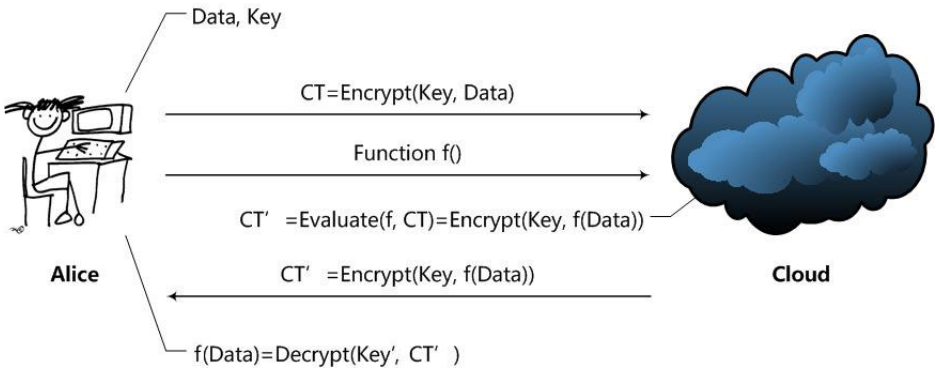

Fig. 2.1 General concept of how FHE works.

Other encryption algorithms are known for having somewhat homomorphic property (see Wikipedia [171]). For instance, RSA is homomorphic with regards to multiplication: If the RSA public key is modulus m and exponent e, then the encryption of a message x is given by:

$$\varepsilon(x) = x^e mod(m) \tag{2.2}$$

The homomorphic property for the multiplication is then:

$$\varepsilon(x_1) \cdot \varepsilon(x_2) = (x_1^e \cdot x_2^e) mod(m) = (x_1 x_2)^e mod(m) = \varepsilon(x_1 \cdot x_2) \tag{2.3}$$

which means if the evaluation function is multiply, the RSA has property of homomorphic.

2.2.2 Related work of FHE

Since 2009 when FHE based on ideal lattice was introduced by Gentry [55], three main branches of FHE schemes have been developed: lattice-based, integer-based and learning-with-errors (LWE) or ring-learning-with-errors (RLWE) based encryption.

The main focus of the theoretical cryptographic research community is currently on LWE and RLWE based FHE (Brakerski and Vaikuntanathan [18], Gentry et al. [57], Gentry et al. [58]). LWE based was introduced by Regev [131], and has been shown to be as hard

as the worst case lattice problems. This problem has been extended to work over rings by Lyubashevsky et al. [95], and this extension increases the efficiency of LWE.

Integer based schemes were introduced by Van Dijk et al. [160] as a theoretically simpler alternative to lattice based schemes and have been further developed to offer similar performance to existing lattice based schemes by Coron et al. [34], Coron et al. [35].

Despite different math basis have different performance, none of them is efficient enough for applications with time constraints. For example, key generation in Gentry and Halevi's lattice based scheme in Gentry and Halevi [56] takes from 2.5 seconds to 2.2 hours. And for the evaluation step, a recent research by Gentry et al. [59] shows a homomorphic evaluation of AES-128 requires 36 hours which is actually incredibly slow compared with the speed of hundreds of MB/s for AES-128 on modern PC's CPU. Very few applications can stand such delays.

Another important limitation of FHE is with the memory usage. FHE generates very large cipher text and uses public key sizes to guarantee adequate security to prevent against possible lattice-based attacks. Gentry and Halevi's FHE scheme [56] uses public key sizes ranging from 17 MB to 2.25 GB.

Current research is aiming at improving performance of FHE either by focusing on new fundamental math to reduce computation complexity or by implementing the existing FHE algorithms on different hardware (GPU or nanotechnology). New algorithms are expected to provide with an actual breakthrough in term of performance; however, on another hand, hardware progression is relatively limited with regards to the need for a vast deployment of FHE.

2.2.3 Performance study

In this section, we provide current research results about performance of the existing algorithms and their implementations. We are adding our own implementation for comparison. As we mentioned earlier, theoretical breakthrough of algorithm may bring a revolution in term of acceptance of FHE, this may need many years of work. In the meantime, it is interesting to search for possible optimized solutions including by using existing powerful hardware to determine whether FHE is ever usable. Although many research articles have claimed the performance of FHE are slow or far from application, it seems important to characterize how slow FHE really is. Performance of the underlying crypto-primitives such as modular reduction and large multiplication are required in many of the FHE schemes. Actually, they are critical these operations could be significantly improved through the use of GPGPU, FPGA, or ASIC technology.

Table 2.1 Performance study of different based FHE and SWHE modified according to [40]

Designs	Schemes	Platforms	Performance
CPU Implementations			
AES [59]	BGV-FHE	2.0 GHz Intel Xeon	5 min/AES block
AES [39]	NTRU-FHE	2.9 GHz Intel Xeon	55 sec/AES block
Full FHE [137]	NTRU-FHE	2.1 GHz Intel Xeon	275 sec/bootstrap
Full FHE (our test)	BGV-FHE	3.0 GHz Intel I7	3-5 min/bootstrap
GPU Implementations			
NTT mul/reduction [166]	GH-FHE	Nvidia C 250	0.765 ms
NTT mul [166]	GH-FHE	Nvidia GTX 690	0.583 ms
AES [38]	NTRU-FHE	Nvidia GTX 680	7 sec/AES block
NTT mul (our test)	GH-FHE	Nvidia GTX 780	0.81 ms
FPGA Implementations			
NTT transform [167]	GH-FHE	Stratix V FPGA	0.125ms
NTT mod/enc [22]	CMNT-FHE	Xilinx Vitrex-7 FPGA	13 ms/enc
AES [40]	NTRU-FHE	Xilinx Virtex-7 FPGA	0.44 sec/block
ASIC Implementations			
NTT mod [41]	GH-FHE	90 nm TSMC	2.09 sec
Full FHE [42]	GH-FHE	90 nm TSMC	3.1 sec/recrypt

The first GPU implementation of a FHE scheme was presented by Wang et al. [166] in 2012. The authors implemented the small parameter size version of Gentry and Halevi's lattice-based FHE scheme in Gentry and Halevi [56] on an NVIDIA C2050 GPU using the FFT algorithm, achieving speed up factors of 7.68, 7.4 and 6.59 for encryption, decryption and the recryption operations, respectively. The Fast Fourier Transform (FFT) was used to target the bottleneck of this lattice-based scheme, namely the modular multiplication of very large numbers.

An overview of FHE implementations on different platforms is shown in Table 1 in Doröz et al. [40]. Clearly, since the platforms vary greatly according to available memory, clock speed, area/price of the hardware a side-by-side comparison is not possible and therefore this information is only meant to give an idea of what is achievable on various platforms.

Much of the development so far has focused on the Gentry-Halevi FHE Gentry and Halevi [56], which intrinsically works with very large integers (million bit range). Therefore, a good number of works focused on developing FFT/NTT (Number Theoretic Transform) based large integer multipliers in Doröz et al. [41], Doröz et al. [42], Wang et al. [166]. Currently, the only full-fledged (with bootstrapping) FHE hardware implementation is the one reported by Doröz et al. [42], which also implements the Gentry-Halevi FHE. At this time, there is a lack of hardware implementations of the more recently proposed FHE schemes, i.e. [34]

and Coron et al. [35], BGV-style FHE schemes Gentry and Halevi [56] and Yagisawa [178] and NTRU based FHE, e.g. López-Alt et al. [94] and Stehlé and Steinfeld [145].

2.2.4 Discussion

Results for different FHE algorithms and for limited evaluation functions (AES-128 bit here) were presented in Table 2.1. We can use this table to conclude as in the European H2020 project [68] that FHE is still far from real application. But here, we can quantify the issue. The AES block is processed in around 1-5 mins on an Intel Xeon CPU which is the type of CPU currently used in workstations. A good GPU (Nvidia GTX 690) could help reducing this processing to about 7 secs. However, considering the AES is processed at a hundreds MB/s on PC's CPU [37], which equals almost 1 million blocks processed per second, the performance of FHE-AES is far too slow to get considered usable. Even if the hardware upgrades, even if the performance of FHE-AES is improved one thousand times faster, it is still too slow for general use.

Table 2.1 shows that we still need to progress by 2 or 3 order of magnitude before deploying FHE. Our own code is on par with current publications for similar schemes and similar platforms. The only hope would be to use partial homomorphic encryption (PHE) or somewhat homomorphic encryption (SHE) but their usage will be very limited to niche applications.

2.3 Traditional full encryption

Cryptography is the science of writing in secret code and is an ancient art; the first documented use of cryptography in writing dates back to circa 1900 B.C. when an Egyptian scribe used non-standard hieroglyphs in an inscription. Some experts argue that cryptography appeared spontaneously sometime after writing was invented, with applications ranging from diplomatic missives to war-time battle plans. It is no surprise, then, that new forms of cryptography came soon after the widespread development of computer communications. In data and telecommunications, cryptography is necessary when communicating over any untrusted medium, which includes just about any network, particularly the Internet.

Within the context of any application-to-application communication, there are some specific security requirements, including:

- **Authentication:** The process of proving one's identity. (The primary forms of host-to-host authentication on the Internet today are name-based or address, both of which are notoriously weak.)

- **Confidentiality:** Ensuring that no one can read the message except the intended receiver.
- **Integrity:** Assuring the receiver that the received message has not been altered in any way from the original.
- **Non-repudiation:** A mechanism to prove that the sender really sent this message.

Encryption is one of the principal means to guarantee **privacy and confidentiality** of information. Traditional encryption algorithms in the recent several decades, which is also widely used in information security in telecommunication fields, perform various substitutions and transformations on the plaintext (original message before encryption) and transforms it into ciphertext (scrambled messages after encryption). The goal of encryption is to make the plain information unreadable, invisible or unintelligible to keep it secure from any unauthorized attackers.

Encryption algorithms are traditionally split into two groups: Symmetric key encryption (also called secret key) and Asymmetric key encryption (also called public key). Symmetric key encryption is a form of cryptosystem in which encryption and decryption are performed using the same key like DES, AES, 3DES, IDEA, etc. It is also known as conventional encryption. The security of symmetric encryption algorithms relied on very large key space and normally faster than asymmetric encryption on modern communication devices.

Asymmetric encryption is a form of cryptosystem in which encryption and decryption are performed using different keys (like RSA) – one public key and one private key. It is also known as public-key encryption. This two-key crypto system makes two parties possible to securely communicate on a non-secure channel without the problem of sharing the single key like in symmetric encryption systems. The most famous asymmetric key algorithm is Rivest-Shamir Adelman (RSA by Rivest et al. [136]). The asymmetric encryption algorithms are much slower than the symmetric ones because they use much more complex math calculations rather than just bit-level operations.

2.4 Selective encryption

2.4.1 Basic concept of selective encryption

Selective encryption (SE) used for protecting data especially multimedia data has been introduced more recently. The basic idea is to go as fast as possible to reduce the overhead involved by securing data. Although traditional data encryption techniques such as Advanced Encryption Standard (AES) [134] have become very popular, they have some clear limitations

for multimedia applications. The main problem is that the majority of existing encryption standards such as DES and AES have been developed for i.i.d. (independent and identically distributed) data sources [32]; however, multimedia data are typically non i.i.d. which will lead to poor speed of encryption pointed out in Fig. 2.2 by Grangetto et al. [64]. This is because the statistics for image and video data are strongly correlated and have strong spatial/temporal redundancy that makes them differ a lot from classical text data. And as pointed by Lookabaugh in [92, 93], the relationship between plaintext statistics and ciphertext security is already highlighted by Shannon in [142]: a secure encryption scheme should remove all the redundancies in the plaintext; otherwise, the more redundant the souce code is, the less secure the ciphtertext is [101]. Based on this viewpoint, the naïve full encryption algorithms are not suitable for protecting the multimedia contents and SE methods are designed to fit the need.

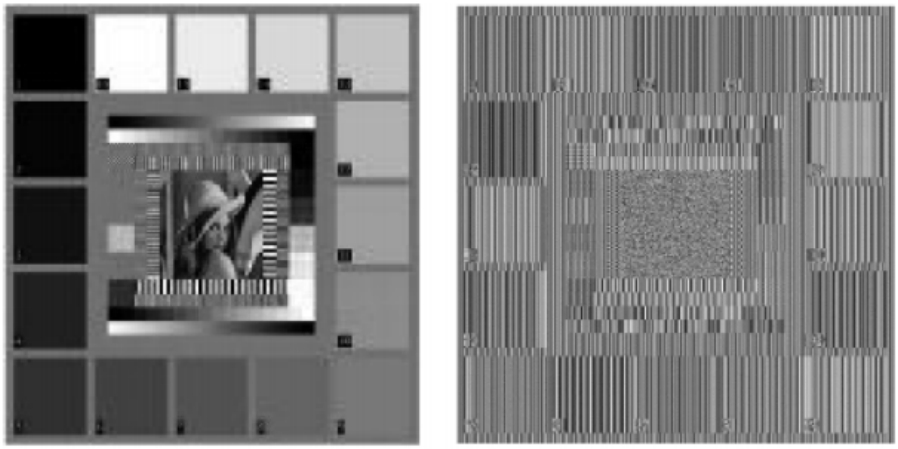

Fig. 2.2 One example in [64]: Original image (left) compared with AES-encrypted image (right).

SE consists in applying encryption to a subset of the original content with or without a preprocessing step like shown in Fig. 2.3. The main goal of selective encryption is to reduce the amount of data to encrypt while achieving a required level of security. The general approach is to separate the content into two fragments. The first fragment is the *public fragment*, it is left unencrypted in most SE cases and made accessible to all users. The second fragment is the *private fragment* which is encrypted. Only authorized users have access to the protected private fragments. One important feature in selective encryption is to make the private fragment as small as possible.

The main question for SE is how to select the private fragment to encrypt while keeping the rest without an information leak. There is no general answer to this question because as shown in related works, the SE methods are most used for soft encryption purposes that

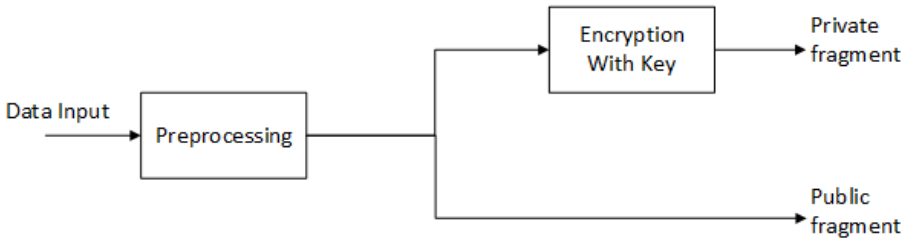

Fig. 2.3 Basic concept of selective encryption.

make them have different protection standards. For example, in some applications (video on demand, database search, etc.), it could be important to encourage customers to pay for the entire content. To this purpose, only a soft visual degradation is achieved, so that everyone could still understand the content but have to pay to access the full-quality original content. In some other use cases like sensitive data (e.g., military images/videos, etc.), hard visual degradation could be desirable to completely disguise the visual content. And sometimes only a part of the image is recognized and protected [162]. Moreover, according to Massoudi et al. [101], many kinds of different methods are adapted to protect different multimedia formats (JPEG, MPEG, etc.) or different multimedia contents respectively, however, state of the art SE methods are designed to protect a given type and nature of data (e.g. bitmap image, jpeg image, mpeg video, etc.). Consequently, they can protect only the kind of data format which they were designed for.

In summary, different use cases and different formats of multimedia contents determine and restraint different purposes of SE designs. The most important trade-off is to make the private fragment as small as possible in order to reduce processing time while securing the whole data content according to a specific requirements.

2.4.2 Related work of SE

SE methods have been described and discussed in many previous works (see an overview by Massoudi et al. [101]). According to Massoudi et al. [101], SE methods can be classified by when the encryption is performed with respect to compression (there are very few multimedia formats that are uncompressed such as bitmap are not within this scope.). So three classes of SE methods are listed: (1) Precompression, (2) Incompression and (3) Postcompression. This classification is based on how most multimedia content is generated from initial pixel information to packets transmitted on Internet (see Fig. 2.4).

According to Massoudi et al. [101], in the process shown in Fig. 2.4, the coding process is always seen as the compression step as the widely used coding techniques especially entropy coding schemes [83] can efficiently reduce the multimedia data size before transmission. So

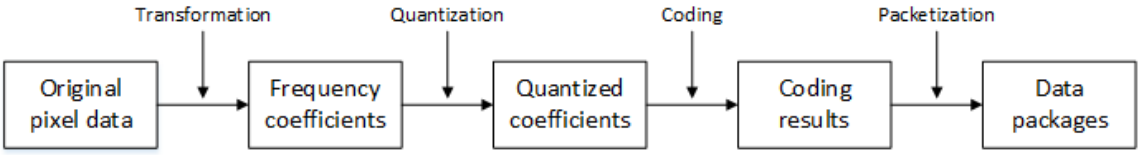

Fig. 2.4 The process of how most multimedia data is generated.

if the selective encryption is performed at the frequency coefficients step, the SE methods are classified as precompression; if it is performed during the coding process, the SE methods are classified as Incompression and the other methods that perform SE after coding step are postcompression.

Precompression SE methods

This category of SE methods are mainly protecting data at its frequency space. In Fig. 2.4, the transformation methods like Discrete Cosine Transform (DCT) [4] and Discrete Wavelet Transform (DWT) [21] are commonly used to generate frequency coefficients in the first step. As from a viewpoint of energy distribution in frequency domain, low frequency areas take less storage space while carrying most of the energy. Studies on the Human Visual System (HVS) have confirmed that humans are more sensitive to lower frequencies than to higher ones [123]. So the most important visual characteristics are to be found in the low frequencies, while details exist in the higher frequencies. And these considerations have had fundamental impacts on image or video compression techniques and also given the hint about the design of SE methods. In fact, most SE methods exploit this energy concentration in their designs.

The very initial SE method based on DCT is proposed by Tang [151] in 1996 to protect some of the DCT coefficients in the I-frame of a MPEG video [82]. The author used DES in CBC mode [33] to protect the DC coefficients and randomly permutated the AC coefficients instead of the zigzag scans.

However permutation of the AC coefficients is not enough. As shown by Qiao et al. [124] and Uehara and Safavi-Naini [157], with setting DC coefficient to a fixed value, a chosen or known plaintext attack [8] can get a semantically good reconstruction. As long as the DC coefficient in the DCT represents the average intensity of the corresponding DCT block which is critical from an energy viewpoint, the rest AC coefficients still carries some information that can help to reconstruct and get an acceptable visual result.

This situation is seen again in Puech and Rodrigues [123], although protecting only the DC value can highly degrade the visual quality of image or even make an image totally

unreadable, the DC coefficients can be recovered from the remaining coefficients which makes the reconstruction of the image possible as pointed by Uehara et al. [158].

More recent works in Krikor et al. [80] and Yuen and Wong [180] protect not only the DC values but also some AC values as well. These methods seems more promising as the coefficients protected (DC coefficient and first 5 AC coefficients in Krikor et al. [80]) carry more than 96% of the whole energy in an image use case. However, this is still not enough as a protection method. Because in some cases there are sharp edges or many detail information contained in an image that makes the rest high frequency coefficients could show some hints about what the image is without any recovery of the protected coefficients. As shown in Qiu and Memmi [126], the reconstructed image by padding random number for the protected DC and first 5 AC coefficients is still able to be understood.

Indeed, protecting the low frequency coefficients of DCT can efficiently degrade the visual quality which fits some use cases. However, degrading the visual quality does not mean providing a good protection of the content. After all, as images are very different, it is difficult to generally determine how many low frequency coefficients should be protected to achieve a good level of protection.

Wavelet based SE methods are also shown in related works like in Chen and Zhao [24], Taneja et al. [150] and Martin et al. [99]. The techniques include frequency selective encryption, block shuffling, encryption of wavelet packet tree structures, etc. Although there are no publications pointing that these techniques can be attacked, however, as pointed by Massoudi et al. [101], these SE methods mainly aim to degrade the visual quality and it necessarily is still difficult to evaluate its security level. That is to say, harder visual distortion does not imply more security.

Incompression SE methods

In 2003, Pommer and Uhl [121] proposed a SE method that encrypts only the head information of the wavelet packets which specifies the subband tree structure. This method can be attacked by chosen plaintext attack as the statistical properties of the wavelet coefficients remain unprotected which gives the possibility to reconstruct the approximation subband. Protecting only head information is far from enough to secure the content, however, their use case could justify this approach.

In 2001, [174] and [173] gives a new viewpoint that SE methods can be done during the entropy coding stage. One method they proposed uses the multiple Huffman tables (MHTs) to protect audio and visual contents by generating millions of different Huffman tables using Huffman tree mutation [174, 173]. Indeed, decoding a Huffman coded stream without any knowledge about the Huffman coding tables is very difficult as shown in Gillman

et al. [61]. However, the basic MHT could still suffer from known and plaintext attacks as shown in Zhou et al. [187].

The other method proposed by Wu and Kuo [174] and Wu and Kuo [173] is to protect during the process of QM arithmetic encoding [85] (an enhancement of the Q coder [119]). As long as the QM coder is based on an initial state index as an entry, 4 published initial state indices is picked and used in a secret order according to the author. There are no known attack to this method but it can only be used for the multimedia format with a QM coding stage inside (e.g. JPEG standard [118]).

The similar technique shows up to protect JPEG2000 [152] images when MQ coder (an enhancement of QM coder, see [152]) is used in JPEG2000 standard. In 2006, Grangetto et al. [64] used a randomized MQ coder that randomly the two alternative coding intervals that can achieve very good visual degradation. In 2014, Xiang et al. [177] gives another protection method for JPEG2000 images by replacing the initial lookup table during the MQ coding process. These methods can be efficiently used by embedding into the JPEG2000 coder and decoder but are also highly format reliance.

Postcompression SE methods

In 2000, Cheng and Li [26] proposed a SE method at the output of quadtree compressor [98]. The author takes the quadtree structure values as the private fragment to encrypt and leave the rest leaf values unencrypted. However, as pointed by Massoudi et al. [101], the brute force attack is practical for low information images and for high information images, the encrypted fragment can reach about 50% of the original image size.

In 2008, Massoudi et al. [100] designed a SE method dedicated for JPEG2000 images on packets level that can degrade the visual quality of images by protecting only a small part of the original data. However, this method can be applied only on JPEG2000 format and the performance could be weak when high level protection is required.

These kind of methods are also seen in Wu and Deng [175], Stutz and Uhl [148] and Engel et al. [44]. These methods did protect the code blcok contribution to packets (CCPs) which can achieve high level of visual degradation but may be weak against side channel attack.

2.4.3 Our SE approach

Massoudi et al. [101] classified SE methods related works in three categories by when the encryption is done with regards to the compression process. However, SE designs are not practical for an end user. As shown in Fig. 2.5, if we consider SE designs from an end user point of view, the digital devices that a normal end user have are normally a digital device

that will generate multimedia content (also including multimedia contents downloaded from Internet) and a device that owns limited calculation capacity (a low-end laptop or a high-end desktop, etc.). In this case, if the end user wants to store the multimedia data (photos or videos) to a cloud server or to share these data through a cloud server, the data has to be protected before going to the insecure channel. However, as long as today's digital cameras are not equipped with hardware or software available for any security calculation, the very first data that an end user gets is the formatted package-level data like JPEG or MP4 files directly generated from the camera (see Fig. 2.5).

Such a situation is not favorable to SE methods belonging to precompression or incompression are efficient because the only way to use these methods would consist in decoding the package-level data like JPEG on the laptop until transformation step (reverse the process of Fig. 2.4) and applying the SE method to reformat everything again, which is of course very time costly and complex. Moreover, even if this kind of scheme is used, the data is still vulnerable as indicated in the previous section: many SE methods have not been published with enough security analysis and are proven either exposed to attack or can be reconstructed somehow leading to information loss.

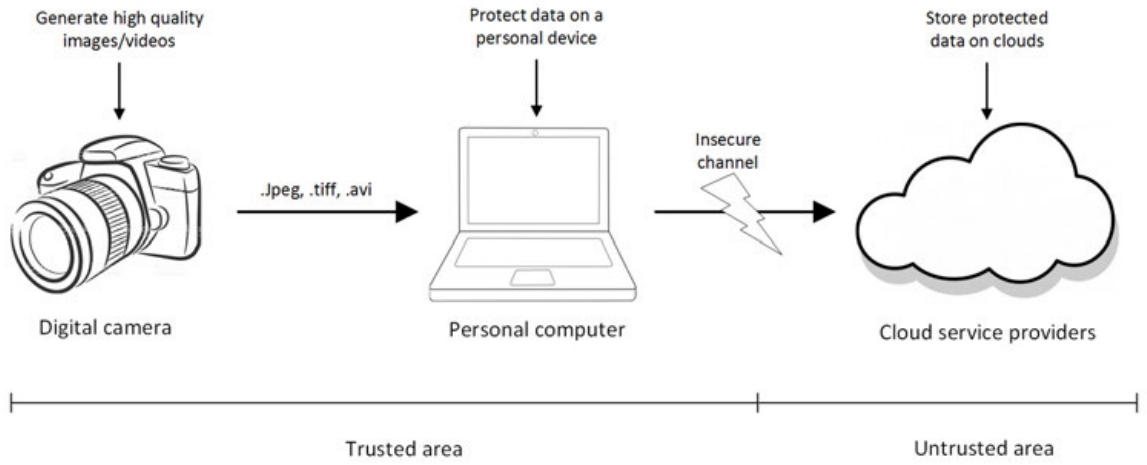

Fig. 2.5 A use case that multimedia data should be protected before sending to could storage.

In our work, we reconsider SE in an end user scenario. On the one hand, nowadays, data security is more important than a decade ago because we have security threats not only from insecure channels as usual but also from possible information leak from cloud providers (see PRISM [122]); on the other hand, however, the multimedia data have many kinds of formats with very different designs which makes using format reliance SE methods difficult. The use case we consider is based on an end user viewpoint that data of an end user should be protected from not only the insecure channel but also the cloud service providers (the whole

untrusted area in Fig. 2.5). Moreover, the SE design should be efficient enough compared with the full encryption methods.

The general concept of our view is shown in Fig. 2.6. Three main steps are defined: Preprocessing, Protection and Dispersion.

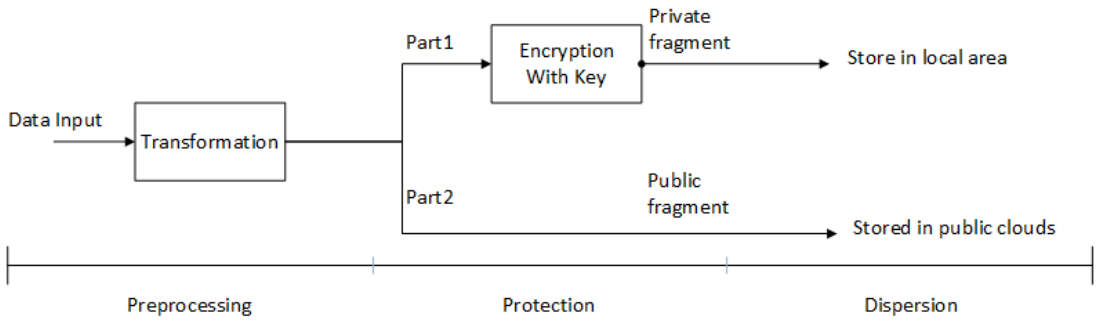

Fig. 2.6 SE conceptual design combines fragmentation with an example use case of efficient dispersion .

In this scenario, data first goes to a preprocessing step that will perform the transformation to help separating data into two fragments (sometimes more than two fragments) with different levels of importance. This is the concept of fragmentation introduced by our work in our SE design. In fact, fragmentation is not a new idea but a general concept used in computer science in many different applications and usages (by operating system to optimize disk space management, by database management or distributed systems to gain in performance particularly in latency, by routing algorithms in communication to increase reliability and support disaster recovery when combining replication and fragmentation together). Here the usage of fragmentation is done by the transformation like DCT or DWT in our design.

The second step is the protection for different fragments. Indeed, data fragments of different security levels should be protected with different encryption methods for efficient purpose. The encryption method used in our design for the most important data fragment is AES-128. Since 2001, Advanced Encryption Standard (AES) [36], is selected as a standard specification for the encryption of electronic data by the U.S. National Institute of Standards and Technology (NIST), it has become the most widely used symmetric encryption algorithm in the world. Although many proposals of side-channel attacks for AES were published in recent years (Piret and Quisquater [120], Ors et al. [113], Schramm et al. [141], Bertoni et al. [13]), AES is still considered secure as long as no key abuse. Moreover, encryption algorithm for the private fragment can be easily replaced by another one if need be. In Fig. 2.6, we fragment data into two parts: *private fragment* and *public fragment*. The *public fragment* can be as large as needed but carry as little information as possible. And the protection method

for the *public fragment* should be light weighted or no protection at all with the target that no recovery should be possible only from the public fragment.

Then the dispersion step should be performed to store different fragments into different storage areas making for an additional hurdle for attackers. In Fig. 2.6, we design to store the private fragment in a trusted area and the public fragment in a public and untrusted area. This design fits the real scenario shown in Fig. 2.5 which can let most of the data stored in public clouds without information leak and save storage space on the user's local device. For the transmission purpose, we have discussed in Chapter 5 that the private fragments can be encrypted and transmitted through different channel which allows our design fits the needs of both secure data storage and secure data transmission.

2.4.4 Performance issue of SE

Speed is a critical criterion and a key rationale for developing SE methods: encrypting a small part of the data ought to be faster than doing it in full. However, the gain in performance is not that obvious, as in some use cases, a complete SE approach adds a preprocessing step that could lead to overall worse performance than full encryption. After all, the proprecessing step also costs time and very few papers discuss and show performance of SE algorithms implementation (Khashan et al. [77]).

Therefore, we should benchmark any new proposed method against existing ones–in particular, the standard full encryption methods (today, AES)– using end to end comparison and similar hardware. The need for regular benchmarking is reinforced by the fast paced progression of hardware architecture and software implementations of full encryption methods, as a particular implementation could reach best in class performance on a well-adapted platform [37]. Overall, when accounting for every step of the process, it is not so clear that full encryption is slower than SE, especially for some methods with the intensive steps.

One point worth consideration is that some random position permutation methods (Li et al. [88], Li and Lo [84], Zhang et al. [183]) and chaotic based cryptosystems (Liu and Wang [90], Bhatnagar and Wu [14], Zhang et al. [184]) are used to encrypt entire or partial image data. These approaches do not have the performance issues we mentioned before. However, the security level of the random position permutation schemes is weak against the known plaintext attack. Zhao et al. [186] proposed to recover the corresponding original image. Moreover, the main constraint of chaos based encryption schemes is that the finite accuracy of numerical calculations on modern computers can lead to an arbitrary change of major chaos properties such as the external parameters or initial conditions. In summary, although these methods have generally high performance, their security levels are not good enough as pointed by Amigó et al. [6] and Kulkarni et al. [81].

Here we give a simple example to compare one DCT algorithm implementation (implemented based on [112]) and AES-128 bit (this simple example uses only two very common AES modes: CBC and CFB modes implemented based on [37]) on two different PCs with Intel CPUs. The result in Table 2.2 shows that DCT 8×8 is around 45% slower than AES-128 bit. Moreover, AES has a counter mode (AES-CTR [155]) which can be implemented in parallel on modern CPUs with multiple cores. The speed is normally three or four times faster (according to number of cores) than CBC mode on CPUs.

In summary, this brief comparison indicates the SE method using DCT 8×8 like Krikor et al. [80] has serious performance problems given that the preprocessing step (DCT 8×8) alone is much slower than standard encryption algorithms such as AES.

Table 2.2 Benchmark of AES 128-bit and DCT 8×8 on current CPUs.

Computer CPU	AES/CBC 128-bit	AES/CFB 128-bit	DCT 8×8
Intel I7-3630QM	374 MiB/s	362 MiB/s	203 MiB/s
Intel I7-4770K	494 MiB/s	480 MiB/s	267 MiB/s

In this work, we define a SE algorithm implementation as *usable* if this algorithm meets both a suitable level of security with regard to the needs for the special use case and a level of performance comparable or better than a full encryption algorithm (in this work, we use AES 128-bit as the standard encryption algorithm to compare). Based on this definition, many of the SE algorithm implementation using DCT 8×8 in the literature are actually 'unusable' as DCT 8×8 implementation is not faster than AES running on the same CPU.

This issue could be solved by introducing additional calculation resource available, such as the common GPUs on today's PCs.

Chapter 3

Hardware acceleration

In this chapter, the development of parallel computing especially General Purpose Graphic Processing Unit is presented. Both the hardware and software development are given to illustrate the huge improvement of GPGPU in the last decade. Then, the GPGPU of Nvidia is chosen as the platform used for this thesis and the detail information is given.

3.1 Background of parallel computing

Moore's law [140], in the form of doubling the number of transistors in a dense Integrated Circuit (IC) every two years was proven to be met from the 60s to late 90s. In the meantime, clock speed, which determines the main frequency of the chip and is a key criteria to measure the commodity computer CPU's performance, also doubled about every 18 months until 2000 [19]. In this period, Bixby [15] pointed that from 1987 to 2000, performance of commercial Linear Programming solvers were increased one million times faster: 1000 times coming from better methods and the other 1000 times benefited from general improvement in performance in computers technology.

From the 1970s, when the first generation of CPU was created, to the year of 2004, most of computer CPUs used a serial model of execution for calculation tasks. The main improvements were more transistors, higher clock speed, and better memory technology.

Among these factors, the clock speed, linked to the IC technology, determines the minimal time one CPU round needs, always increased at every new generation of computer CPUs until 2004. As pointed by Brodtkorb et al. [19], the main frequency of computer CPUs seem to reach some physical limit in early 2000s. It is also reported by Owens [114] that CPU main frequency increased from 0.5 GHz in 1991 (HP PA-RISC) to 3.6 GHz in 2005 (Intel Xeon). But nowadays, clock frequencies seem stabilized: on Intel CPUs we see even less than 3.6 GHz (commonly between 2.0 GHz and 3.5 GHz without boost). At the same time,

however, we see parallelism keeping growing in CPU architecture from two cores inside one CPU to dozens of cores integrated within one CPU. From then on, parallel implementation for calculation tasks became so important that solutions for complex algorithms need to be optimized to fully exploit the multi-core architecture of modern CPUs.

Parallel computing is not a new idea. Since the 1960s, as the first computers with multiple processors were built up and deployed, parallel computation became a wide spread programming technique. Indeed, according to [19], there are different types of parallel computing in different levels and formats: e.g. parallelism at IC instruction level is common today [163]; parallelism for tasks and for data are the main optimization used by modern IC designs. The task parallelism consists on processing a large number of input elements in to a pipeline that feeds output of each successive task into the input of the next task. This is commonly seen on a computer CPU's working way that divides this pipeline by time and calculate each pipeline stage in turn. However, data parallelism has a different approach that divides the calculation of the pipeline by space instead of time. This model makes it possible that different parts of hardware can be customized with dedicated-purpose for different task calculation to achieve a generally greater computation efficiency over a general-purpose solution.

The different parallel designs for computing are according to the application needs. In this recent decade, huge number of applications for digital contents especially multimedia contents show up with a different feature for the needs of computing. An important feature of these applications need is that the data can be processed independently and in any order on different processing elements for similar operations which is called throughput computing [91]. The throughput computing applications are also seen as the most important classes of future applications [9, 76].

In such a situation, the traditional philosophies of designing CPUs which is to provide calculation capacity for different applications and fast response time for a single task were not suit for these application needs now. Moreover, due to the cost of technology complexity and power consumptions, the main stream CPUs in recent years are integrating only a small number of processing general-purpose cores on one die like Intel-I7 series CPUs [23].

At the same time when we see the parallelism keeps growing in CPU architecture, Graphic Processing Unit (GPU), built on different initial philosophies, as an alternative parallelism model, showed up to fit the needs of these application calculation. In the beginning, designed as subordinate processors, GPUs are built specially for rendering and other graphics applications for multimedia data. This category of applications determined Single-Instruction-Multiple-Data (SIMD) as the basic execution model of GPU. This is borrowed from vector computers [11] built in 1970s.

In this recent decade, driven by the needs of multimedia applications especially gaming industry and needs for accelerating some general-purpose applications that fits more data parallelism, GPU was well developed with both hardware upgrades and software adaption that gives rise to a wider General-Purpose-Graphic-Processing-Unit (GPGPU) field [115]. And until today, not only three of the world's five fastest supercomputers use GPU acceleration [72], but also almost every personal computer is equipped with a high performance GPGPU to accelerate special applications.

3.2 Development of modern GPGPU

The initial role that the GPU play was just a normal component in common PCs. Nowadays, high performance GPUs are common on not only on professional workstations, servers, or super-computers but also personal computers with different capability. Initially, GPU cards are dedicated to video memories and special calculation units. Today, the need for speed of dedicated memories and calculation units are still the main requirement for the GPU performance.

In this section, the development in hardware and software of GPUs for personal computers is presented to elaborate on how GPUs become so efficient for calculation tasks. The Nvidia GeForce series GPUs (for PC users) will be used as examples as we will be comparing their evolution. However, the development of dedicated GPGPUs for workstations or super-computers will also be briefly mentioned but they are not utilized for the use cases we discuss and evaluate.

3.2.1 Hardware development

In this section, the hardware evolvement of modern PCs is introduced. As shown in Fig. 3.1, the host memory (CPU memory) is controlled by CPU and communicates with GPU through PCI Bus. And there is a specific memory (DRAM) for GPU.

In the last two decades, the hardware and industrial process for making GPUs have improved so much that now owning a high performance GPU on a personal computer is common. However, unlike the development of CPUs in the past 40 years, the most performance gain of GPU does not come from the increase of main frequency but from the increasing number of calculation cores and architecture of their dedicated memory.

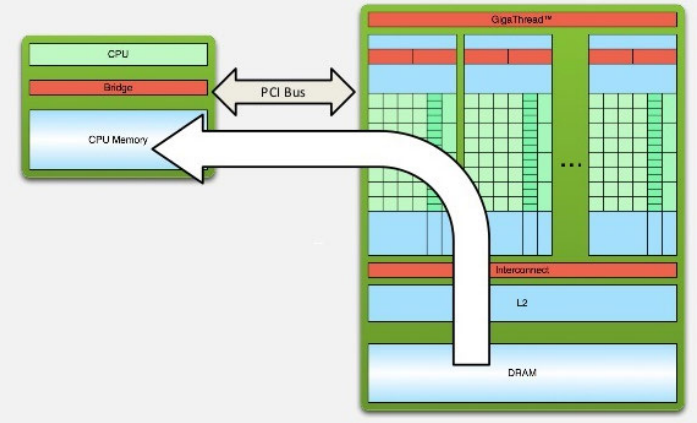

Fig. 3.1 Memory architecture of CPU and GPU on modern PCs [110].

Memory

GPU memory, also called as video RAM, is an independent memory card integrated on GPU board communicating with the host memory on motherboard through bus. The GPU memory we mentioned in this section is only about the memory on GPU board (called 'global memory' in Nvidia CUDA) not in GPU chip (caches, called 'shared memory' or 'texture', etc in Nvidia CUDA).

The speed of GPU memory is measured by the memory bandwidth, which is basically the speed of the read and write operations of the dedicated video memory by the calculation cores. Normally, it's measured in gigabytes per second (GB/s). The reason why there is an independent memory for GPUs is that the GPU cores are calculating much faster than the bus transfer speed and in recent decades, even the speed of the host memory cannot meet the calculation needs. If the memory is not fast enough, GPU cores will wait for data transfer after each operation and the memory can become a series bottleneck. As a result, since a decade ago, dedicated memory became widely used in GPU with size ranging from 512 MB to today's 2-12 GB.

The memory bandwidth today is mainly determined by two factors: memory clock and memory width. The memory clock means the clock rate of the memory chips and memory width is the width of the interface bus. They are all determined by the standard processing at each generation [10]: DDR (Double Data Rate), DDR2, DDR3/GDDR3, DDR4/GDDR4, DDR5/GDDR5 and GDDR5X. If we consider Nvidia GPUs as examples, in 2006, when DDR2 memory is still used for host memory by PCs, Nvidia GeForce 8800 Ultra has the DDR3 memory clock rates at more than 1000 MHz. Today, as DDR3 memory is used commonly by CPU memory, Nvidia GPUs are equipped with GDDR5 or GDDR5X that provides more than 5000 MHz clock rates [109]. Moreover, the DDR5 generation

memory supports 256-bits or 384-bits for bus width which produces the theoretical maximum bandwidth by multiplying memory width and memory clock.

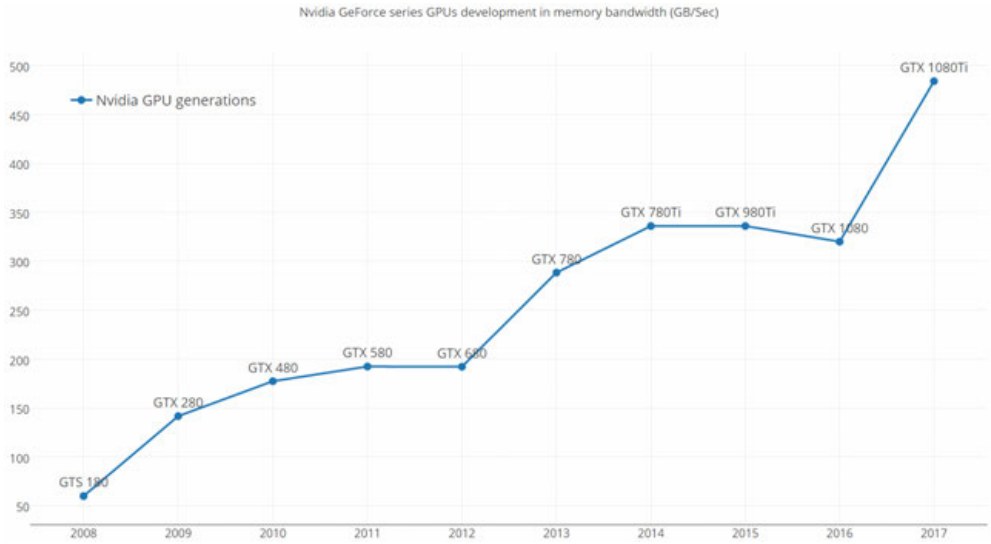

Fig. 3.2 Increase of memory bandwidth (CUDA cores on Nvidia GeForce series GPUs since 2008).

The memory bandwidth of the best Nvidia GeForce series GPUs (high-end GPUs for PCs) are shown in Fig. 3.2 in each year from 2008 to 2017 (data collected from Nvidia website). The memory bandwidth increases about 10 times faster in the past 9 years from about 50 GB/Sec to 484 GB/Sec. One point should be noticed is the GTX 780Ti is the enhanced version of GTX 780 but with a difference that Ti means a very enhanced version. The GTX 780 is one of the GPU card used in this thesis.

Calculation cores

Today, all GPU manufacturers including both AMD and NVIDIA are building architectures with unified, massively parallel programmable units at their cores. However, as pointed by Owens et al. [115], a decade ago, the GPU was just a fixed-function processor, building around the graphics pipeline, it could excel at three-dimensional (3-D) graphics but little else.

In fact, the initial design of GPUs was to treat computer graphics primitives such as vertices and pixels inputting as a stream model. For one piece of data input, there is a vertex processor calculating points (seen as multiple component vectors) and another processor calculating pixel color and so on. Inside one GPU chip, many processing units with this simple architecture are integrated and connected via data flows to perform this simple operation and use the spatial parallelism of graphic applications (e.g. for one frame, which

pixel is calculated first is not important). In 2003, the GPU ATI R300 had eight-pixel pipelines handling single-instruction, multiple-computing processing [96].

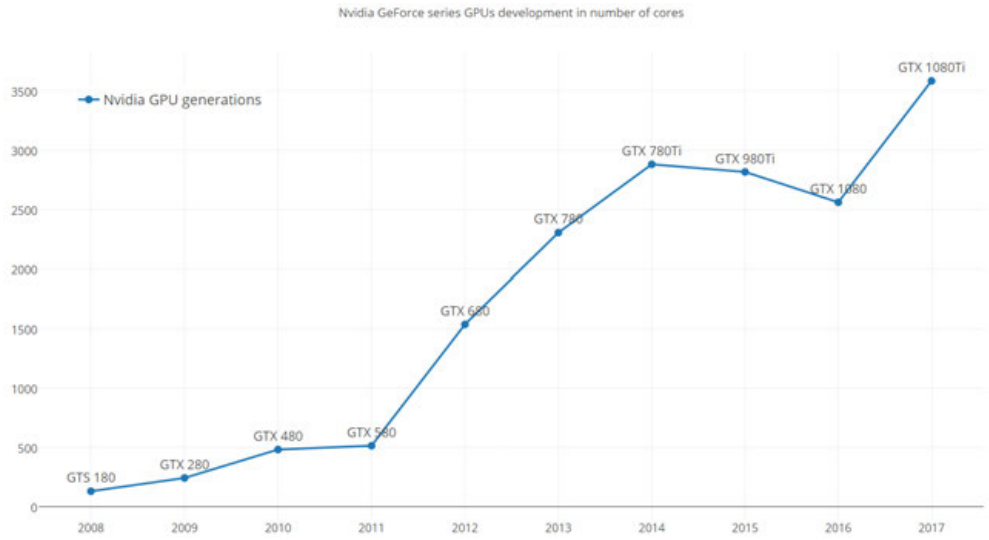

Fig. 3.3 Increase of calculation cores (CUDA cores on Nvidia GeForce series GPUs since 2008).

This simplicity of GPU architecture made it possible to use large areas of chip real estate for computation engines. In 2003, the ATI R300 chip has more than 110 million transistors which is almost same as Intel's Xeon microprocessor with 108 million in the same year. However, more than 60% transistors of the Xeon are devoted to cache [96]. Nowadays, in 2016, the Intel CPU for PCs contains 1-2 billion transistors in die [71] and Nvidia GPU has 5.2 billion transistors on GTX 980 and 7.2 billion transistors on GTX 1080 [109] with a much larger improvement than CPU's progression compared with one decade ago.

Another direct comparison of hardware improvement is the number of CUDA cores in Nvidia series GPUs in Fig. 3.3. The CUDA cores counted here is the special single-precision calculation cores of Nvidia GPUs in GeForce series (designed for PCs, mainly for gaming purpose) and more details of CUDA will be explained in following sections. From 2008 to 2017, the Nvidia GPUs produced in each year have evolved from less than 200 CUDA cores to more than 3500 CUDA cores.

3.2.2 From GPU to GPGPU

Initially driven by specific needs for gaming applications, the computation capacity of GPUs are mainly fixed-function. Since 2006, as pointed by Owens et al. [115], the GPU has evolved into a powerful programmable processor and GPU evolution has been focusing on

the programmable aspects of the GPU. This is due to the development of calculation capacity, it became more and more biverse application utilizing GPUs as accelerators for computing bound tasks in general-purpose computing.

In the early days of programming, graphics specific APIs such as OpenGL [172] or DirectX [65] were be used to perform computations. And the shader programming [46] is the most common method to execute user defined computation on GPU. For example, the operation of adding two matrices on GPU is one in following steps: creating a window with each pixel corresponding to one output element; rendering one quadrilateral to cover this window; then the texture unit will render this quadrilateral with two textures as every color value inside each texture means the value of the input matrices; finally the color value will be added to get a new texture which can get the output result based on the output quadrilateral. During this process, as long as there was no API for matrix addition, the operation had to be written to fit the existing API. This can be a really cumbersome process when dealing with more complex general-purpose operations like matrix multiplication or DCT transform like in Fang et al. [47]. In fact, Fang et al. [47] achieve 50% more performance gain with shader programming compared to CPU with SSE implementation which is not a huge improvement.

In 2003 parts of GPUs' fixed-function pipeline became programmable with the release of the NVIDIA GeForce 256 GPU and C for Graphics language [49] (see Fig. 3.4).

In 2006, GPUs started to support the unified Shader Model 4.0 on both vertex and fragment shaders [16]. The instruction set specially started to support both 32-bit integers and 32-bit floating-point numbers and the hardware allowed an arbitrary number of both direct and indirect operations from global memory (texture) which makes the single-precision calculation much easier to accelerate. Since then, the design of GPUs are increasingly focusing on the programmable units in the graphics cores and instead of being seen as a a fixed-function pipeline, GPUs started to be described as a programmable engine supported by large number of high efficient fixed-function units.

In 2007, NVIDIA released the first general-purpose language for programming GPUs, Compute Unified Device Architecture (CUDA [110]). Also, as shown in Fig. 3.4, two other alternative tools to CUDA have emerged: OpenCL (successor of OpenGL) and DirectCompute (successor of DirectX).

Since then, the GPGPU developing entered a new era that the designing of GPU hardware are for different purpose computing with parallel model and platform gives programmers direct access to the GPU's virtual instruction set, parallel computational elements and arbitrary memory operations. It is possible to implement and optimize complex computation tasks at very low level on GPU and the recent researches show the performance gain compared with CPU are increasing very fast [19]. In the following sections, CUDA platform and

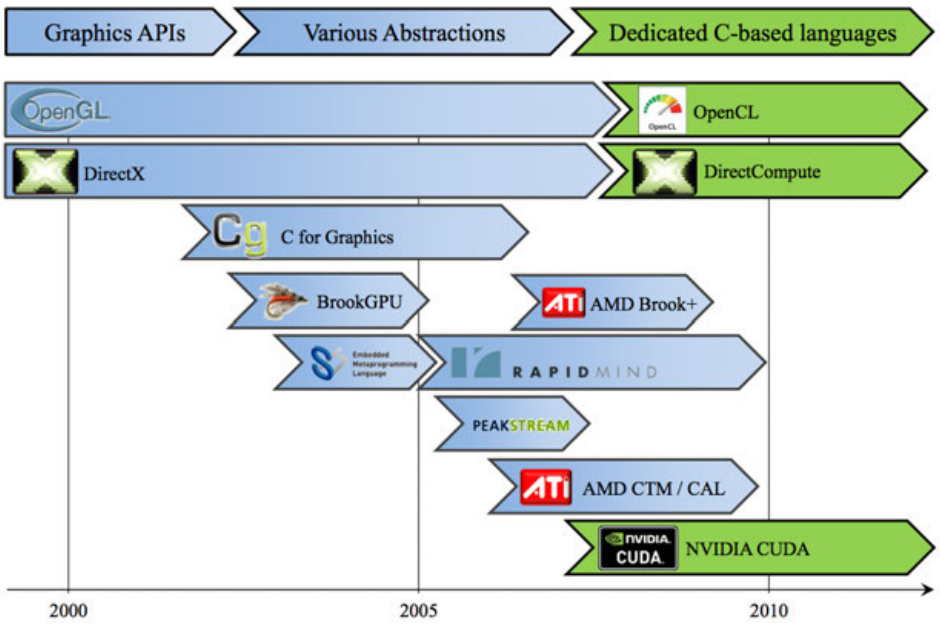

Fig. 3.4 Evolution of GPU programming languages. Initially: since 2007 general purpose languages such as CUDA, DirectCompute, and OpenCL have appeared. [19]

corresponding Nvidia series GPUs are chosen to be elaborated on implementation and architecture details.

3.3 CUDA platform

As indicated by [110], the Nvidia Compute Unified Device Architecture (CUDA) programming model was created as an inexpensive (since it is present as a graphic card in every computer), highly parallel hardware and software architecture available to a continuously larger community of more and more various application developers.

The main purpose of this CUDA platform is to manage computations on the GPU as a data-parallel computing task without mapping them to a graphics APIs. Also, not only the software level is designed to give a new general-purpose C-like programming language, but also the hardware is adapted to support multi-threads at a hardware level.

It is available for the Nvidia GeForce series GPUs (for PCs), Nvidia Quadro series GPUs (for professional rendering), Nvidia Tesla series GPUs (for science especially math calculation) and Nvidia Tegra GPUs (for mobile platforms). Although different Nvidia series GPUs have the same CUDA architecture, the design purpose and hardware configurations are very different. In this subsection ,we elaborate the three most important factors in CUDA

paltform and explain the details for implementing calculation on CUDA-enabled GPUs. More details of different GPU series will be mentioned later in this chapter.

3.3.1 CUDA cores

The most common way to measure a Nvidia GPU calculation capacity is counting the CUDA cores. High-end PC GPUs today have more than 2000 CUDA cores. However, it is not fair to compare GPU and CPU by them. Basically a core in a CPU means an independent core with large cache that can handle each single operation a computer does including calculation, memory fetching, I/O, interrupts with a highly complex instruction set. In CUDA, the corresponding concept should be Multiprocessors (namely Streaming Multiprocessor, shortly as SM) instead of CUDA cores as shown in Fig. 3.5.

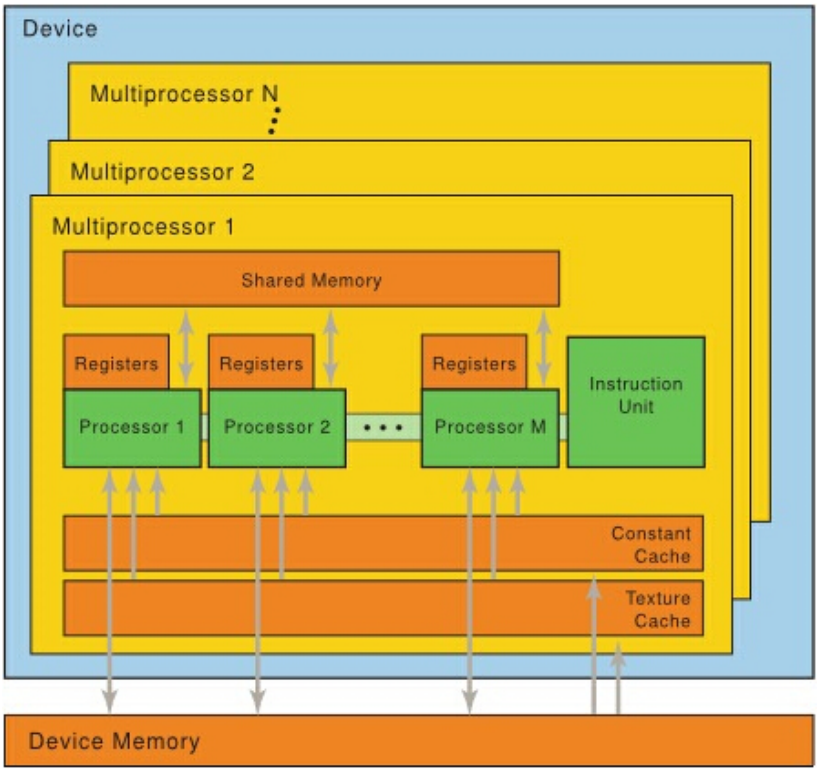

Fig. 3.5 CUDA-enabled Nvidia GPGPU device architecture. [78]

As shown in Fig. 3.5, each SM (Multiprocessor in Figure) has its own instruction unit, registers, different caches and from 8 to 128 CUDA cores based on different version of architectures (also called stream processors, SP in previous version of Nvidia docs). This SM can perform the complex functions that similar to what a CPU core can do. The actual CUDA cores inside each SM are just weak calculation cores that can only perform simpler

calculations but in a real hardware-level parallel (all CUDA threads are mapping to different CUDA cores and executed in different hardware calculation unit in parallel). This is the SIMD model that lets the CUDA cores within the same SM execute same instruction on different pieces of data. Besides, CUDA cores on the same generation of GPUs are the same, and different generations of CUDA cores are similar except different technology process and power consumptions, etc.

3.3.2 CUDA threads model

Normally in a CPU scenario, thread, a component of a process, means the smallest sequence of programmed instructions that is handled by the operating systems. Also, definition of Multi-threads on a computer architecture normally corresponds to how many physical cores the CPU has. For instance, systems with a single processor generally implement multi-threads program by slicing the time which is to make the CPU switch between different software threads. This switch between processes make the user cannot tell that the threads are not physically parallelized. Modern CPUs equipped with several physical cores like Intel PC CPUs can execute multiple threads in physical parallel with every processor or core executing a separate thread simultaneously.

Threads used in GPU case have a different definition with the one used for CPUs. Based on a totally different design method, the GPUs are designed mainly for calculation instead of managing tasks or logic operations. So the usage of physical parallel threads is much more important than the number in CPU case (normally more than tens of thousands). These threads are more likely to be only simple calculation tasks. Not like the CPU threads, CUDA threads have to be in a very regular fashion with no branches and inter-thread communication to maintain the efficiency. For implementation, CUDA threads normally are patched into warps and sent down to the pipeline together. As a result, the irregular and branch operations are difficult for GPU threads.

For Nvidia GPUs, CUDA platform extends C language by allowing the programmer to define C functions, called 'kernels', that, when called, are executed N times in parallel by N different CUDA threads, as opposed to only once like regular C functions. As shown in Fig.3.6, the thread hierarchy architecture is that threads are grouped into blocks and blocks are grouped into a grid. In the end, a kernel is executed as a grid of blocks of threads. The key factors of the threads hierarchy architecture are:

• Each thread is executed by one core

• Each block is executed by one SM and does not migrate

• Several concurrent blocks can reside on one SM depending on the blocks' memory requirements and the SM's memory resources

- Each kernel is executed on one device
- Multiple kernels can execute on a device at one time

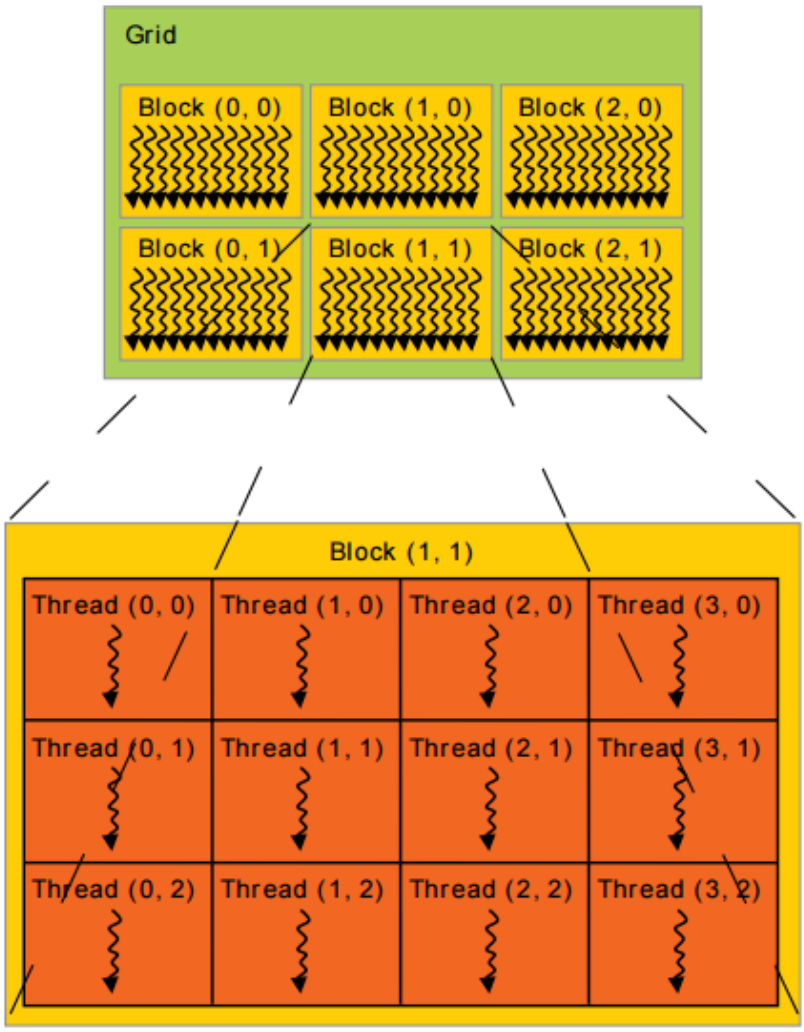

Fig. 3.6 CUDA threads model in layers built of grid and block [110].

Thread blocks are required to be executed independently which is to say they can be executed in parallel or in series. This independence requirement allows thread blocks to be scheduled in any order across any number of SMs which enables programming to adapt with the number of cores. This feature provides adaptability to CUDA programs that allow to fit different GPUs and to get efficiency even the configuration of these GPUs are different (e.g. GPUs equipped with different numbers of CUDA cores or SMs).

3.3.3 CUDA memory access management

The memory bandwidth increase shown in Fig. 3.2 are the largest piece of memory on GPU board also called as global memory which is also the largest and the slowest memory on GPU board. Other types of memory are mainly many different kinds of caches and registers inside the GPU chip as shown in Fig. 3.5.

There are many memory technologies both in software level and hardware level for the computer to accelerate the memory operations. The most common way for hardware level is the usage of faster memory and wider bus. As shown in Fig. 3.2, GPUs are always using the state-of-the-art memory hardware which can provide the best memory bandwidth. On the other hand, for the software level of design, the most common way to accelerate is to exploit memory by not only using faster memory hardware integrated on chip but also optimizing to avoid cache miss. However, although the CPU has multiple levels of cache with high performance, the operations with these caches are managed only by the operating system and are not accessible to programmer.

Unlike CPUs, CUDA-enabled GPUs allows user to access different kinds of memory during execution. As shown in Fig. 3.5, each thread corresponding to a 'Processor' has a private local memory which is the registers; each thread block corresponding to a SM has shared memory visible to all threads of this block and with the same lifetime as this block; and all threads can access to the global memory. There are also two additional read-only memory spaces accessible by all threads: the constant and texture memory spaces. These two kinds of memory are designed for some specific data formats. The constant memory is used to stored the constants which can reduce the required memory bandwidth. Because the constant memory space is cached, a read from constant memory costs one memory read from device memory only on a cache miss; otherwise, it just costs one read from the constant cache. For the threads, reading from constant memory is as fast as reading from registers as the constant memory is cached on chip. The other special memory, texture memory, is designed for threads likely to read from an address "near" the address that nearby threads read. Normally it is used when the program ought to read the data often but update the data rarely and the reading access fits the pattern of spatial locality. For example, in matrix multiplication, the nearby threads access nearby locations of memory (neighbour matrix elements) which can profit the texture memory. Moreover, texture memory can provide additional speedups if we utilize some of the conversions that texture samplers can perform automatically, such as unpacking packed data into separate variables or converting 8-bit and 16-bit integers to normalized floating-point numbers.

In summary, the core design of GPU memory access management is to not only provide fast memory hardware as in Fig. 3.5 but also optimize the software level to let the user have

the access to different elements of a complex memory hardware architecture. This could accelerate calculation tasks quite noticeably. However it makes virtualization like in cloud computing difficult for GPUs.

3.4 Different hardware platforms

Different GPU hardware architecture may have huge difference in all aspects. As limited by factors like cost design purpose, or power supply, GPU configurations can be categorized as low-end PC GPUs (for laptops or some low-end desktop), high-end PC GPUs (normally for high-end desktops, but also on some gaming laptops, professional GPUs (for professional math calculations) and mobile GPUs (with totally different designs). In this section, several main GPU platforms will be mentioned and compared. Also, details of the two very different GPU platforms used in our evaluation will be given.

3.4.1 PC GPU platform

In this subsection, a brief overview of the GPU hardware specifications is given by introducing PC GPUs including low-end laptop GPUs, high-end desktop GPUs, state-of-the-art PC GPUs. The main terms that determines a GPU's performance is the number of CUDA cores, memory configuration, and hardware version (also named "compute capacity version" in Nvidia official documents).

We can notice that in 2011, the calculation speed of GPU varied a lot (can up to more than 50 times faster) according to different GPU types because of their different hardware configuration. This huge difference is rarely seen between PC CPUs. According to Gregg and Hazelwood [66], the Geforce GTX 480 card runs sort algorithm more than 10 times faster than 330M card. The reason for this situation is because of different design purposes and limit of cooling system or power supply in different PC computers. In recent years, the gap between high-end and low-end GPUs increased even more rapidly.

We categorize PC GPUs into three main categories according to which type of computer they equip: laptop GPUs, desktop GPUs and cutting edge ones. Professional gaming laptops equipped with very powerful GPUs and low configured desktops equipped less powerful GPUs should be considered.

However, this category fits most of the use cases that high-end GPUs are more widely used on desktop for gaming experience and low-end GPUs are normally designed for laptop to reduce power consumption and physical space usage. The most advanced ones in recent two years are listed as well to compare the main hardware configuration.

In Table 3.1, we compare six Nvidia GPUs along three product lines. The performance of Nvs 330M GPU and GeForce gtx 480 GPU (manufactured ain the same year 2010) used in Gregg and Hazelwood [66] have very different CUDA cores inside which leads to different performance for the same algorithm. The next laptop GPU (Nvs 5200M) and desktop GPU (GeForce gtx 780) released in 2012-2013 both increased in all aspects including CUDA cores and memory space. However, the huge difference between laptop GPU and desktop GPU still exists due to the initial design purpose. By the year of 2016-2017, the newest generation of Nvidia GPUs are using the newer generation technology in the micro-architecture manufacturing. As pointed out in [109], the GeFroce gtx 1080 GPU combines benefits of the new Pascal architecture and implementation which is 16 nm FinFET manufacturing process, and the latest GDDR5X memory technology. These benefits allows it to be 3 times more efficient than the GeForce gtx 780 with the similar CUDA core numbers and even less memory width.

Table 3.1 Main characteristics of a laptop GPU and a desktop GPU.

	Nvidia card	Year	Hardware version	CUDA cores	Memory (MB)	Clock (MHz)	Memory Width
Laptop	Nvs 330M	2010	1.2	48	256	1265	128 bit
	Nvs 5200M	2012	2.1	96	1024	1344	64 bit
Desktop	GeForce gtx 480	2010	2.0	480	1024	1401	320 bit
	GeForce gtx 780	2013	3.5	2304	3072	941	384 bit
Most advanced	GeForce gtx 1080	2016	6.1	2560	10k	1733	256 bit
	GeForce gtx 1080Ti	2017	6.1	3584	11k	1582	352 bit

The Nvs 5200M and GeForce gtx 780 are the GPUs used to implement our design in this thesis. In fact, the two different GPUs are used to present the results for two different use cases: a laptop with a limited calculation power GPU and a desktop with a much more powerful GPU.

In the Chapters 4 and 5, benchmark evaluation for different calculation tasks on two different GPU platforms shows that implementation details can be varied a lot due to the different performance of GPUs. As long as CPU are also involved in calculation, it is important to consider at least two very different GPU platforms since the difference in performance of the GPU may modify the level of involvement of the CPU.

3.4.2 Mobile GPU platform

During the past decade, mobile phones especially smart phones have changed from just handling dull text-based menu systems to a device equipped with powerful calculation cores

and being able to render high-quality graphics at high frame rates. In recent years, due to the development of the battery technology and circuit design, the CPU and GPU in today's smart phones have more capabilities than just being used for rendering graphics.

According to Akenine-Moller and Strom [5], a mobile device (mobile phone) is by definition powered with batteries and also has to be small in size in order to be portable. As a result, most limitations stem from constraints of battery-driven and small size. To provide long use-time on the battery, the system of the mobile phones are designed to save energy which limits the calculation power.

For the CPU case, the main difference between the mobile phone and personal computer is that the mobile phone CPU normally has limited CPU instruction set and a lower clock frequency (e.g., sometimes the division instruction is missing and often floating-point support is not available). Moreover, due to lack of fans or other cooling devices,even if batteries would suddenly become much more powerful, CPU calculation power could not be increased rapidly just like in PC scenarios.

For the memory design, the memory architecture is quite different from that of PC systems as in Fig. 3.7. A flash memory often plays the role of 'hard disk' which can keep the data even when the power is off. And there is a small system RAM that is located off chip. As the feature of flash memory is the reading operation is faster than writing, some data that are often used like videos or photos are stored in flash and loaded into RAM when needed. In many cases, there is no dedicated graphics memory and no separate bus for graphics-related memory designs.

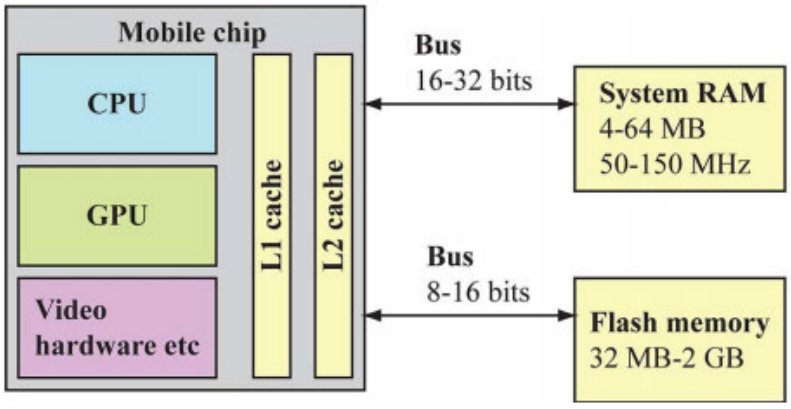

Fig. 3.7 One example for mobile phone CPU and GPU system shown in [5].

In summary, because of all the factors listed above, the mobile phone GPU today cannot be such power calculation chip as for PC GPGPUs. However, there is still a large development both for hardware and software level. For instance, as pointed by Akenine-Moller and Strom

[5], in 2008, the L2 cache shown in Fig. 3.7 is still seldom seen. However, today, the A8 processor used by iPhone 6 has a per-core L1 cache of 64 KB for data and 64 KB for instructions, a L2 cache of 1 MB shared by both CPU cores, and a 4 MB L3 cache that services the entire chip [7].

More importantly, in recent years, many researchers have already been exploiting to make the dedicated graphics APIs on phone GPUs fit to general-purpose calculation. In [30] the computational speed of the FAST corner detection algorithm is increased 24 times by using GPU parallel computing on an iPhone 4. In [156], the Metal [139] and Swift based Deep Learning library for Apple devices like iPhone or Apple TV is introduced and the authors aim to make the iPhone GPU support using deep learning models trained with popular Deep Learning frameworks.

Although the most popular tools used to develop the general-purpose computing task on a mobile phone GPU are still graphics dedicated, it is possible to predict a general-purpose platform like CUDA will emerge and the potential calculation resources of mobile phones will be exploited.

3.5 Discussion

Over the last several decades, parallel computing has evolved significantly both on software aspects and hardware aspects. The computation process has moved from dedicated algorithm on costly equipped super computers to general programming model on almost every personal computers and even many smart phones. Today, the field of parallel computing is having one of its best moments in history of computing and its importance will only grow as long as computer architectures keep evolving to a higher number of processors.

And as shown in our comparison of the Nvidia series GPGPUs released recently, the Nvidia GPGPUs have multiple branches of products with very different hardware configurations which will lead to different software designs. On the other hand, the rapid development pace in hardware manufacturing will continually influence the algorithms implementation.

It seems like almost all problems of calculation could be accelerated by the usage of GPGPU. However, there are still some reasons that limits the GPGPU usage. One of the most common problems is the bottleneck of memory transfer between the host memory and GPGPU's memory. As pointed out by Gregg and Hazelwood [66], due to the reason that the memory transfer speed is not so fast as the calculation speed, the GPU could be idle while the PCI bus are busy which leads to the decrease of whole performance. This fact rises two open challenges which are how to update the hardware to accelerate the memory transfer and

how to design the algorithm to make the execution time of GPU overlap the memory transfer time.

Chapter 4

DCT based selective encryption for bitmaps

In this chapter, the improved selective encryption methods are shown based on DCT and GPGPU acceleration. There are two levels of design with different purpose. First, the DCT related bitmap protection is introduced. It is pointed that high frequency coefficients of DCT could be used to recover some of the contents. Then, the performance issue mentioned in chapter 2 is solved by employing GPGPU as a hardware accelerator. The two levels of our improved designs are followed with many details to guarantee the minor loss of image quality. Then, the security analysis is presented. At last, the calculation allocation for accelerating process speed is presented to make the designs fit into two typical different hardware platforms.

4.1 DCT transformation and selective image protection

The Discrete Cosine Transform (DCT) is a Fourier-like transform, which was first proposed by Ahmed et al. [4]. The purpose of DCT is to perform decorrelation of the input signal and to present the output in the frequency domain just like other transformation algorithms. Compared with Fourier Transform, which represents a signal as a combination of sines and cosines, DCT performs only the cosine-series expansion.

DCT is widely used in many selective encryption algorithms (Shi et al. [144], Chiaraluce et al. [28], Yen and Guo [179], Tang [151], Tosun and Feng [154], Qiao et al. [124], Shi and Bhargava [143], Zeng and Lei [181], Wang et al. [165], Wu and Kuo [174], Wu and Kuo [173], Kankanhalli and Guan [74]). The reason that DCT is used in many SE methods is because DCT itself is widely used in multimedia content compression algorithms. And

DCT only has the cosines coefficients which makes it map real numbers to real numbers. Compared with DCT, the FFT algorithm always has complex numbers that is difficult to store and process. The second reason is that DCT is known for its property of very high 'energy compaction', meaning that the transformed low frequency coefficients are very large and high frequency coefficients are relatively very small. As a result, this transformed results can be easily compressed by using quantization to keep only a few low frequency components (see JPEG standard [164]).

DCT has different types shown in Kresch and Merhav [79]. The most popular DCT algorithm is two-dimensional symmetric variation of the transform that operates on 8×8 blocks (DCT 8×8) and its inverse (iDCT 8×8). This DCT 8×8 is utilized in JPEG compression routines [164] and has become an important standard in image and video transformation algorithms and many other areas. The two-dimensional input signal is divided into the set of non-overlapping 8×8 blocks and calculation for one DCT 8×8 two-dimensional block is defined as follows:

$$C(u,v) = \alpha(u)\alpha(v) \sum_{x=0}^{7} \sum_{y=0}^{7} f(x,y) \cos\left[\frac{\pi(2x+1)u}{16}\right] \cos\left[\frac{\pi(2y+1)v}{16}\right] \tag{4.1}$$

The inverse of two-dimensional DCT 8×8 is defined as:

$$f(x,y) = \sum_{u=0}^{7} \sum_{v=0}^{7} \alpha(u)\alpha(v)C(u,v) \cos\left[\frac{\pi(2x+1)u}{16}\right] \cos\left[\frac{\pi(2y+1)v}{16}\right] \tag{4.2}$$

where

$$\alpha(u) = \begin{cases} \sqrt{\frac{1}{8}}, u = 0 \\ \frac{1}{2}, u \neq 0 \end{cases} \tag{4.3}$$

As can be seen from equation 4.1, especially, in the forward DCT 8×8, the substitution of $u, v = 0$ yields:

$$C(0,0) = \alpha(0)\alpha(0) \sum_{0}^{7} \sum_{0}^{7} f(x,y) \tag{4.4}$$

which is eight times of the mean of 8×8 sample. In fact, this value is called the DC coefficient of the transform results and the others are called the AC coefficients which are independent of the average value. Normally in the image compression case, the DC coefficient is relatively large in magnitude while the AC terms become lower in magnitude as they move farther from the DC coefficient. This means that by performing the DCT 8×8 on the input raw image, the representation of the image (the main elements carried by an

image) is concentrated in the upper left coefficients of each of the output 8×8 matrix (i.e. low frequency area), while the lower right coefficients of the output matrix contains less important information like details (high frequency area).

From the energy viewpoint, the DC coefficient takes most of the signal energy of the input matrix. In most DCT-based compression algorithms like JPEG standard, there is a quantization step (see Fig. 2.4) to rounding mainly the high frequency coefficients. However, for protecting the bitmap image, compression is not an option.

As pointed out in Chapter 2.4, protecting only the DC coefficient of each 8×8 block for an input bitmap image is far from enough to guarantee security. Other researches explored in protecting some of the important AC coefficient as well [80], as long as in most image use case, the DC coefficient and first 5 AC coefficients take more than 96% of the signal energy. If the DC and first 5 AC coefficients (chosen as [80] but this is a changable parameter) and padded with zeros and iDCT with the rest 58 AC coefficients, the visual content that can be seen is really limited as shown in Fig. 4.1(d-f). In fact, selecting more AC coefficients could help the visual degradation but does not help providing security.

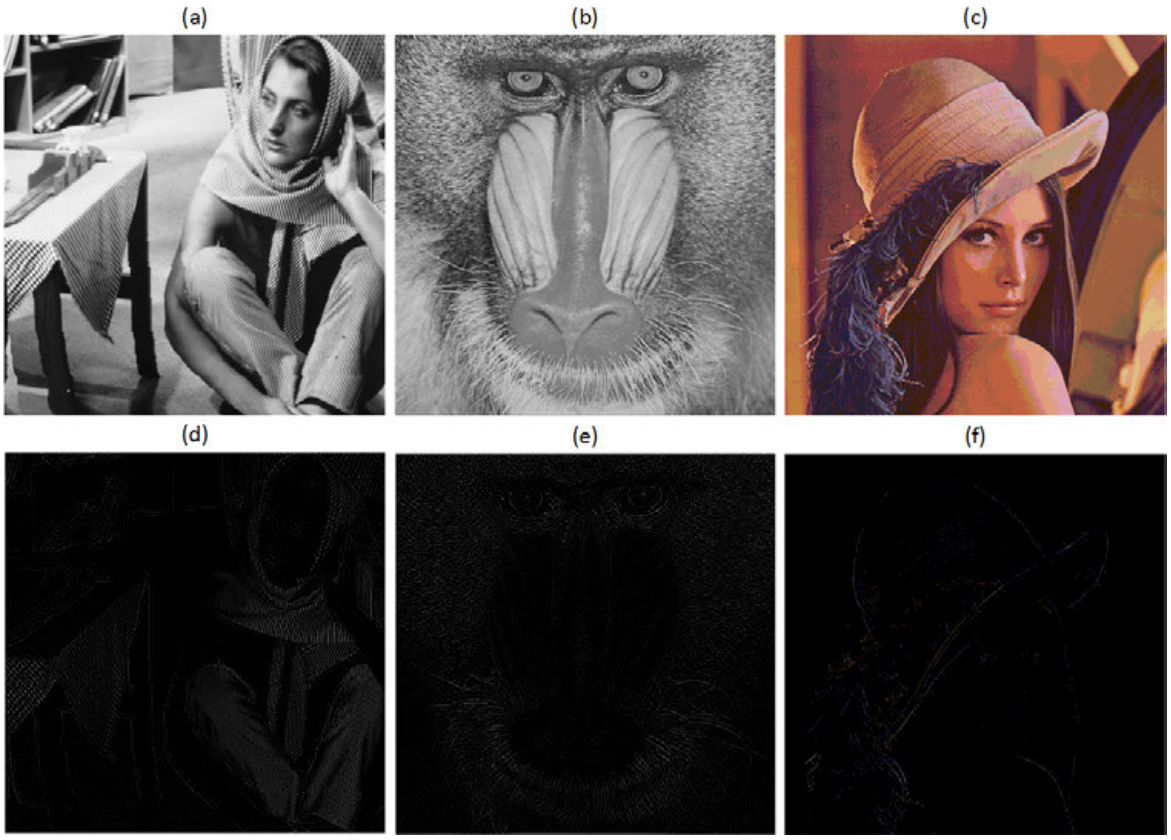

Fig. 4.1 Theoretical protection results in [80, 125]: original images (a-c) and images that the low frequency area is padded with zeros (d-f).

However, SE methods like [80] (protecting the first 6 coefficients of each 8×8 sub-matrix of a bitmap's DCT 8×8 results) is still not enough if the purpose is to protect the whole image content rather than to only disguise the image visual quality. As the remaining 58 AC coefficients carries very little energy, the iDCT 8×8 result for these 58 coefficients seems almost clean. However, in some cases when the bitmap has many sharp edges, just padding zeros to the first 6 coefficients can show some critical contour to help attackers guess the original content by just visual like shown in Fig.4.1 (d-f).

Moreover, there are possibilities to guess the protected DC values from the know high frequency values in each of the blocks. In fact, in the JPEG standard, original image data will subtract 128 from each pixel intensity in each block to form the range [-128, +127]. And in some SE methods this subtract is not performed. We calculate means of absolute values of the rest 58 AC coefficients for each 8×8 block and renormalize them to a interval [0, 1]. The guessing DC value is given by multiplying these renormalized means and 2048 (upper limit of DC coefficients if no subtraction) or 1024 if there is subtract.

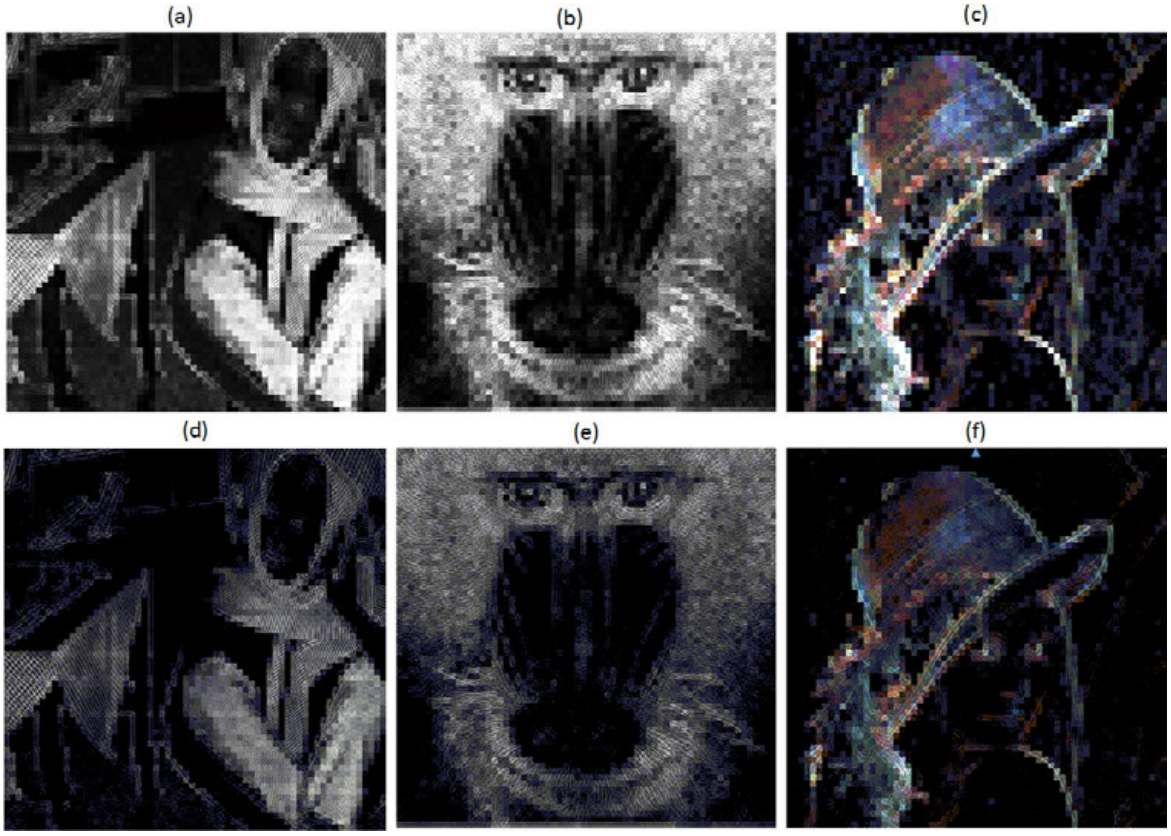

Fig. 4.2 Three examples to recover original images by guessing DC coefficient.

Fig. 4.2 (d-f) and (g-i) give the recovery results for no subtract and with subtract respectively which can clearly show the original image contents. This is because a smaller range and more accurate of the DC coefficient of a block can be estimated from the remaining 58 AC coefficients of the same block. Moreover, as pointed by Li et al. [87], recovering an arbitrary set of missing DCT coefficients (except for the case when all DCT coefficients are missing) at an acceptable level is possible.

In summary, although all DCT coefficients of one block can be seen as separate layers with different importance according to energy distribution, SE methods based on protecting only few low frequency area can just fit the use cases of disguising the image quality. When protecting the image content is the purpose of SE design instead of degrading the visual quality, protecting only the low frequency coefficients and leaving the rest coefficients as plain is far from enough.

4.2 DCT acceleration on GPGPU

4.2.1 DCT implementation on CPU

A lot of effort has been put into optimizing DCT routines on existing hardware. Most of the implementations of DCT 8×8 on computer CPUs are well-optimized, which includes the transform separability utilization on high-level and fixed point arithmetic, cache-targeted optimization on low-level [52].

However, very few papers discuss and show performance of SE methods based on DCT 8×8 by giving implementation. It is important to benchmark DCT 8×8 to watch over performance as long as hardware evolves at a fast pace which makes DCT implementations outperforming against a full encryption. E.g. the AES 128-bit can reach about 200 MB/s on a PC's CPU [37] in 2009 but the same code can run almost twice faster today. In this section, we compare the DCT implementation on CPU and GPU today and elaborate on how DCT 8×8 is accelerated by GPU.

4.2.2 DCT implementation on GPU

GPU acceleration of DCT 8×8 has been possible since creation of shader languages long time ago. However, it requires a specific setup to use common graphics API such as OpenGL [172] or Direct3D [45] for general-purpose computing which is difficult to implement. Since the appearance of CUDA [110], it is easy to have a transparent implementation of GPU accelerated DCT 8×8 on a recent Nvidia GPU with a natural extension of C language programming.

We should notice that most of the traditional low-level optimizations commonly used in CPU implementations are unnecessary in GPU scenario. The floating point calculation is native to GPU and the MUL, ADD and MAD operations on chip are executed with the same speed. The optimization of DCT on GPU is mainly based upon two aspects: first to make the calculation process fit the GPU calculation model; then to optimize the implementation at hardware level (memory usage, data transfer, avoid bank conflict, replace multiplications by reciprocals or arithmetic shifts, etc).

Accelerating DCT by CUDA is discussed in many previous works [112]. Normally, the DCT 8×8 on two dimensions is actually a separable transform according to equation (4.1). By definition, DCT is firstly applied to the columns of the input 8×8 block (on one direction of the 2D block), and then DCT is calculated along the rows of results in last step (on the other direction of the block). Each time the DCT on one direction is applied, it is actually a matrix multiplication of the value matrix and cosine value matrix (or its transpose). This can be seen as twice matrix multiplication as shown in the following equation:

$$DCT_{2D} = C \times Input \times C^T \tag{4.5}$$

In this matrix multiplication implementation of DCT, the cosine value matrix (presented as C) is never calculated on the fly but pre-calculated and stored as a 8×8 constant matrix. The value of C is given in following equation

$$C = \begin{bmatrix} 0.35355 & 0.49039 & 0.46194 & 0.41573 & 0.35355 & 0.27779 & 0.19134 & 0.09755 \\ 0.35355 & 0.41573 & 0.19134 & -0.09755 & -0.35355 & -0.49039 & -0.46194 & -0.27779 \\ 0.35355 & 0.27779 & -0.19134 & -0.49039 & -0.35355 & 0.09755 & 0.46194 & 0.41573 \\ 0.35355 & 0.09755 & -0.46194 & -0.27779 & 0.35355 & 0.41573 & -0.19134 & -0.49039 \\ 0.35355 & -0.09755 & -0.46194 & 0.27779 & 0.35355 & -0.41573 & -0.19134 & 0.49039 \\ 0.35355 & -0.27779 & -0.19134 & 0.49039 & -0.35355 & -0.09755 & 0.46194 & -0.41573 \\ 0.35355 & -0.41573 & 0.19134 & 0.09755 & -0.35355 & 0.49039 & -0.46194 & 0.27779 \\ 0.35355 & -0.49039 & 0.46194 & -0.41573 & 0.35355 & -0.27779 & 0.19134 & -0.09755 \end{bmatrix} \tag{4.6}$$

As we mentioned in Chapter 3, GPU can accelerate calculations like matrix multiplications. As shown in Patel et al. [117], the authors use this twice matrix multiplication methods to accelerate DCT/iDCT 8×8 process on GPU and get a performance gain of 10 to 20.

However, as pointed by Obukhov and Kharlamov [112], the elements in matrix C still contains many clear symmetric which can be used to accelerate the calculation again. Here,

we use the DCT optimized algorithm from Nvidia technical report [112]. In Table 4.1, we compare the acceleration for DCT 8×8 on two different computers, a laptop with an Nvidia 5200M GPU and an Intel I-7 3630QM 2.4GHz CPU and a desktop with an Nvidia GTX 780 GPU and an Intel I7-4770K 3.5GHz CPU.

From this evaluation, we first see that CPUs on a laptop and desktop computer are not that different as performance of CPUs mainly account on factors like main frequency and caches. For the same generation of Intel CPUs, performance are actually quite similar compared with the vast difference of GPU performance of similar generation which mainly relies on the number of the CUDA cores (which could vary from 100 to 2300). Secondly, as performance gain for the laptop (low-end GPU use case) reaches a factor 10 which is similar to the gain found in [117], the acceleration obtained for the desktop (high-end GPU use case) reaches a factor over 70.

Table 4.1 DCT 8×8 accelerated by GPU for laptop and desktop GPUs.

Image size	1024×768	1600×1200	3240×2592	4800×4800
Laptop CPU time	3.78ms	9.24ms	39.4ms	108.4ms
Laptop GPU time	0.41ms	0.79ms	3.67ms	9.98ms
Performance gain	9.2	11.7	10.7	10.8
Desktop CPU time	2.88ms	7.0ms	29.9ms	82.4ms
Desktop GPU time	0.04ms	0.09ms	0.41ms	1.12ms
Performance gain	72	77.8	72.3	73.6

As we pointed out in Chapter 3, according to Gregg and Hazelwood [66], the calculation ability of GPU varies a lot (can up to more than 50 times faster) in different GPU types because of their different hardware configuration. Gregg and Hazelwood [66] show that the Geforce GTX 480 card (high-end desktop GPU) runs sorting algorithm more than 10 times faster than 330M card (low-end laptop GPU). We see the similar difference between our two GPUs in Table 4.1. The huge difference of hardware configurations results in corresponding huge difference of GPU performance. This is an important difference which explains why a SE architecture dedicated to a laptop can benefit from using CPU and GPU while the corresponding desktop solution will look at using only the GPU.

4.3 Design of SE for bitmaps based on DCT

As mentioned in Chapter 2, different SE methods are designed for different protecting purpose and use cases. Here, in this section, we introduce two designs of SE based on DCT 8×8 for bitmap images: a first level of protection when speed is of the essence and disguise

image visual quality fit with the use case requirements, and a more complex second level of protection when a more global protection of the image is required. One the one hand, our second level of design proves that by encrypting DC and a few AC coefficients while still protecting the rest AC coefficients in DCT 8×8 blocks can achieve a good level of protection; on the other hand, our work shows that the data-parallel execution model of GPU fits nicely with the preprocess step, DCT 8×8. This fitness will make GPU provide a critical performance gain for selective encryption based on DCT 8×8 since it is only through a GPU implementation that SE is more efficient than a full encryption. Also we point the allocation for arranging calculation tasks would change depending on hardware configuration by providing evaluations on two typical different computers. The following results have been published in [125] and [126]. We provide here additional test cases and a few more details for instance or accuracy.

4.3.1 First level protection

In Chapter 2, we defined the fragmentation step to label the preprocessed data with different levels of importance. Here, firstly, the input data will be preprocessed using DCT 8×8. Then the results of the DCT 8×8 which are the frequency coefficients will be fragmented into two parts according to the selection ratio with respect to the required visual disguise level. The encryption system will be used for the private fragment (Fragment 1 in Fig. 4.3) and the public one (Fragment 2 in Fig. 4.3) is let to be plain.

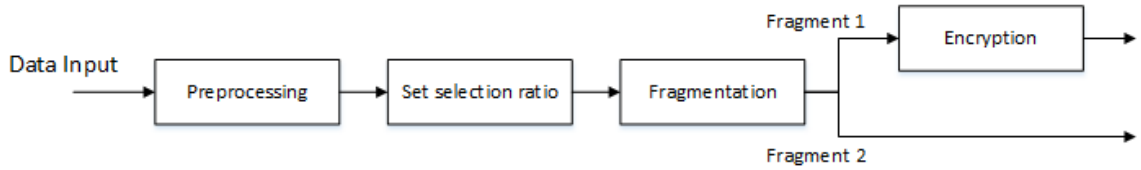

Fig. 4.3 General design method for first level protection where Fragment 2 is let to be plain.

Although the visual information cannot be totally protected and having the risk the coefficients could be somewhat recovered, this method significantly reduces the need for the data to be fully encrypted and improve the output performance. The fragmentation step possesses selection ratio done in the frequency domain to increase or decrease the private fragment to be encrypted allowing the user to increase or decrease the desired level of protection. The selection ratio can be set by user, however, the coefficients [0,0], [0,1], [1,0], [2,0], [1,1], [0,2] of the DCT 8×8 block cited from Krikor et al. [80] constitute the default selection and is recommended from experience.

This protection method will erase most important visual characters from an image (like people's face) as shown in Fig. 4.1 (d-f). It is recommended if for instance, the user's target is to protect against a mild level of attack from knowing who is in the image. More generally, this first level of protection is good for soft encryption when high performance is required at the same time. In the following sections we will elaborate how GPU is used to accelerate the whole process and how to achieve the best performance on different hardware platforms.

4.3.2 Second level protection

As pointed out in Chapter 2.4 and elaborated in Section 4.1, Coefficients in high frequency area of DCT 8×8 sometimes can be used to reveal some information about the original image especially some sharp edges or clear details are contained. For some use cases like protecting whole image content without any information leak, a second level protection is needed to protect ont only low frequency coefficients but also high frequency coefficients. In order to guarantee that performance for the whole SE process will still be better than the full encryption, a lightweight protection method is used to protect the high frequency coefficients (see Fig. 4.4, generally, encryption for Part1 and light protection for Part2).

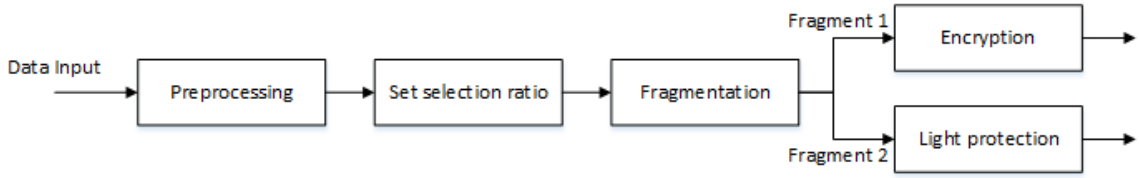

Fig. 4.4 General design method for second level protection where Fragment 2 is also protected.

A dispersion step is added to separate the storage of the two parts of protected data. This fragmentation method is using Fragment 1 to build up a lightweight protection for the high frequency coefficients (Fragment 2).

We go in more details in Fig. 4.5: the lightweight protection step uses the SHA-512 function [153] to get a unique fixed-length string (512-bit long) from the 6 selected coefficients (Fragment 1 in Fig. 4.4). The SHA-512 function has a feature that can generate two totally different and unpredicted fixed length strings even if only one bit of the input string is different. Moreover, according to [153], it is not possible to recover the input data if only the output 512-bit string is known. This feature will guarantee that the 512-bit string cannot be used to do prediction, recovery or guessing even adjacent 8×8 blocks of a bitmap image are very similar. Because the block we processed is 8×8, the reverse DCT (iDCT in Fig. 4.5) result of the rest DCT coefficients (DC position padded with 1024 and rest AC coefficients

padded with zeros) contains 64 pixels. If we store these 64 pixels in 8-bit integers (Byte), the total length is exactly 512 bits. Then the XOR step can protect every bit pixel by pixel within each block.

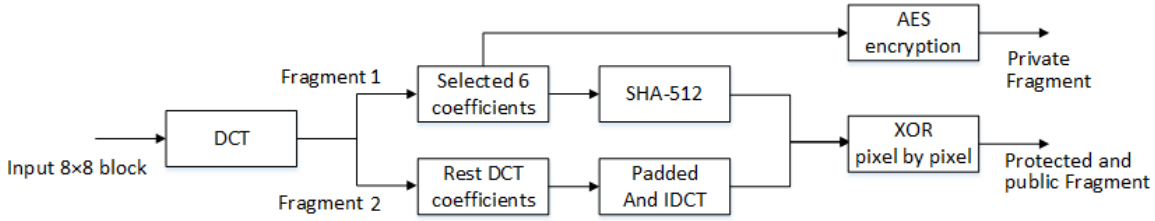

Fig. 4.5 Design to enhance the protection level.

4.4 Storage space usage and numeric precision

There is a classic trade-off between the memory occupation (both footprint and storage space) and numeric precision when it comes to handling floating point numbers. This problem is rarely considered in traditional DCT based SE methods. The possible information loss caused by not designing the numeric format transform between integers and floating-point numbers seems to be ignored by many related works (Krikor et al. [80] Pareek et al. [116] Puech and Rodrigues [123] Guan et al. [67]). This is because most of the DCT based SE methods are protecting contents with the compression step which is the quantization step that rounded most of the high frequency coefficients, so no need of the design to store the floating point numbers.

However, in bitmap protection cases, if we take [80] as an example, each pixel in bitmap files is usually stored as an 8-bit integer (two more bytes are used for 'Highcolor' and two additional bytes are used for 'Truecolor'). During the forward DCT computation, these integers are transformed into floating point (32 bits) numbers increasing the footprint by a factor 4. At the end of the computation, numbers are turned back to integer and this is repeated during the computation of iDCT. These value type changes involves truncation as the range of encrypted coefficients are very different and some rounded values have to be ignored in order to fit the storage space. This could lead to image distortion or information loss when decrypting and rebuilding the original image. Moreover, recursive rounding error cannot be avoided in this case if one bitmap image is encrypted and decrypted multiple times by this scheme.

In our implementation, we firstly calculate the possible value range to determine how to store the results. Then we measure the possible distortion or information loss in image

processing by using PSNR (Peak Signal-to-Noise Ratio) [73] to show how much signal is lost for different images. Moreover, more specific comparison between original images and multiple encrypted and decrypted images are compared to show the possible information loss.

4.4.1 Storage space design

For the bitmap case, we consider the gray scale image as an example (for 3 layer color images, each color layer can use the same scheme for one gray scale image).

For each pixel of a gray scale bitmap, the input range is between 0 and 255. Since DC coefficients are bounded by 1024 (subtract 128 from each pixel to reduce DC value range from [-2048, +2048] to [-1024, +1024]), we used an 11-bit storage space to store only the integer part (1 bit for sign and 10 bits for absolute value). For AC coefficient, it is easy to calculate that the range is within -1023 to +1023 by using the definition and equations (4.5), (4.6) (no matter the input range is from 0 to 255 or from -128 to 127). Our design is to use 11-bit storage space for each selected AC coefficients: first bit for the sign and the other 10 bits for the value (10-bit can store integers from 0 to 1023). For color images, the protection is done for the different layers of pixels respectively. We call this design as 11-bit store method and use it as default in this design.

After storing the selected important values, the remaining AC coefficients will need an iDCT to re-transform to a 8×8 matrix with each element as an 8-bit integer. Here the initial DC value is padded with 1024 and the 5 selected AC values are padded with zeros. The reason why not just pad every selected element as zero is because as long as the DC values and first 5 AC coefficients are zeros, the iDCT results will contain a lot of negative values or positive values very near to zero. It is difficult to store all these values within 8-bit storage space. However, if the DC value is set to be 1024, the average value is set to be 128 in the iDCT result which is easier for keeping the coefficients. Then the value range is to be set as between 0 and 255 to round all iDCT coefficients to 8-bit unsigned integers.

The extra storage space of 11-bit store method is just the extra bits used to store the selected DC coefficient (11 bits) and the 5 AC coefficients (55 bits in total) which is 66 bits more per 8×8 block. In summary, the total extra storage usage is $66/512 = 12.9\%$ of the original space usage. Considering the fragmentation step, the private fragment only takes 66 bits and the protected and public fragment takes the same storage space with the original image. The visual results for the designs is shown in Fig. 4.6.

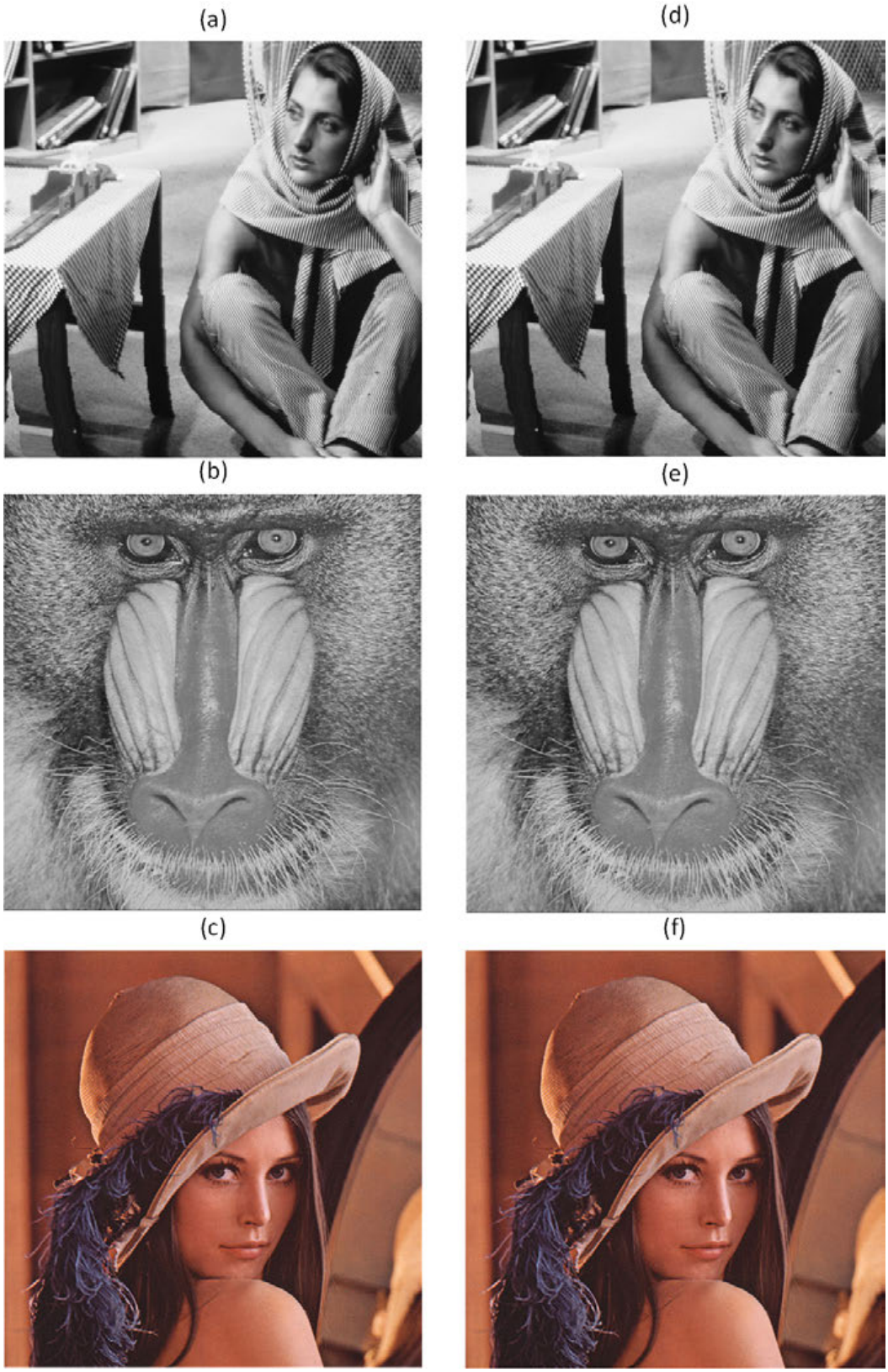

Fig. 4.6 Visual effect of 11-bit store method (a-c): original images and (d-f): decrypted and rebuilt images with PSNR values are 63.1, 62.7 and 62.9 respectively.

4.4.2 Numeric precision analysis

In Fig. 4.6, we gives the example of visual results of the decrypted images (d-f) compared with the original images (a-c). And the value of PSNR after encryption and decryption is more than 62 dB as shown in Table 4.2. PSNRs of 50 dB for 8bpp (bit-per-pixel) images usually results in almost identical images according to [73].

Table 4.2 PSNR for the selective encryption of different images.

Image size	PSNR (enc and dec)
256×256	62.78 dB
512×512	63.10 dB
1024×768	62.76 dB
1600×1200	62.82 dB
3240×2592	62.85 dB
4800×4800	62.89 dB

In Table 4.2, we tested multiple bitmap images as input to show the PSNR of the images before and after protection keeps about 62 dB which means the loss caused by rounding in the design is really tiny. In fact, there are two places where the information details are missing: first one is the rounding step of the DC coefficient and selected 5 AC coefficients; second one is to store the remaining coefficients after rounding each of the iDCT results into 8-bit unsigned integers. second one is to store the remaining coefficients after rounding each of the iDCT results into 8-bit unsigned integers.

In order to give a complete idea of the bit value loss due to the integer and float conversion, a more straight forward way is used by comparing the different values in the gray pixel value. Firstly, we take one image 'fofo' (image (b) in Fig. 4.6) as the plain image. And each pixel value of the reconstructed image is compared with the initial plain image. There are only about 3% of the pixel values are different due to the integer and float conversion. Then we select randomly one block to show the visual difference with this kind of minor pixel value difference on visual effect. The following two blocks are the pixel values and only three values are slightly different and are located at $(3,1)$, $(4,6)$ and $(5,6)$. In Fig. 4.7, the minor difference in visual is shown by comparing the original block with the reconstructed block. The red small blocks in the right image are the ones different with original ones and all pixel values corresponds to the following matrix.

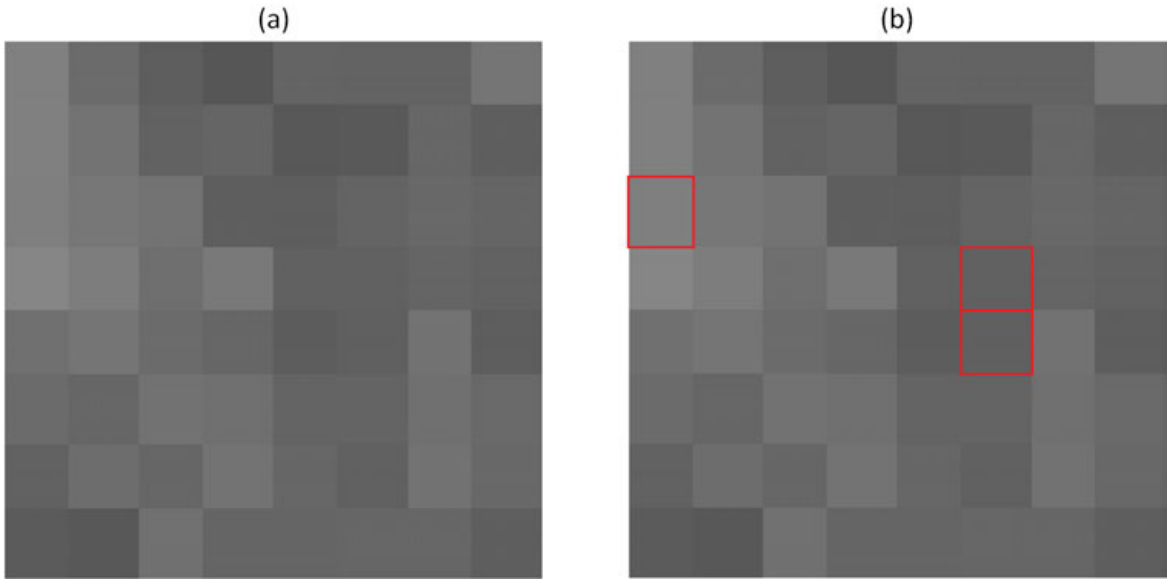

Fig. 4.7 Visual effect of one 8×8 block with only 3 pixel value different (original block and reconstructed block).

$$\begin{bmatrix} 128 & 107 & 94 & 86 & 100 & 99 & 99 & 117 \\ 128 & 115 & 98 & 101 & 87 & 89 & 102 & 95 \\ 127 & 119 & 115 & 95 & 94 & 100 & 104 & 101 \\ 134 & 125 & 110 & 121 & 97 & 97 & 101 & 98 \\ 111 & 117 & 107 & 102 & 92 & 96 & 114 & 94 \\ 107 & 102 & 114 & 111 & 100 & 100 & 111 & 105 \\ 98 & 109 & 102 & 115 & 102 & 97 & 114 & 104 \\ 91 & 88 & 112 & 101 & 101 & 102 & 102 & 95 \end{bmatrix}, \begin{bmatrix} 128 & 107 & 94 & 86 & 100 & 99 & 99 & 117 \\ 128 & 115 & 98 & 101 & 87 & 89 & 102 & 95 \\ (128) & 119 & 115 & 95 & 94 & 100 & 104 & 101 \\ 134 & 125 & 110 & 121 & 97 & (98) & 101 & 98 \\ 111 & 117 & 107 & 102 & 92 & (97) & 114 & 94 \\ 107 & 102 & 114 & 111 & 100 & 100 & 111 & 105 \\ 98 & 109 & 102 & 115 & 102 & 97 & 114 & 104 \\ 91 & 88 & 112 & 101 & 101 & 102 & 102 & 95 \end{bmatrix}$$

As long as every time the protection and rebuild process would introduce the truncation and rounding, recursive rounding error [70] is also introduced. In Fig.4.8, Fig.4.9, and Fig.4.10, 15 rounds of protected and rebuild process for three bitmaps (images (a): fofo, (b): barbara, and (c) lena in Fig.4.6) are done, and in each round, two results are compared between the rebuilt image in current round with the original image: PSNR and the percentage of changed pixel values. From the experimentation, the PSNR and percentage of changed pixel values keep unchanged after several rounds which means the storage design avoids the recursive rounding error after some rounds loss. In the end, PSNR is 60.919 for fofo case, 60.735 for barbara case, and 61.788 for lena case. And totally less than 5% (around 4.6%) pixel values are slightly changed like in Fig.4.7.

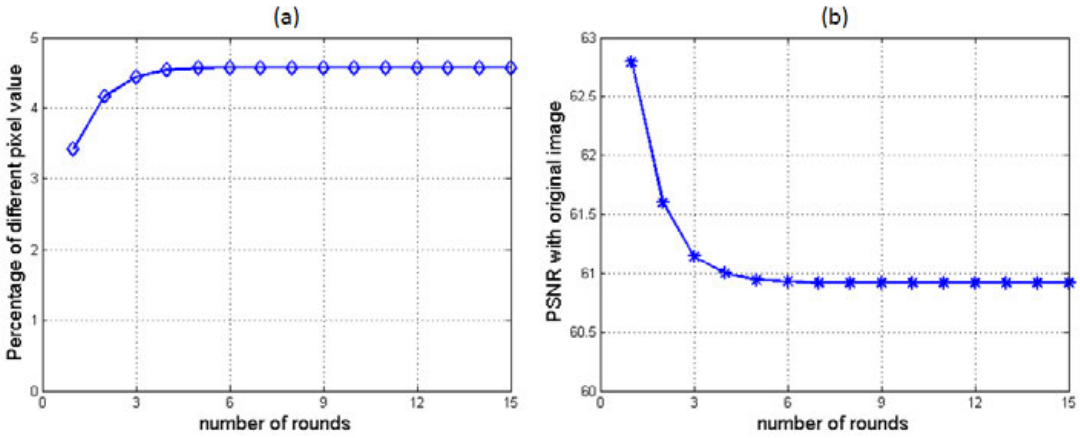

Fig. 4.8 Percentage of different pixel values (a) and PSNR (b) stop changing after several rounds for fofo image.

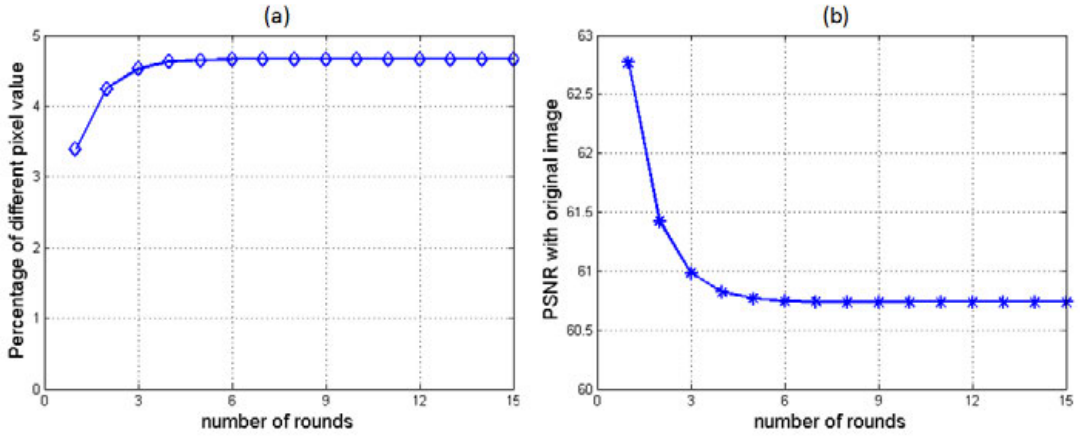

Fig. 4.9 Percentage of different pixel values (a) and PSNR (b) stop changing after several rounds for barbara image.

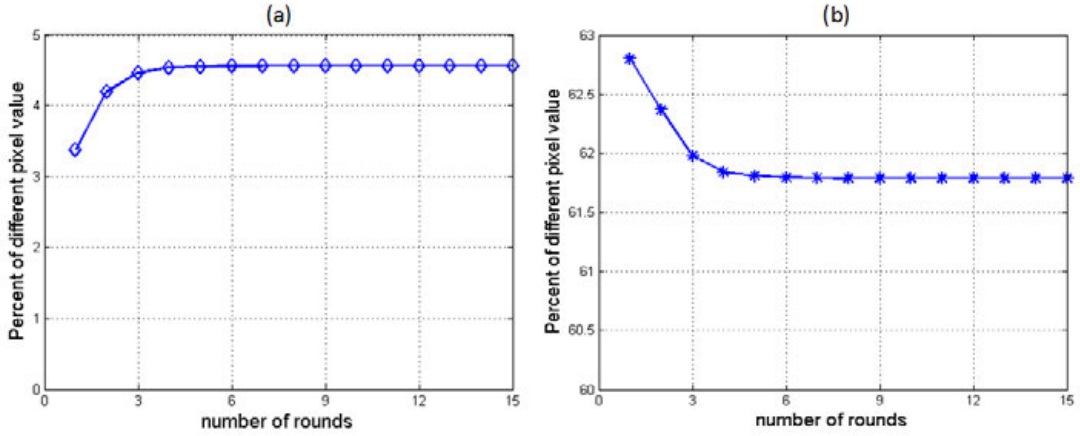

Fig. 4.10 Percentage of different pixel values (a) and PSNR (b) stop changing after several rounds for lena image.

4.5 Result analysis

In this section, probability density function (PDF) and correlation coefficient computation are used to evaluate the protection quality. As pointed out before, our method will fragment the image into two (a confidential fragment to be stored locally or in a high-level security place, a public fragment to be stored in a public server). Also, the first level protection method is only for disguising the image quality instead of protection, only the second level protection of our designs will be analyzed here. And the analysis is only for the protected public fragment as long as the private fragment is seen as secure by employing AES (It is easy to replace AES to any other kind of encryption algorithms).

As pointed by Pareek et al. [116], it is known that many encryption algorithms have been successfully analyzed by statistical analysis and several statistical attacks. In most cases, visual degradation is used to evaluate the security property of SE methods for images. To test the robustness of our encryption method, we will perform statistical analysis by giving the PDF and the correlations for two adjacent pixels in the protected public part.

4.5.1 Probability Density Function analysis

A probability density function (PDF) of the image byte representation illustrates how pixels in an image are distributed by graphing the number of pixels intensity level. For a gray scale image case, Fig. 4.11 gives an example that the PDF of the protected and public fragment of the image are fairly uniform and significantly different from the respective PDF of the original image.

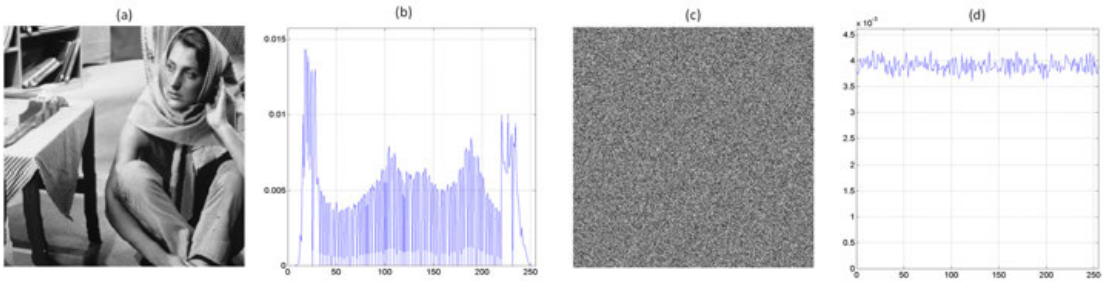

Fig. 4.11 Plain gray-scale image (a) and its PDF (b) compared with protected and public fragment (c) and its PDF (d).

Respectively, Fig. 4.12 gives an example that for a truecolor image (RGB image) case, the distribution for three color layers are all uniformly distributed after protection. This property guarantees that the protected and public fragment of the image will not provide any clue to employ any statistical attack [116].

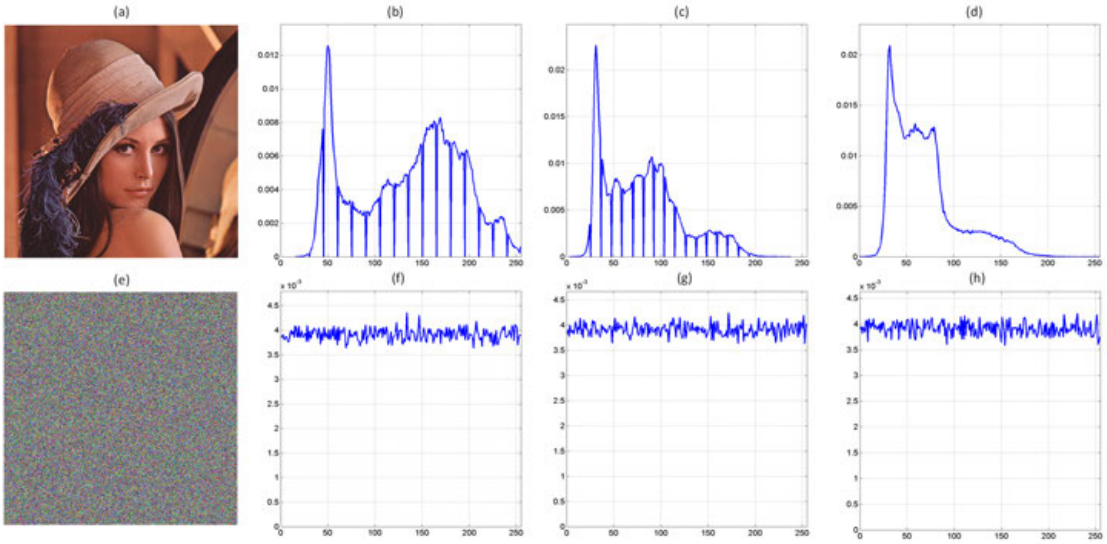

Fig. 4.12 Plain RGB image (a) and its PDF on RGB layers ((b),(c),(d) correspond to red, green, blue layers) compared with protected and public fragment (e) and its PDF on RGB layers ((f),(g),(h) correspond to red, green, blue layers).

4.5.2 Coefficients analysis

Lower correlation between original and encrypted data is an important factor that permits to validate the independence between them. Having a correlation coefficient uniformly distributed means that a high degree of randomness is obtained. According to Wang et al. [168], to test the correlation between two adjacent pixels, the following procedures are carried out. First, randomly select 10,000 pairs of two adjacent pixels in horizontal, vertical and diagonal direction, then compute the correlation coefficient r_{xy} of each pair using:

$$r_{xy} = \frac{cov(x,y)}{\sqrt{D(x) \times D(y)}} \tag{4.7}$$

where

$$E(x) = \frac{1}{N} \times \sum_{i=1}^{N} x_i$$

$$D(x) = \frac{1}{N} \times \sum_{i=1}^{N} (x_i - E(x))^2$$

$$cov(x,y) = \frac{1}{N} \times \sum_{i=1}^{N} (x_i - E(x))(y_i - E(y))$$

x and y are values of the two adjacent pixels in the image for the gray scale image case.

Then, the same operations are performed along the vertical and the diagonal directions. As shown in Fig. 4.13, the correlation coefficient distributions of the cipher images seem uniform compared with the original plain image. In Fig. 4.14, the analysis for the protection results of a three layers of a RGB format bitmap image is given. In this format, every pixel is stored using 24 bits with every 8 bits for one color layer. The protection will mix the correlation coefficient distributions for each of the layer.

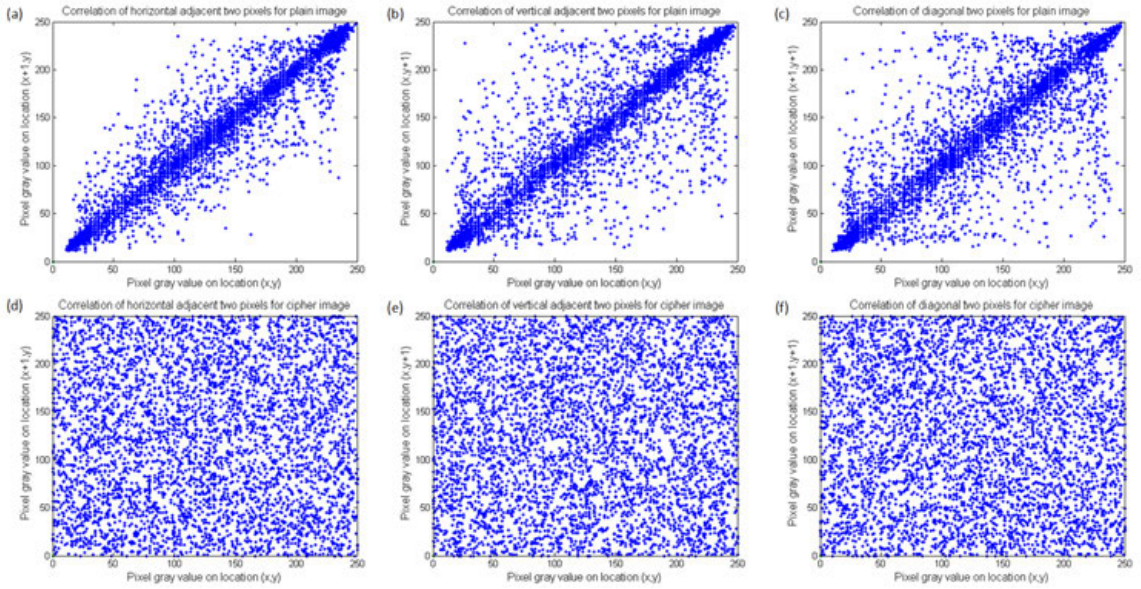

Fig. 4.13 Correlation of adjacent pixels in horizontal, vertical and diagonal direction for a gray scale bitmap image.

4.6 Evaluations with different computer architecture

In this section, we mainly discuss the implementation of allocating calculation tasks to GPU and CPU and evaluate their performance. As we pointed out in Chapter 3, the huge difference between low-end GPU and high-end GPU makes the calculation and design for program very different. Here a common low-end laptop GPU (Nvidia Nvs 5200M equipped with a CPU of Intel I7-3630QM) is used to test allocation. Then using a high-end desktop gaming GPU (Nvidia GTX 780 equipped with a CPU of Intel I7-4770K) leads to change and improve the design.

One circumstance of the hardware worth pointing out is that the other devices equipping by the two computers are similar (CPU, bus, motherboard, host memory, etc). Therefore the difference in performance allows comparing with the GPUs and the respective designs.

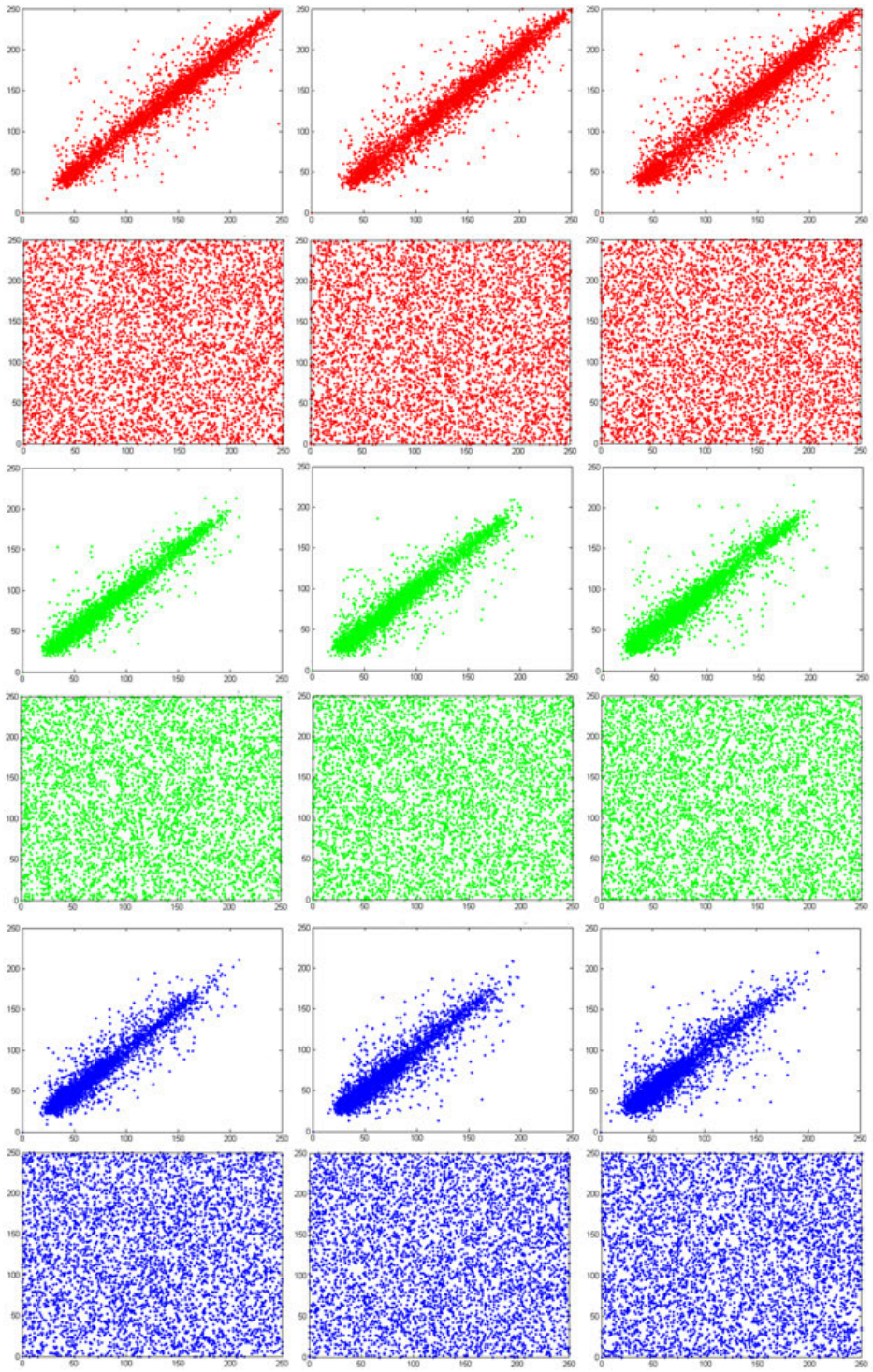

Fig. 4.14 Correlation of adjacent pixels in horizontal, vertical and diagonal direction for Red, Green and Blue layers.

4.6.1 Allocation of calculation tasks for a moderately powerful GPU (laptop)

Fig. 4.15 shows the design steps to process a single bitmap image. The image content will be copied into GPU memory and fragmented by GPU after DCT 8×8 preprocess. Then the selected coefficients which are considered as the private fragment will be transferred to host memory and encrypted using AES 128-bit by CPU. In parallel, the remaining DCT coefficients will be padded and transformed by iDCT 8×8 to build the public part. Then the public fragment will be transferred to host memory for further dispersion.

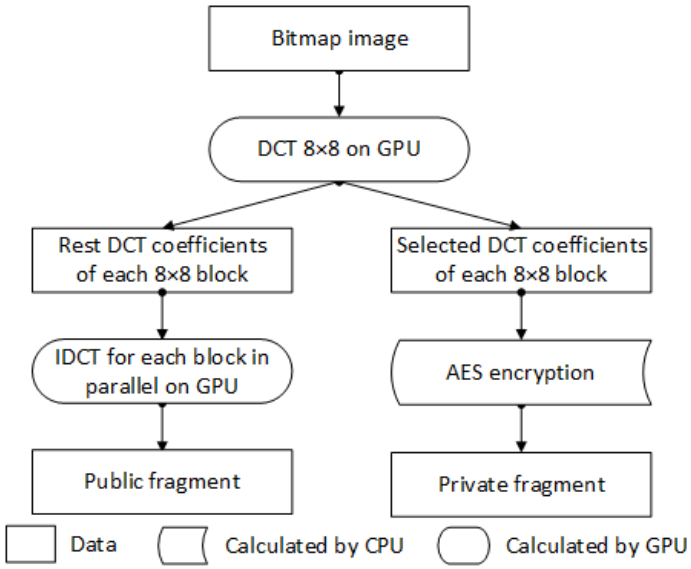

Fig. 4.15 Process steps for first level protection.

This design is aiming at fully utilizing both the CPU and GPU resources on a laptop by accelerating DCT processing using GPU. The total execution time depends on a race between CPU and GPU. As we evaluate separately the execution times of on CPU and GPU: the time spent by DCT on GPU is greater than the AES time spent by AES on CPU as shown in Table 4.3. This is because although GPU is able to accelerate DCT, CPU just need to encrypt a small part of the original data. The overlay and parallel design is very simple: it uses the GPU to calculate DCT and then when GPU is calculated, the iDCT for the public part, CPU is only calculating the AES for the private part.

This design based on laptop hardware configuration works well for a series of images in the same format (bitmap) as input because of the overlay design of the GPU and CPU. As GPU are calculating the DCT 8×8 and iDCT 8×8 of each input image and CPU are encrypting the selected parts (data amount about 10% of the original image) in parallel. The total run time depends on which processor is slower (on laptop use case, the GPU execution

is always slower due to its limited calculation capacity). The working flow of operations is shown in Fig. 4.16.

Table 4.3 DCT time on GPU and AES time on CPU of the laptop use case.

Image size	1024×768	1600×1200	3240×2592	4800×4800
DCT on laptop GPU	0.41 ms	0.79 ms	3.67 ms	9.98 ms
AES on laptop CPU	0.19 ms	0.47 ms	2.05 ms	5.87 ms

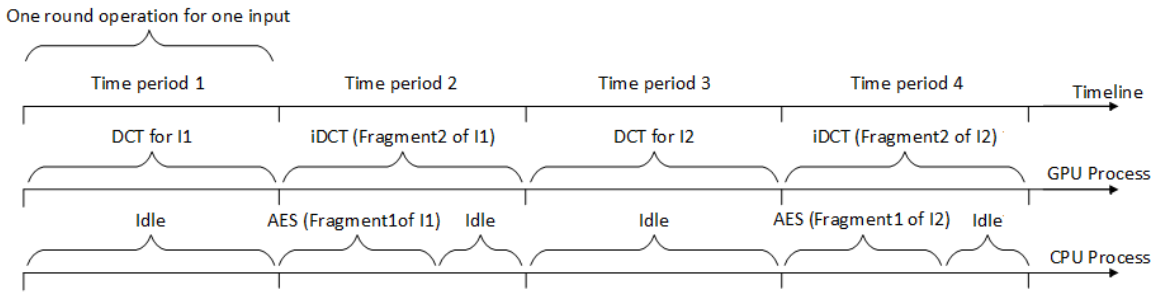

Fig. 4.16 Time overlay design of first level protection for multiple bitmap images as series input.

In fact, as long as the encryption run time on CPU for Fragment 1 of I1 is less than total time of period 2 and period 3 in Fig. 4.16, this design of overlay makes it adapted for the second level protection method. The main difference is the hash function which becomes a new calculation task. The initial plan for second level protection is to use the idle time space of CPU to calculate the hash value of Fragment 1 of the image to be protected along the scheme (Fig. 4.17). This is the right option as long as the laptop GPU is limited and cannot calculate hash function fast enough. However, Table4.4 shows that the SHA-512 calculation becomes the key element and our time overlay design in Fig. 4.16 will not suit anymore as we would love to let GPU hold at time Period 2 to wait for the hash calculation. So the overlay design in Fig. 4.16 should be modified.

It is important to evaluate time cost for all calculation tasks for second level protection in laptop scenario. As shown in Table 4.4, the execution time of SHA-512 algorithm and AES on CPU is still possible but it has to be covered by the execution time of DCT and iDCT on GPU which makes a new overlay design still possible in the case of a series of images as input.

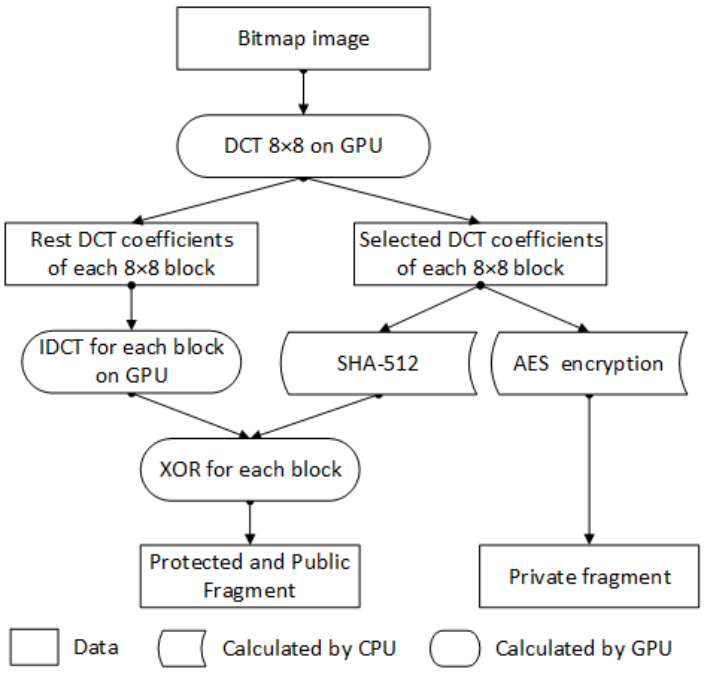

Fig. 4.17 Process steps for the second level protection.

Table 4.4 DCT time for one input image on GPU; AES and SHA-512 time for selected DCT coefficients on CPU for the laptop use case.

Image size	1024×768	1600×1200	3240×2592	4800×4800
DCT on laptop GPU	0.41 ms	0.79 ms	3.67 ms	9.98 ms
AES on laptop CPU	0.19 ms	0.47 ms	2.05 ms	5.87 ms
SHA-512 on laptop CPU	0.29 ms	0.73 ms	2.8 ms	7.69 ms

If we consider the two same size bitmaps (e.g. two 512×512 bitmap images) as the input together, while the SHA function for the first image is calculated by the CPU (one hash per block), the GPU will calculate the DCT for the second input image in parallel. For every two DCT operation on GPU, the GPU turns to calculate the iDCT for the first image (XORed with the hash results) while CPU continues the SHA calculation for the second input image. And AES will be performed for the selected coefficients of two images together while iDCT is performed for the second image. The time flow is shown in Fig. 4.18 to elaborate the whole design. The 'Idle' period in the CPU timeline can be considered as the redundancy prepared for the possible delay caused by the memory transfer between host memory and GPU memory (this memory transfer is always controlled by the CPU instructions).

The evaluation of performance is shown in Table 4.5. The execution time for one input image is not exactly twice of the DCT time on GPU because the DCT and iDCT are not

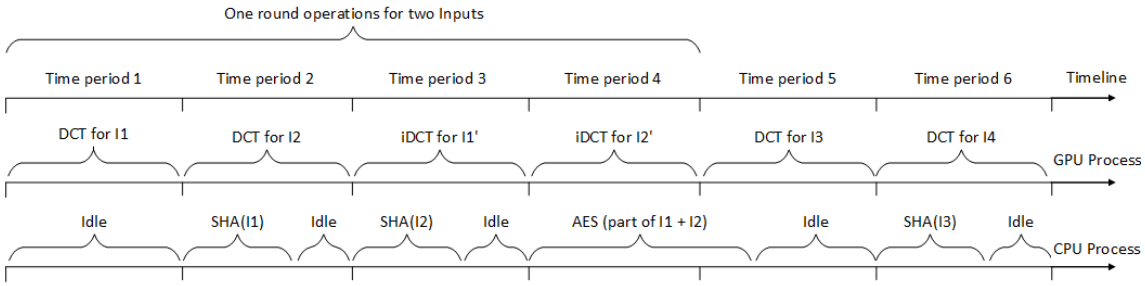

Fig. 4.18 Time overlay design for the second level protection.

exactly the same. The evaluation shows that the total run time is almost the half of the DCT speed on GPU which is over 1.1GB/s (faster than full AES on CPU in [37]).

Table 4.5 Speed of full AES for the input image on CPU, our SE design, and AES for the input image on GPU for laptop scenario.

Image size	1024×768	1600×1200	3240×2592	4800×4800
AES on laptop GPU	5.5 ms	13.5 ms	59.2 ms	162.3 ms
AES on laptop CPU	2.1 ms	5.0 ms	21.9 ms	60.2 ms
SE on laptop CPU + GPU	0.89 ms	1.94 ms	8.38 ms	20.91 ms

However, as shown by Li et al. [86] and Gervasi et al. [60], GPUs can also accelerate AES computation. However, as shown in Table 4.1, GPU run times vary widely according to their architecture. In Table 4.5, we compare the performance of full encryption using AES on CPU and GPU with our SE method. Due to the limitation of the GPU compute capability on laptop, the AES on GPU is even slower than on CPU. This means the design of calculation task arrangement is highly based on the hardware configuration. And for a low-end GPU laptop use case, using GPU and CPU in parallel for both first and second level SE methods is the best implementation option.

4.6.2 Allocation of calculation tasks for a powerful GPU (desktop)

We saw in Chapter 3 that the evolving of the GPUs are so fast that the computation allocation can vary over time according to GPU configurations. In our work, this fact makes it possible to do all SE steps including DCT 8×8 and AES on the GPU in some special situations. The situation worth dealing with the situation on most desktops today where GPUs are so powerful that can calculate DCT for all piece of data still faster than AES for only a small part of data on CPU. This leads to a serious question: the overlay design of Fig. 4.16 and Fig. 4.18 are not working anymore. Evaluations in Table 4.6 shows that, on Nvidia GTX 780, the GPU

time period for computing iDCT is so short that it cannot cover for the calculation of AES on CPU.

Table 4.6 Run time in period 2 on desktop GPU and CPU.

Image size	1024×768	1600×1200	3240×2592	4800×4800
iDCT on desktop GPU	0.04 ms	0.09 ms	0.41 ms	1.12 ms
AES on desktop CPU	0.16 ms	0.38 ms	1.72 ms	4.67 ms

According to Li et al. [86], AES speed can reach more than 50 Gbps on an Nvidia GPU of a desktop machine with CUDA implementation (In our work, it can reach almost 40 Gbps on our desktop as shown in Table 4.7). In such a situation, the parallel design in Fig. 4.16 is definitely not suitable anymore as we are getting a scheme of GPU always idle and CPU always fully used. Although the performance is still better than the full AES on CPU, the hardware resource in GPU is not fully exploited.

In fact, according to these evaluations, we move all SE calculations including DCT and AES to GPU for the first level of SE. This design uses GPU to work three steps in sequential for each input image: DCT for original image, AES for selected coefficients and iDCT for the rest coefficients. In Table 4.7, we list the evaluation for full encryption on CPU and GPU compared with SE on GPU.

Table 4.7 Speed of AES on CPU and GPU, our SE (first level protection) on GPU.

Image size	1024×768	1600×1200	3240×2592	4800×4800
AES on desktop GPU	0.19 ms	0.46 ms	1.91 ms	5.46 ms
AES on desktop CPU	1.56 ms	3.8 ms	16.6 ms	45.5 ms
SE on desktop GPU	0.10 ms	0.21 ms	1.01 ms	2.76 ms

We can see that the SE we use is still faster than naïve AES on either CPU or even on GPU. This results benefits from the idea that all the calculations of SE are moved to the GPU. Based on these observations, we can see that using a GPU as an accelerator for our SE algorithm is always a better choice compared with naïve AES. The main reason for this situation is because although the AES can be accelerated a lot by GPU, the DCT 8×8 calculation itself suits better than AES to the GPU design. A deeper reason is that DCT 8×8 is optimized by many previous works that the calculation is adapted to fit Nvidia GPU architecture; in the mean time, the design of AES algorithm utilized logic operations at the bit level which is not as easy as DCT to optimize for GPU. This main difference makes AES always slower than DCT on the same GPU platform. Moreover, the SE method of both the

first and the second level protection generates only about 13% of original data to do the AES operation which indeed does not add much burden for calculation.

For the strong level of protection method on desktop, the only difference is how to allocate the hash calculation task. As pointed out in Chapter 3, according to tests based on programs in Steube [146], the SHA-512 performance on the desktop GPU, Nvidia GeForce GTX 780 is around 136 MH/s (means 136 million hash calculation per second). We should notice that for each 8×8 block, there will be one hash calculation, so we can evaluate the run time by SHA-512 as in Table 4.8.

Table 4.8 Speed estimation of SHA-512 of once per 8×8 block on desktop GPU.

Image size	1024×768	1600×1200	3240×2592	4800×4800
SHA-512 once per block	0.09 ms	0.22 ms	0.96 ms	2.65 ms

The speed is much faster than SHA-512 on CPU based implementation from [37]. Also, SHA-512 implementation on CPU is too slow to fit the overlay design shown in Fig. 4.18 in our desktop scenario. In the evaluation of second level protection, we allocate this hash task to the GPU also. In the end, we compare the strong level of protection method on GPU with AES on GPU in Table 4.9.

Table 4.9 Evaluation of AES on GPU, our SE (strong level of protection) on GPU.

Image size	1024×768	1600×1200	3240×2592	4800×4800
AES on desktop CPU	1.56 ms	3.8 ms	16.6 ms	45.5 ms
AES on desktop GPU	0.19 ms	0.46 ms	1.91 ms	5.46 ms
SE level 2 on GPU	0.19 ms	0.43 ms	1.97 ms	5.41 ms

Table 4.9 shows that the SE in second level protection mode on desktop GPU has the same performance as AES-128 on GPU. In summary, the allocation of calculation of HASH and AES tasks always depends on the computation capacity of the GPU while the DCT task always can be allocated to the GPU.

4.7 Discussions

In this chapter, we implemented two levels of selective encryption methods both using DCT 8×8 preprocessing based on GPU acceleration. We defined a first level of protection which is lightweight and is designed to disguise image quality. Then, we defined a strong second level of protection that can provide a good level of security.

The first level of protection design combines CPU and GPU resources available on most PCs, tablets, or even smartphones today. It provides a very fast speed to perform selective encryption in the frequency domain for bitmap images. The second level of protection method addresses the issue with better protecting the public fragment which is left plain in the first level of protection. The idea is to use a small number of high frequencies to rapidly protect the low frequencies of the public fragment; indeed, the second level of protection implementation also uses the acceleration offered by the GPGPU. Evaluations show that it is about twice faster than AES on a laptop; as Table4.9 shows that SE performance are comparable to AES with a high-end GPU as the ones equipped on a desktop. By two different statistical analyses, it shows that the second level protection method offers a good level of protection to resist recovery.

The separation of an image data into a private fragment and a public and protected fragment can be used to address the issue with efficiently protecting large amount of bitmap images using but not completely trusting remote storage servers like a cloud storage provider. We separate the original data as putting the important private fragment to be stored locally and putting the remaining fragment protected to a remote server. For instance, in a cloud with the additional protection offered by the cloud provider. Doing so, we make the best usage of the local memory where we store only about 13% of the data depending of a tunable number of coefficients selected to constitute the private fragment. To perform one or the other of the two methods, we refined the implementation architecture using both the GPU and the CPU available on a PC and reach a level of performance that much faster than CPU based AES and comparable with GPU based AES and never slower.

Indeed, one have to realize that GPGPU architectures as well as encryption algorithms are progressing at a fast pace. For instance, late in 2014, a new generation Nvidia Geforce series GPUs (http://www.nvidia.com/object/geforce_family.html) was released with more CUDA cores, higher clock frequency and wider memory bandwidth, improving effective speed by 40% compared to GPU for desktop we used (manufactured in 2013). And this increase keeps showing up in 2015 and 2016 with different generations of calculation core architecture introduced, faster memory equipped. We are convinced that performance for computing the DCT 8×8 and other algorithms benefiting from GPU like SHA-512 or even AES will still progress. As pointed by Gregg and Hazelwood [66], the memory transfer between host and GPU memory could be a bottleneck due to the limitation of the PCI Express bus connecting them (normally several GB/s). During this work, we have seen that unfortunately, this can influence the load to assign to the CPU vs. the GPU in order to obtain the best performance. This would suggest developing a software adaptor to smartly allocate the computation task according to the hardware architecture available. As pointed in Chapter 3,

the mobile platform that lets CPU and GPU use the same memory which maybe a solution to this problem. However, it is still difficult to see solutions for replacing PCIE bus showing up in today's PC manufactures.

Nonetheless, our work is clearly showing that selective encryption can potentially become widely used for bitmap image protection since it provides excellent processing time, a minimal visual content loss, a good level of protection by fragmenting bitmap into two separate storage space, and a moderate increase of its total memory storage.

Chapter 5

DWT for general purpose protection

In this chapter, first we present the GPGPU based acceleration of DWT-2D. Then, the design is given with both general architectures and details. The security analysis followed, for different types of files, are presented to prove the good effect of our design. Then, the benchmark section gives a general comparison of our experimentation on two different computer platforms with other encryption algorithms. At last, we present the use case with the transmission and secure sharing architecture.

5.1 Discrete wavelet transform and GPU acceleration

In previous sections, DCT (Discrete Cosine Transform) was used to support fragmentation decision before performing encryption for bitmap image protection. However, DCT cannot guarantee the total losslessness due to conversions between integers and floating point numbers which will result in rounding errors (sometimes even recursively). These rounding errors can be reduced by using more storage space with more detailed designs but cannot be totally avoided. This is the reason why DCT cannot provide the integrity required for dealing with any kind of data type.

Discrete Wavelet Transform (DWT) [21] is sometimes used in selective encryption (see previous work [63] [138] [121]), but most of the time it is used as a standard compression step for formatting rather than as a preprocessing step for selecting in multimedia use cases. In our design, DWT is used as a preprocessing step before fragmentation with a special filter Le Gall 5/3 [21] which has an important lossless property by mapping integers to integers. The DWT-2D based on Le Gall 5/3 filter fits best for our design for it can provide data integrity and also be efficient both in performance and storage space usage.

Performance against full encryption is constantly required. The transform used in the preprocessing step of SE can legitimately be removed from the benchmark when SE and

compression are integrated and that transform is used by both applications. In these cases, SE performs a light weight protection within the compression or coding process for a specific format like MPEG4 [133] or JPEG2000 [31]. However, our use case aiming at dealing with any kind of data will have to take into account the entire process when it comes to performance evaluation since it should be able to deal with agnostic data type and even formatted data. This will lead us to implement DWT on a GPGPU to benefit from its acceleration [50].

5.1.1 DWT

DWT is a signal processing technique for extracting information mostly used in compression standard such as JPEG2000 [31]. It can represent data by a set of coarse and detail values in different scales. Naturally, it is a one-dimensional transform. But, it also can be used as a two-dimensional transform as applied in the horizontal and vertical directions. For the image case, this DWT-2D transform will generate four small images which each one is one quarter size of the original image with one level transform: one with low resolution (LL), one with high vertical resolution and low horizontal resolution (HL), one with low vertical resolution and high horizontal resolution (LH), and one with all high resolution (HH). Then the second level transform will only be performed for the first quarter ('LL' part) of the first level's result which is called dyadic decomposition as shown in Fig. 5.1.

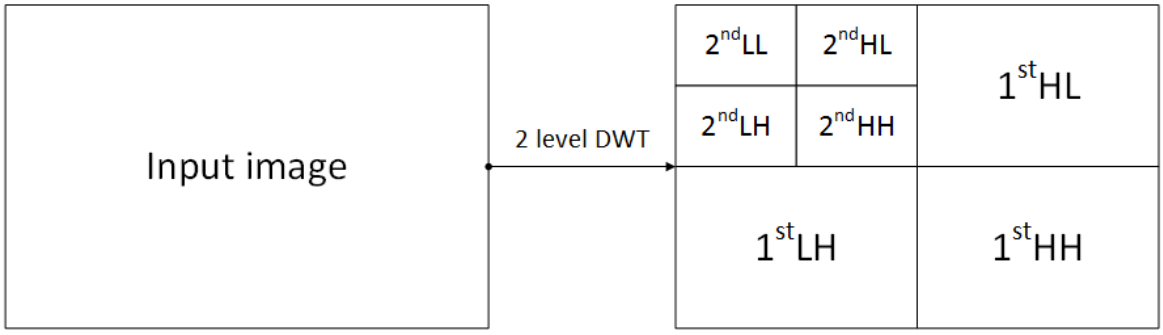

Fig. 5.1 Two level Discrete Wavelet Transform 2D result [31].

To perform the forward DWT, a one-dimensional sub-band is decomposed into a set of low-pass samples and a set of high-pass samples. In our design, the "Le Gall 5/3 filter" by Burrus et al. [21] is used so no data will be lost due to numerical rounding. And the lifting-based filtering scheme [1] is used which updates odd sample values with a weighted sum of even sample values, and updating even sample with a weighted sum of odd sample values. The lifting-based filtering for the 5/3 analysis filter is achieved by using equations (5.1) and (5.2) [31]:

$$y(2n+1) = x_{ext}(2n+1) - \lfloor \frac{x_{ext}(2n) + x_{ext}(2n+2)}{2} \rfloor \tag{5.1}$$

$$y(2n) = x_{ext}(2n) + \lfloor \frac{y(2n-1) + y(2n+1) + 2}{4} \rfloor \tag{5.2}$$

where x_{ext} is the extended input signal, y is the output signal and $\lfloor a \rfloor$ indicates the largest integer not exceeding a.

DWT can be performed at different levels, we chose a two-level DWT as illustrated in Fig. 5.1. In Fig. 5.4, the selected coefficients to build the private fragment are the 2^{nd} LL which takes about 1/16 of the storage space and carries the basic elements (coarse information) of the original image. The reason for using two-level DWT is that the one-level DWT still has a large low frequency part (1/4 of the whole DWT-2D result) to be protected. Three or more DWT levels make the value range of the high frequency coefficients too large to waste more storage space (more details about value range given later in this section).

5.1.2 DWT acceleration based on GPGPU

There are two main categories of DWT implementations on hardware: by convolution operations [97] and by the lifting scheme [149]. In early GPU-based DWT implementations (Hopf and Ertl [69], Garcia and Shen [53]), the convolution operations were preferred as the early developing tools for GPU such as OpenGL or Cg. The performance gain compared with CPU implementations was limited due to not only the limited GPU calculation capacity but also the lack of a general purpose GPU development platform to fully exploit the GPU parallel computing resources. In fact, the lifting scheme is more suitable for GPU computation as each coefficients in this scheme is computed using the coefficient that in the even or odd position and its two neighbours. As a consequence, all coefficients can be calculated without dependencies therefore can be performed in parallel. This important feature is not fully used until CUDA is released [78]. Not only it provided operation level parallelism, but it also gave access to arbitrary memory operations. CUDA architecture along with the Nvidia GPGPUs accelerates DWT 10 to 20 times faster than an optimized CPU implementation (multi-core CPU based on OpenMP) in 2009 [50].

The reason why GPGPU brought such a huge performance acceleration is because unlike modern CPUs with only a few powerful physical cores (4 or 8 on a Intel CPU for PC) that allows only limited number of actually parallel threads, a GPGPU could contain hundreds even thousands of threads at the same time. This can fit the scheme based feature to allow each of the output coefficients calculated separately with a hardware level parallelism. The

CUDA platform allows to realize the first generation of DWT-2D implementation by simply using the parallel computing cores in CUDA enabled GPGPU since 2009.

More optimization came out after 2009 like optimizing the memory usage to avoid the time consuming operations like matrix transpose. For example, the calculation rounds in [50] are to load the data from global memory to shared memory and calculate the horizontal direction of DWT; then the result matrices are loaded back to global memory and transposed to become the input data for the next round. In the next round, the same calculation operations are performed as the data are transposed so the vertical DWT can be easily done. This method loads data between fast shared memory and slow global memory twice and transposes the matrix once which is not efficient as pointed out by Enfedaque et al. [43].

Further improved methods [102] explored minimizing memory transfers between the global memory and the shared memory by computing both the horizontal and the vertical filtering in one step. The improvement is based on carefully arranging the input matrix into rectangular blocks before computing and loading them to the shared memory by a thread block. Then both the horizontal and the vertical DWT can be calculated in these blocks which successfully avoided the matrix transpose or further memory transfers. However, there is a drawback of such an approach: adjacent blocks have data dependencies that can only be avoided by extending all blocks with some rows and columns that overlap with adjacent blocks.

More recent research [159] shows better performance with more optimization in handling the problem of data block dependencies by more memory transfer steps. And the result shows that a 10 to 14 times speedup can be reached compared with a CPU implementation using instruction level accelerations (MMX and SSE extensions). In 2015, the fastest implementation of the DWT found in the literature is proposed by Enfedaque et al. [43]. In this chapter, an optimized scheme is implemented with the state-of-the-art hardware (Nvidia GTX Titan GPU). The DWT-2D with "Le Gall 5/3" filter for a 4096×4096 image can be done in 0.467 ms.

In summary, as pointed out in Chapter 3, the development for CUDA enabled GPGPU is highly dependent on both the software and the hardware architecture. In recent years, there is continuing optimization for DWT as different CUDA versions and different GPGPU are released.

In our implementation, the lifting scheme is used and the main method according to van der Laan et al. [159]. As we are not focusing on the best optimization of implementing DWT-2D on GPGPU, the performance evaluations are just based on the hardware we have instead of the most powerful GPGPUs.

5.2 Design of DWT based SE

5.2.1 Designs

In our design [127], as shown in Fig. 5.2, in order to deal with sizable input data it is being proposed to cut it into several chunks of the same given size 2D matrix (e.g. seen as a 512×512 or 1024×1024 byte block which is chosen to accommodate further transformation or the hardware platform architecture). Then every chunk (D_i) goes to the SE process to generate three fragments which are the private fragment D_iA, the first public and protected fragment D_iB, and the second public and protected fragment D_iC. Then the D_iA fragments go to the trusted area like a local machine under the user's control and the D_iB, D_iC fragments may be transmitted to the public area like a public cloud with little fear of an attack since D_iB, D_iC are supposed to carry little information and also to be protected. This will be shown later in Section 5.3 where a number of security analysis will be performed.

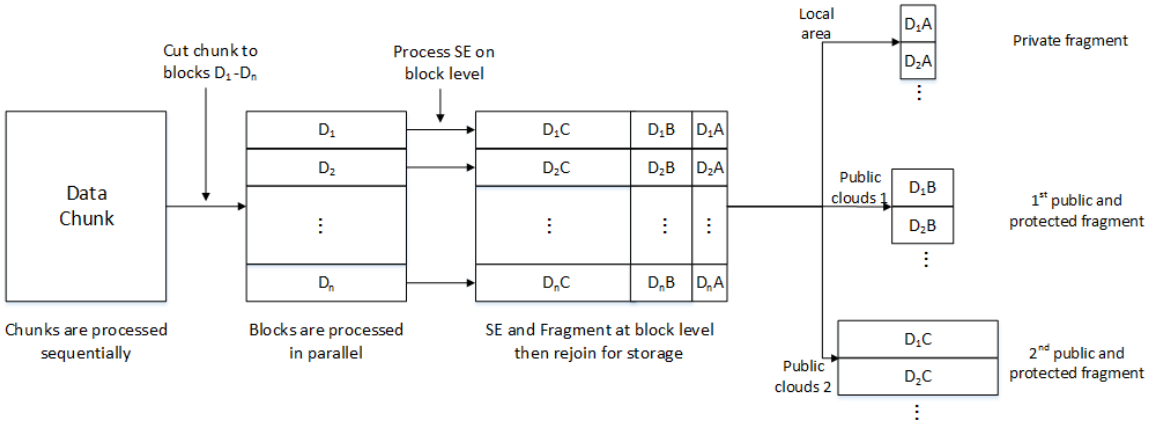

Fig. 5.2 SE General method for processing large amount of data.

The main idea is to consider every block D_i as a matrix and be treated as such by the SE process. That is to say any kind of data formats can be seen as a matrix by considering every byte of data as a pixel to form a bitmap gray scale image. Then every "image" D_i is simply processed using the SE method block by block with block size 8×8 shown in Fig. 5.4. The block size chosen can be changed according to the size of the original data. This tiling step is used to achieve a nice fitting with the GPGPU architecture (will be mentioned later).

The first step for the 8×8 block is to do the Discrete Wavelet Transform (DWT). In our work we perform two successive levels of the DWT with the Le Gall 5/3 filter so the low frequency coefficients which are considered as the private fragment (shown in Fig. 5.3). This fragment takes only 4 out of 64 coefficients (with $k = 4$ in our implementation) but carries most of the original frequency feature. The AES-128 bit [62] will be used (In our design, however, the implementation is structured such that another encryption algorithm can easily replace AES-128 if need be) to protect this fragment if further transmission is needed.

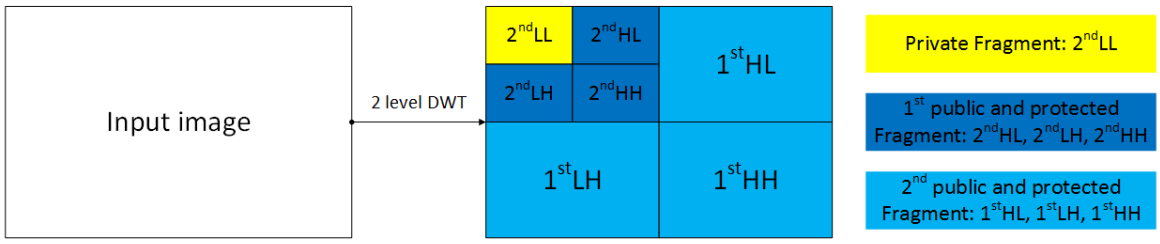

Fig. 5.3 DWT-2D and fragmentation process for the single 8×8 block.

Then the private fragment of each 8×8 block will be used to generate a 256-bit sequence by using SHA-256 [153] which can guarantee very different bit sequence generated even when the corresponding coefficients of the private fragments in neighbor blocks are very similar (encryption key is used to guarantee the key sensitivity in Fig. 5.4). This bit sequence is used to protect the 1^{st} public and protected fragment (the rest coefficients of 2^{nd} level DWT shown in Fig. 5.3) by performing an XOR operation. This fragment is defined as the 1^{st} public and protected fragment as shown in Fig. 5.3. For the rest DWT coefficients which forms the 2^{nd} public and protected fragment, a bit sequence generated from SHA-512 [153] results of 1^{st} public and protected fragment and encryption key is used to do protection.

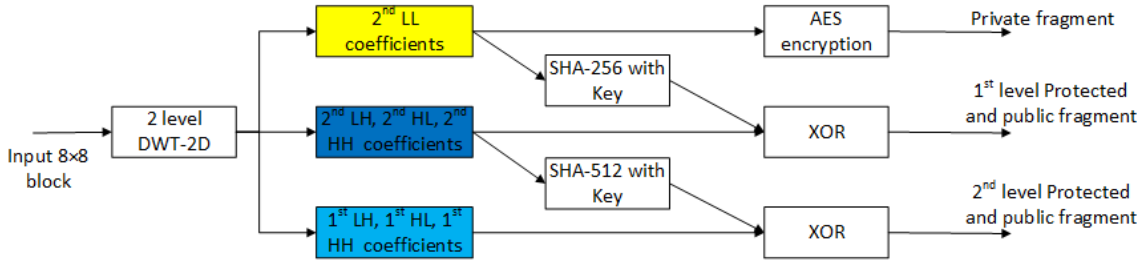

Fig. 5.4 SE process for the single 8×8 block.

The protection for the 'protected and public fragments' provided by a XOR operation is based on the randomness guaranteed by the HASH algorithms. For example, in bitmap case, as long as there are redundancies, the $L3$ coefficients could be very similar especially between neighbor blocks. However, the SHA-256 and SHA-512 will generate totally different bit sequences even when there is only one different bit in inputs. This randomness will be added by XORing the to the 'protected and public fragment' which is the next level of DWT coefficients and random hash value of the current fragment. For other kinds of files as input, this design also has good effect. More security analysis for the protection will be shown later.

5.2.2 Evaluation of the storage necessary for DWT

Evaluation for the first level of DWT-2D transform

Input matrix is a 8×8 matrix with all elements are 8-bit integers (consequently within a range 0 to 255 or -128 to +128). As shown in Fig. 5.5, the Discrete Wavelet Transform has two steps: first, in horizontal direction. This will generate all coefficients in all lines: the first 4 are low frequency and last 4 are high frequency. It is easy to find out that the range for high frequency is -255 to +255 (double the range of input). And the range for low frequency is -192 to +192 (1.5 times of the input range). Then, the transform in vertical direction transforms the $1^{st}LL$ and $1^{st}H$ blocks respectively. This step will generate four blocks: $1^{st}LL$ (low frequency of the $1^{st}L$ block), $1^{st}LH$ (high frequency of the $1^{st}L$ block), $1^{st}HL$ (low frequency of the $1^{st}H$ block), $1^{st}HH$ (high frequency of the $1^{st}H$ block).

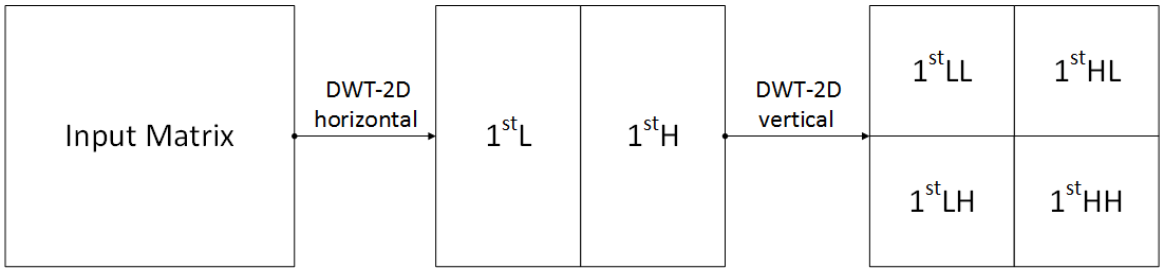

Fig. 5.5 Discrete Wavelet Transform 2D is calculated in two steps for the 1^{st} level.

It is easy to calculate the range for the $1^{st}HH$ is largest: -511 to $+511$ and the range for $1^{st}LL$ is $1.5 \times 1.5 = 2.25$ times of the input range (-128 to $+127$).

In summary, the possible max or min values of the 1^{st} level DWT-2D results can be stored with 10-bit long integers (-512 to +512).

Evaluation for the second level of DWT-2D transform

The 2^{nd} level transform only calculates the $1^{st}LL$ block (shown in Fig.5.5) which is a 4×4 block. The calculation will also be performed in two directions. Finally, the transform generates three 4×4 blocks and four 2×2 blocks (Fig. 5.1).

In order to calculate the possible max and min value in the 2^{nd} level four blocks, we need to get the equations for the coefficients presented by the input values. In order to get the max and min values for the output, the input values are either -128 or +128 (reach the max abstract values). So the rounding process can be ignored as we just want to estimate the output values in this case. The equations (5.3) and (5.4) can be simplified as follows:

$$y(2n+1) = x_{ext}(2n+1) - \frac{x_{ext}(2n) + x_{ext}(2n+2)}{2} \tag{5.3}$$

$$y(2n) = x_{ext}(2n) + \frac{y(2n-1) + y(2n+1)}{4} \tag{5.4}$$

In this case, the transform can be calculated by using the input matrix to multiply the coefficients matrix. And for the 1^{st} level DWT, the coefficients matrix A is:

$$\begin{bmatrix} 0.75 & -0.125 & 0 & 0 & -0.5 & 0 & 0 & 0 \\ 0.5 & 0.25 & 0 & 0 & 1 & 0 & 0 & 0 \\ -0.25 & 0.75 & -0.125 & 0 & -0.5 & -0.5 & 0 & 0 \\ 0 & 0.25 & 0.25 & 0 & 0 & 1 & 0 & 0 \\ 0 & -0.125 & 0.75 & -0.125 & 0 & -0.5 & -0.5 & 0 \\ 0 & 0 & 0.25 & 0.25 & 0 & 0 & 1 & 0 \\ 0 & 0 & -0.125 & 0.625 & 0 & 0 & -0.5 & -1 \\ 0 & 0 & 0 & 0.25 & 0 & 0 & 0 & 1 \end{bmatrix}$$

If we define the input matrix as IN, the first step of wavelet for the horizontal direction can be presented as: $Output1 = IN \cdot A$. Then the vertical direction is calculated: In fact, it can be represented as $Output2 = Output1^T \cdot A$ (use the transpose of $Output1$ to multiply matrix A again) which will get the transpose of the result we want. Then the coefficients of the 2^{nd} level DWT can be calculated:

$$\begin{bmatrix} 0.75 & -0.125 & -0.5 & 0 \\ 0.5 & 0.25 & 1 & 0 \\ -0.25 & 0.625 & -0.5 & -1 \\ 0 & 0.25 & 0 & 1 \end{bmatrix}$$

It is the same to calculate the 2^{nd} level DWT but only on the $1^{st}LL$ block. If we define the final output matrix as F, we list the $F(4,4)$ as follows:

$$\begin{aligned} F(4,4) =& 0.015625 \times IN[2,2] - 0.03125 \times IN[2,3] - 0.109375 \times IN[2,4] + 0.09375 \times IN[2,6] \\ &+ 0.03125 \times IN[2,7] - 0.03125 \times IN[3,2] + 0.0625 \times IN[3,3] + 0.21875 \times IN[3,4] \\ &- 0.1875 \times IN[3,6] - 0.0625 \times IN[3,7] - 0.109375 \times IN[4,2] + 0.21875 \times IN[4,3] \\ &+ 0.765625 \times IN[4,4] - 0.65625 \times IN[4,6] - 0.21875 \times IN[4,7] + 0.09375 \times IN[6,2] \\ &- 0.1875 \times IN[6,3] - 0.65625 \times IN[6,4] + 0.5625 \times IN[6,6] + 0.1875 \times IN[6,7] \\ &+ 0.03125 \times IN[7,2] - 0.0625 \times IN[7,3] - 0.21875 \times IN[7,4] + 0.1875 \times IN[7,6] \\ &+ 0.0625 \times IN[7,7] \end{aligned} \tag{5.5}$$

It is easy to calculate the max and min values if input of IN is within -128 to $+128$. The max value is 648 and min value is -648. Then we calculate all the max values for all 16 values of 2^{nd} level DWT output and put them in the same matrix (min values are the same absolute value but negative):

$$\begin{bmatrix} 338 & 260 & 468 & 468 \\ 260 & 200 & 360 & 360 \\ 468 & 360 & 648 & 648 \\ 468 & 360 & 648 & 648 \end{bmatrix}$$

According to this calculation, there are only four values that could possibly exceed the range of $(-512, +512)$. The storage method for the four values should be designed as 11-bit long $(-1024, +1024)$. Then the $2^{nd}LL$ block (the private fragment) storage space is 40 bits. The $2^{nd}HL, 2^{nd}LH, 2^{nd}HH$ blocks (1^{st} public and protected fragment) take $40+40+44=$ 124 bits in total. The $1^{st}LL, 1^{st}HL, 1^{st}LH, 1^{st}HH$ blocks (2^{nd} public and protected fragment) take 480 bits.

5.2.3 Storage space usage and numeric precision

Because of the transformation step used for the SE, the footprint of the data before and after the transformation could be different. This would lead to the difference of the storage space usage or rounding errors caused by conversions between integers and floating point numbers. In Guan et al. [67], the authors claim all variables are declared as type *double* with a bit-length of 64 bits. This is unnecessary in our case as the input data are stored as integers especially *int* type with a bit-length of 8 bits as the storage of the results will require 8 times more storage space compared with original data. In Qiu and Memmi [126] we already designed how to optimize integer representation but still could not avoid possible rounding errors caused by the calculation of DCT.

In this chapter, the preprocessing step is the DWT based on "Le Gall 5/3" filter which is designed to be an invertible integer-to-integer map, such that the DWT Le Gall 5/3 is lossless. As a result, on one hand, any rounding error is avoided; on the other hand, the extra storage space usage caused by the *int* to $float$ conversion does not exist. The only possible extra storage usage could be caused by the different value range of the input 8-bit *int* and the output *int* coefficients. And the output value range can be calculated as long as the input values are always stored Byte by Byte, the input value range (seen as unsigned value) is from 0 to 255 which can be considered as from -128 to $+127$ (the range is seen as from -128 to $+128$ during the following calculation). Then the storage methods can be optimized according to the value range distribution.

The first level DWT-2D transform is actually calculated by twice DWT-1D transforms (equation (1) and (2)) on the 8×8 block in horizontal and vertical directions sequentially. The first horizontal transform generates two sub-matrices which are $1^{st}L$ and $1^{st}H$ that take each half of the result matrix horizontally. The vertical transform is done on each of the two sub-matrices which generates four sub-matrices like in Fig. 4 ($1^{st}LL, 1^{st}HL, 1^{st}LH, 1^{st}HH$).

In the first horizontal transform, the range for $1^{st}H$ is -255 to +255 (double the range of input) and the range for the $1^{st}L$ is -192 to +192 (1.5 times of the input range). Then the transform in vertical direction, which is transform of the $1^{st}L$ and $1^{st}H$ blocks respectively, gets the following results: $1^{st}HH$ is from -511 to $+511$ and the range for $1^{st}LH$ is from -384 to $+384$. All the coefficients in the three sub-matrices of first level DWT-2D transform can be stored using 10-bits storage space.

The value range of second level DWT-2D coefficients are generated by the same two direction DWT-1D transform of the $1^{st}LL$ sub-matrices coefficients. Range of the second level DWT coefficients can be estimated by simplifying the equations (5.1) and (5.2) and then directly get results from calculating final formula of each elements in the four sub-matrices in Fig. 5.1 ($2^{nd}LL, 2^{nd}HL, 2^{nd}LH, 2^{nd}HH$). The max and min values for each of the value estimated are shown in the following matrices. And the storage method for the second level DWT-2D coefficients is: 11-bit long for each of the lower left corner four coefficients ($2^{nd}HH$) and 10-bit long for rest of the coefficients.

$$\begin{bmatrix} 338 & 260 & 468 & 468 \\ 260 & 200 & 360 & 360 \\ 468 & 360 & 648 & 648 \\ 468 & 360 & 648 & 648 \end{bmatrix}, \begin{bmatrix} -338 & -260 & -468 & -468 \\ -260 & -200 & -360 & -360 \\ -468 & -360 & -648 & -648 \\ -468 & -360 & -648 & -648 \end{bmatrix}$$

As shown in Fig. 5.4, the private fragment we selected is the $2^{nd}LL$ DWT coefficients and all rest coefficients are fragmented into two public and protected fragments.

The storage design for the three fragments could be flexible. If the avalanche effect [170] must be a concern (communication channel is unreliable and transmission error rate is high), the private fragment and 1^{st} public and protected fragment should be stored locally to avoid avalanche effect. In such case, the storage space requirement locally for one block is 164-bits storage in total (40-bits for private and 124 bits for 1^{st} public and protected fragment) and cloud storage usage is 480 bits (the 2^{nd} protected and public fragment). However, if the channel is reliable and error transmission are rarely to be seen, the 1^{st} public and protected fragment can also be put on clouds so the local storage is optimized which is important for a smart phone use case. Anyway, the total storage space usage is 644-bits for one block (initial 512 bits) which is about 26% more but in both cases most of the data can be stored on clouds.

In summary, the preprocessing step is the DWT-2D based on “Le Gall 5/3” filter which is designed to be an integer-to-integer map, such that the DWT is lossless. As a result, on one hand, any rounding error is avoided; on the other hand, the extra storage space usage caused by the *int* to $float$ conversion does not exist. Moreover, in our design, we consider any kind of data type as *int* with bit-length of 8 bits. That is to say, no matter what kind of original data type it is, we process the data by reading one byte one time and deal with it as an 8-bit integer. Then the input bytes will form an "image" (2D matrix) of a configurable size ready for the whole SE process. In this process, the storage method of output data is carefully designed to provide integrity for any kind of input data.

5.3 Security analysis

A secure encryption algorithm ought to resist a various array of classic attacks [111, 29]. In this section, different security tests on the proposed scheme are performed to establish its high level of security.

The basic assumption is that the selected private fragment of data can easily be secured by using AES-128 (also, it is easy to replace AES-128 with any other encryption algorithms as in Fig. 5.4), so the security property of this private fragment is not analyzed here either it is stored locally or for further securing sharing.

To validate a vast deployment (robustness) of the proposed method, the public and protected fragment which is stored on clouds in our use case are analyzed in terms of security performance to verify whether it reaches the required cryptographic performance. In Fig.5.4, the design is to put the two public and protected fragments on clouds. Thus, only these two fragments should be analyzed. However, according to our work, the security property of the 1^{st} public and protected fragment is very similar to the 2^{nd} public and protected fragment so we only present the results for the 2^{nd} public and protected fragment here.

In the following, we present the figures for the security analysis and all statistical results for an image, three kinds of video files, and English texts can be found in Table 5.1, Table 5.3, and Table 5.2 respectively. As long as the video and text files are larger than single image files, the statistical results for the videos and texts are the average one of 100 randomly picked chunks (chunk size 1024KB) inside the video file contents. Some criteria like PSNR and SSIM just suit for measuring images while not for text files.

Here the analysis measures on original data chunk and public and protected fragment used following are given: 1. *Uniformity analysis* is given by calculating the Probability Density Function (PDF); 2. *Information entropy analysis* is given by calculating the Entropy; 3. *Correlation analysis* is given by calculating correlation coefficients; 4. *Difference analysis*

is to test the difference in bit level and also the Normalized Mutual Information (NMI); 5. *Sensitivity analysis* is given by calculating the sensitivity when input plain-text and key changes; 6. *Visual Degradation analysis* is only for bitmaps by calculating Peak Signal-to-Noise Ratio (PSNR) and Structural Similarity (SSIM); 7. *Errors propagation* is also discussed.

Table 5.1 Statistical results of sensitivity for public and protected fragment (stored in Cloud) for Lenna image.

Statistical results for images				
	Min	Mean	Max	Std
PSNR	9.1943	9.2303	9.2616	0.0093
SSIM	0.03	0.0359	0.0412	0.0016
Dif	49.8886	49.9990	50.1077	0.0351
KS	49.8943	50.0011	50.1280	0.0347
$\rho 2$	0.0189	0.0193	0.0196	0.0001
$\rho - h$	-0.0614	0.0002	0.0492	0.0156
$\rho - v$	-0.0515	0.0001	0.0522	0.0154
$\rho - d$	-0.0448	0.0005	0.0580	0.0157
NMI	0.0189	0.0193	0.0197	0.0027

Table 5.2 Statistical results of sensitivity for public and protected fragment (stored in Cloud) for a English text (ASCII coding).

Statistical results for texts				
	Min	Mean	Max	Std
Dif	49.7008	50.0042	50.3350	0.0992
KS	49.7417	49.9978	50.4112	0.1030
ρ	-0.0145	0.0002	0.0192	0.0055
NMI	0.0669	0.0685	0.0701	0.0005

Table 5.3 Statistical results of sensitivity for public and protected fragment (stored in Cloud) for videos.

Statistical results for MP4				
	Min	Mean	Max	Std
Dif	49.8211	49.9918	50.1684	0.0632
ρ	-0.0098	-0.0004	0.0078	0.0031
NMI	0.1005	0.1145	0.1198	0.0018
Statistical results for MKV				
	Min	Mean	Max	Std
Dif	49.9985	49.8323	50.2008	0.0731
ρ	-0.0090	0.0001	0.0085	0.0039
NMI	0.1010	0.1027	0.1035	0.0067
Statistical results for RMVB				
	Min	Mean	Max	Std
Dif	49.8344	49.9994	50.1013	0.0792
ρ	-0.0096	-0.0005	0.0112	0.0037
NMI	0.2616	0.2745	0.2773	0.0022

5.3.1 Uniformity Analysis

The encrypted data should possess certain random properties such as uniformity, which is essential to resist against frequency attacks. Accordingly, the Probability Density Function(PDF) of the public and protected fragment should be as uniform as possible. This means that each symbol (pixels in image case) has an occurrence probability close to $\frac{1}{n}$, where n is the number of symbols ($\frac{1}{256} = 0.0039$ in byte level). We start by analyzing the image data and then other data to prove that the proposed method can attain the uniformity independently for its public and protected fragment.

The original plain image Lenna and its corresponding PDF are shown in Fig. 5.6-(a),(b). While, in Fig. 5.6-(c),(d), the corresponding fragment stored in cloud (c) to their corresponding PDF (d) is shown, respectively. It can be observed that the PDF of the public and protected fragment is close to uniform distribution since the probability of different symbols in the PDF figure are very different with the original one and tends to be uniform.

Also, in Fig. 5.7, the byte representation (read the data chunk byte by byte and form the matrix with each element is the value of the byte before DWT-2D) of an original chosen text file is presented in (a) and its corresponding PDF in (b) in addition to its corresponding fragment byte representation that is stored in cloud (c) and with its corresponding PDF (d). The obtained result indicates that the public and protected fragment of the text file posses also a uniform distribution. The similar results can be observed in Fig.5.8, Fig.5.9, and Fig.5.10.

From these results, we have shown that the distribution of the public and protected fragment tends to the uniform one no matter of the input data type. For the video cases, as long as the input chunks are video file contents which are already compressed and encoded, the original byte representations have no visual information. But the PDF of the public and protected fragments correspondingly have shown a tend of uniform distribution.

Moreover, to validate this result, an entropy test is realized in the sub-matrix level of size 8×8 (same size of the input block).

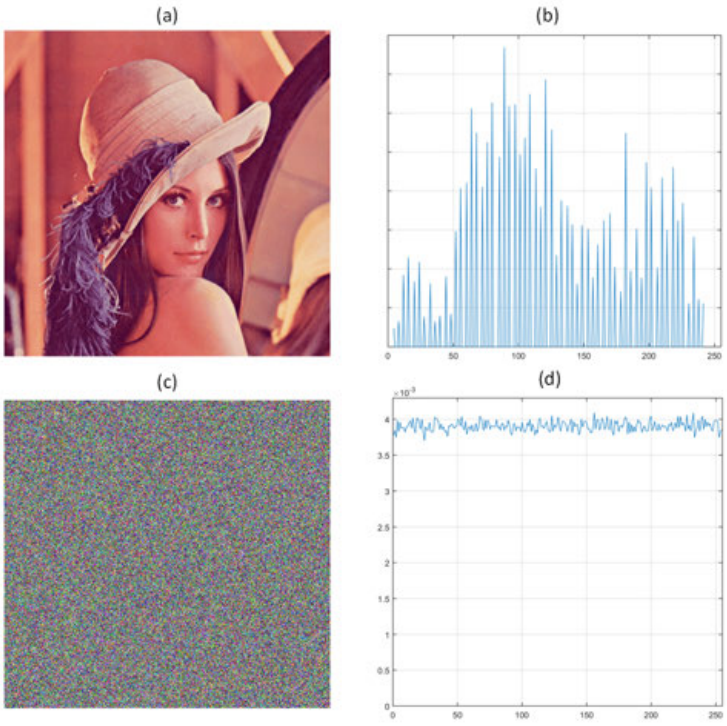

Fig. 5.6 (a) Original Lenna, (b) PDF of original Lenna512, (c) Public and protected fragment, (d) PDF of public and protected fragment.

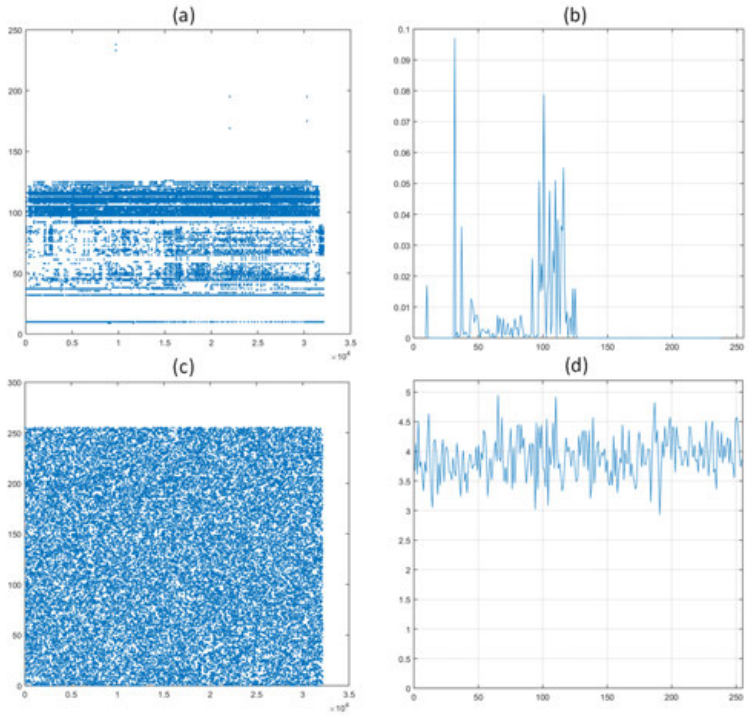

Fig. 5.7 Randomly chosen original text byte representation (a) and its PDF (b), Corresponding protected and public fragment (c) with its PDF (d).

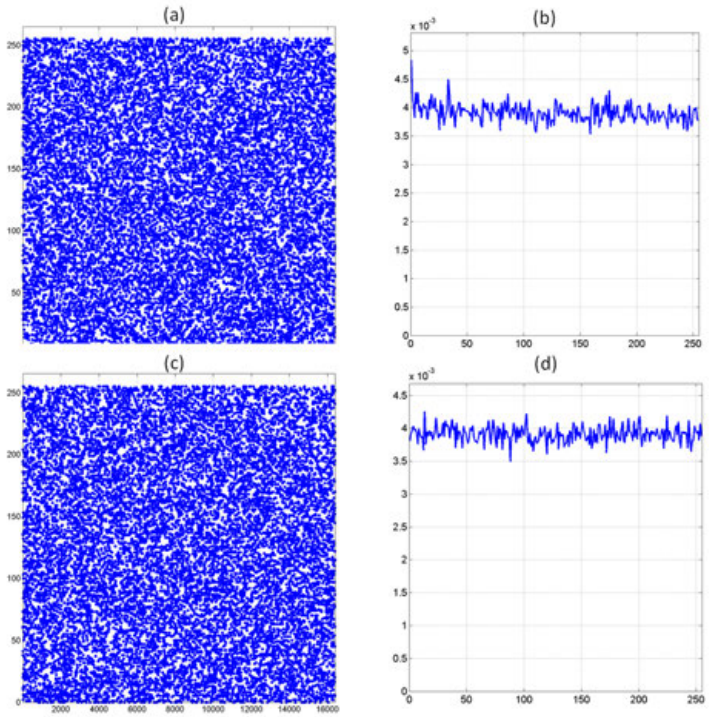

Fig. 5.8 Randomly chosen original MP4 file byte representation (a) and its PDF (b), Corresponding protected and public fragment (c) with its PDF (d).

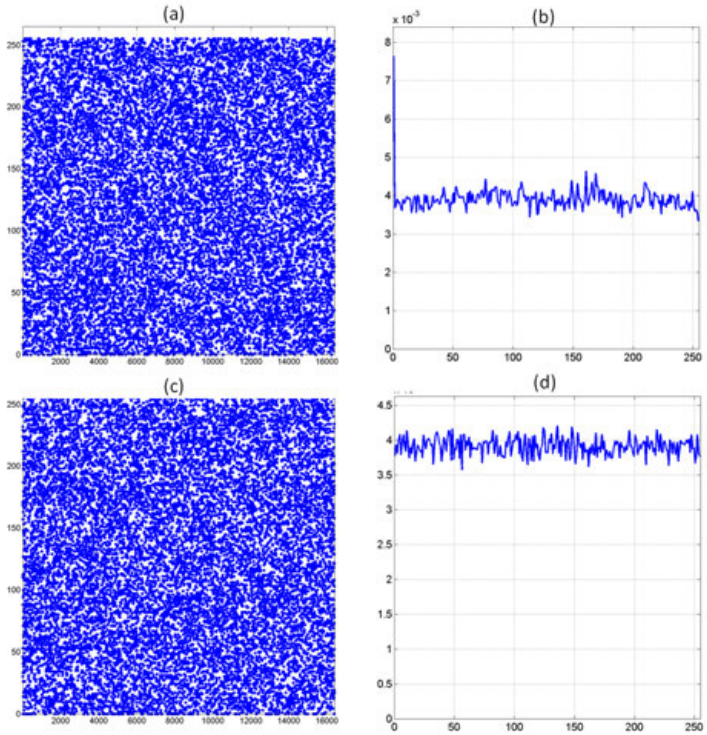

Fig. 5.9 Randomly chosen original MKV file byte representation (a) and its PDF (b), Corresponding protected and public fragment (c) with its PDF (d).

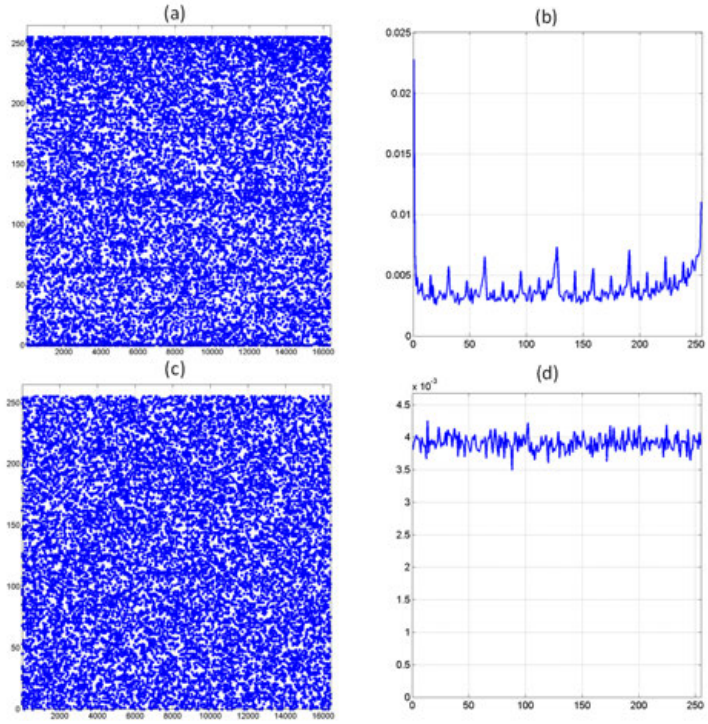

Fig. 5.10 Randomly chosen original RMVB file byte representation (a) and its PDF (b), Corresponding protected and public fragment (c) with its PDF (d).

5.3.2 Information Entropy Analysis

The information entropy of a data sequence M is a parameter that measures the level of uncertainty in a random variable [182] and is expressed in bits, defined using equation (5.6):

$$H(m) = -\sum_{i=1}^{n} p(m_i) \log_2 \frac{1}{p(m_i)} \tag{5.6}$$

where $p(m_i)$ denotes the probability of symbol m_i. It is easy to calculate for a random source emitting 2^N symbols, the entropy should be N. In this design, as the data are always seen as 8-bit per element, the pixel data have 2^8 possible values. As such, the entropy for a "true random" information source must be 8. For the bitmap case, the entropy of the public and protected fragments for different images are always more than 7.999 which proves high randomness.

In this subsection, the entropy tests are done on the public and protected fragments for not only bitmap files but also for English text files and three different video formats. For each file formats, 100 data chunks (each one is 1MB) are randomly chosen for the entropy test. As shown in Table5.4 and Fig.5.11-(d), the public and protected fragment of text chunks always have high randomness with entropy values are always between 7.9992 to 7.9995.

Table 5.4 Entropy test for 100 random chunks for videos and texts.

Entropy test results for videos and texts.				
	Min	Mean	Max	Std
$text(original)$	4.5961	4.6423	4.6938	0.0239
$text(protected)$	7.9992	7.9993	7.9995	0.0000
$mkv(original)$	7.96399	7.99726	7.99928	0.0055
$mkv(protected)$	7.99916	7.99930	7.99945	0.00006
$rmvb(original)$	7.91174	7.96303	7.98120	0.13383
$rmvb(protected)$	7.99914	7.99930	7.99944	0.00006
$mp4(original)$	7.99467	7.99851	7.99930	0.0006
$mp4(protected)$	7.99912	7.99930	7.99941	0.00005

As long as video files are already compressed, encoded and formatted, the entropy of the original video data chunks are already close to 8. However, in Table5.4 and Fig.5.11-(a),(b),(c), there are still improvements of the randomness for the three video formats. Therefore, the proposed scheme can achieve a very low entropy effect that can resist an attack based on entropy analysis for the file formats tested.

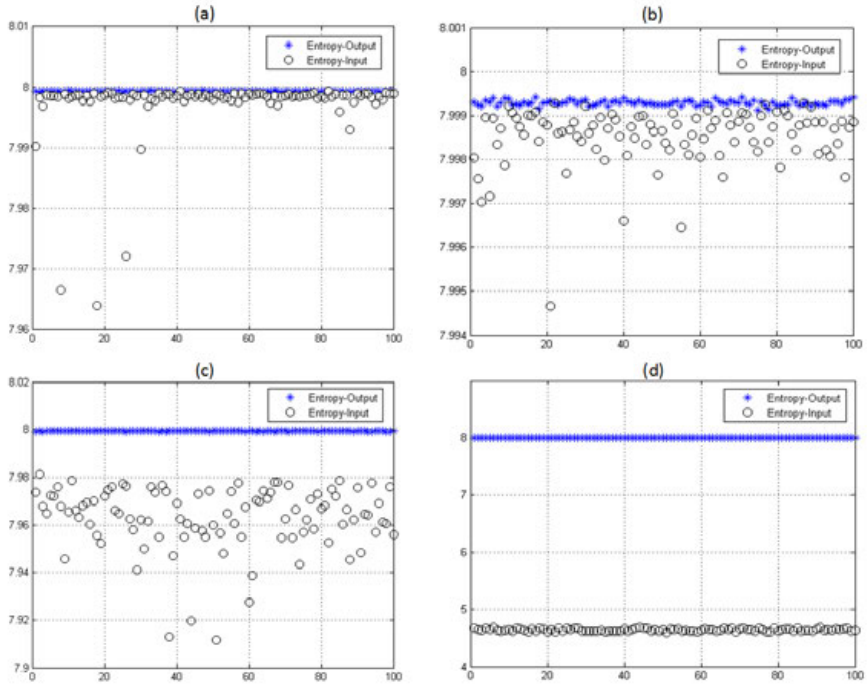

Fig. 5.11 Entropy test results distribution for 100 random chunks for videos and texts: (a) mkv, (b) mp4, (c) rmvb, and (d) text.

5.3.3 Test Correlation between Original and protected and public fragments

Lower correlation between original data and public and protected fragment is an important factor that allows validating the independence between them. Having a correlation coefficient close to zero means that the high degree of randomness is obtained. The correlation coefficient r_{xy} is calculated using the following equations (5.8):

$$r_{xy} = \frac{cov(x,y)}{\sqrt{D(x) \times D(y)}} \tag{5.7}$$

where

$$E(x) = \frac{1}{N} \times \sum_{i=1}^{N} x_i$$

$$D(x) = \frac{1}{N} \times \sum_{i=1}^{N} (x_i - E(x))^2$$

$$cov(x,y) = \frac{1}{N} \times \sum_{i=1}^{N} (x_i - E(x))(y_i - E(y))$$

In this test, we use image, text and video files as input for analyzing correlation. Indeed, the variation of coefficient correlation between original data and the public and protected fragment is obtained by applying the upper equations and the result is shown in Table 5.1, Table 5.2, and Table 5.3 (see value distribution of ρ^2 for image case and ρ for text and video case). The obtained result indicates that the coefficient correlation varies in a small interval very close to 0. This means that low correlation coefficient is attained by employing the proposed scheme and consequently the independence between the original data and the fragment is attained.

Additionally, to validate that the spacial redundancy is removed [108, 132], for the image case, the correlation between pixels of original image and the public and protected fragment are performed. This test selects randomly $N = 4096$ pairs of two adjacent pixels in horizontal, vertical, and diagonal direction. The obtained results are presented in Fig. 5.12, for the original (a)-(c) and the fragment (d)-(f) in horizontal, vertical and diagonal direction, respectively (same for text file from (g) to (l)). The result in this figure indicates clearly the high correlation between adjacent pixels in original image (correlation coefficient close to 1). While, for the public and protected fragment, the correlation coefficients become very low (close to 0) which clearly shows that the proposed scheme reduces severely the spatial redundancy.

Moreover, the variation of the correlation coefficient between adjacent pixels of public and protected fragment of Lenna image versus 1000 random keys are shown in Table 5.1 ($\rho - h$, $\rho - d$, $\rho - v$ respectively). The results are close to 0, which confirms that spatial redundancy is almost eliminated and very little detectable relation can be found in the public and protected fragment for both image and text case. Similar results are obtained using text file as input (see Fig. 5.12 (g)-(l)). For the video cases, the results in Table 5.3 are the average values for 100 randomly picked chunks.

5.3.4 Difference Between input Data and the public and protected fragment

The public and protected fragment must be statistically different from the original data (50%) in bit level. The proposed scheme has achieved a high value of difference before and after process for all data formats tested. For example, the plain image Lenna was tested and the obtained result in Fig. 5.13-(a) shows that 50% of bits is being changed between the public and protected fragment and the plain image. Additionally, similar result is obtained for text and video files, and statistical value is shown in Table 5.2 and Table 5.3(see value distribution of Dif for all cases).

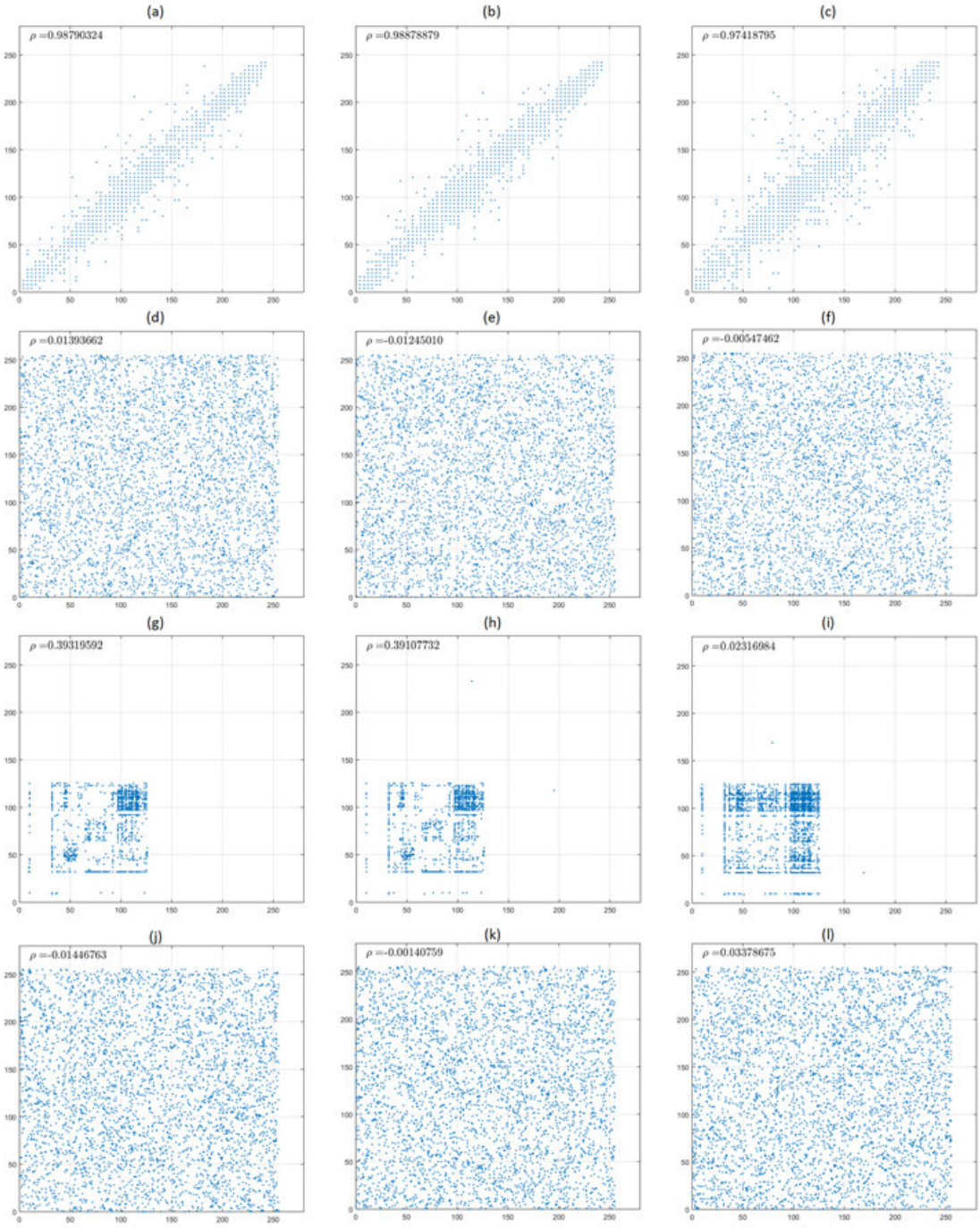

Fig. 5.12 Correlation distribution in adjacent pixels in original Lenna: (a) horizontally, (b) vertically, (c) diagonally.
Correlation in adjacent pixels in the public and protected fragment:(d) horizontally, (e) vertically, (f) diagonally.
Correlation distribution in adjacent pixels in text:(g) horizontally, (h) vertically, (i) diagonally.
Correlation in adjacent pixels in the public and protected fragment: (j) horizontally, (k) vertically, (l) diagonally.

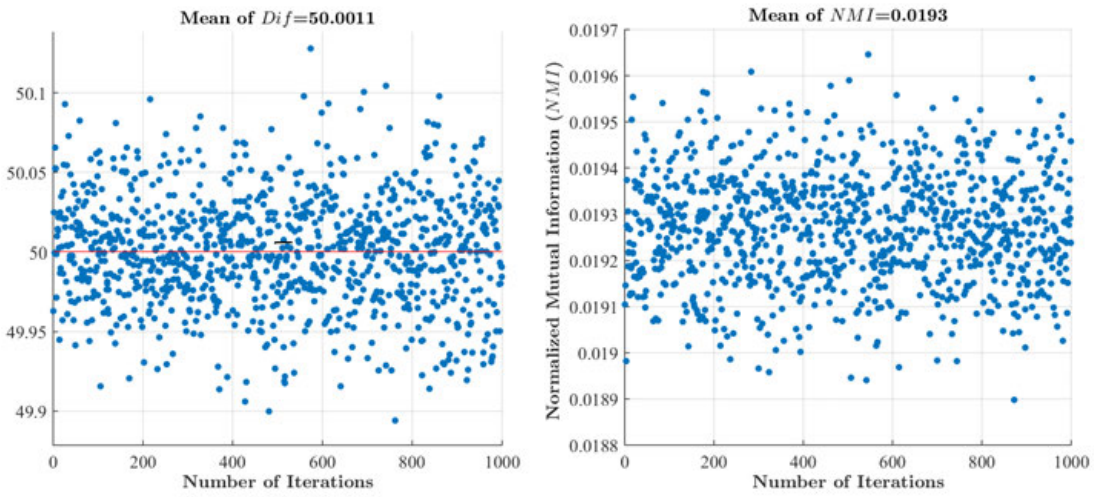

Fig. 5.13 Difference (a) and NMI (b) between original Lenna and the public and protected fragment versus 1000 random different keys.

To confirm this result, we also applied the Normalized Mutual Information (NMI) [161] between the original data blocks and public and protected fragments and the obtained results (for 1000 random secret keys: image case in Fig. 5.13-(b), Table 5.1 and text case in Table 5.2; for 100 randomly picked data chunks: video case in Table 5.3) shows that NMI value is always close to 0. Consequently, this indicates that no detectable information can be extracted from the public and protected fragment.

5.3.5 Sensitivity Test

Differential attacks are based on studying the relation between two encrypted data resulting from a slight change like usually one different bit in the original plain-image or in the key. A successful sensitivity test shows how much a slight change will affect the cipher data. In other words, the higher the ciphered data changes when slight change happens in input, the better sensitivity of the encryption algorithm is. Here we analyze different types of sensitivity.

For the **Plain-text Sensitivity**, it is designed that in current version, the very similar blocks will have the very different public and protected fragments due to the randomness introduced by SHA algorithms. In fact, as long as most file transmitted on Internet are compressed and formatted, many same blocks within one chunk are rare to see. For this specific case, a counter (nouce) could be added as the input of the SHA algorithm in Fig.5.4 to generate different output for the same input blocks.

Concerning the **Key Sensitivity** tests, it is one of the most important tests and permits to quantify its sensitivity against any slight change in the secret key. In fact, for the private

fragment, the encryption algorithm used (AES-128) could meet such sensitivity requirement. For the public and protected fragments, to study the key sensitivity, two secret keys are used : SK_1 and SK_2 that differ in only one random bit. The two plain images are processed separately and the Hamming distance of the corresponding public and protected fragments C_1 and C_2 is computed and also for the chosen text file (same methods used in [48]), and illustrated as Table 5.1 (see KS for both cases) versus 1000 tests.

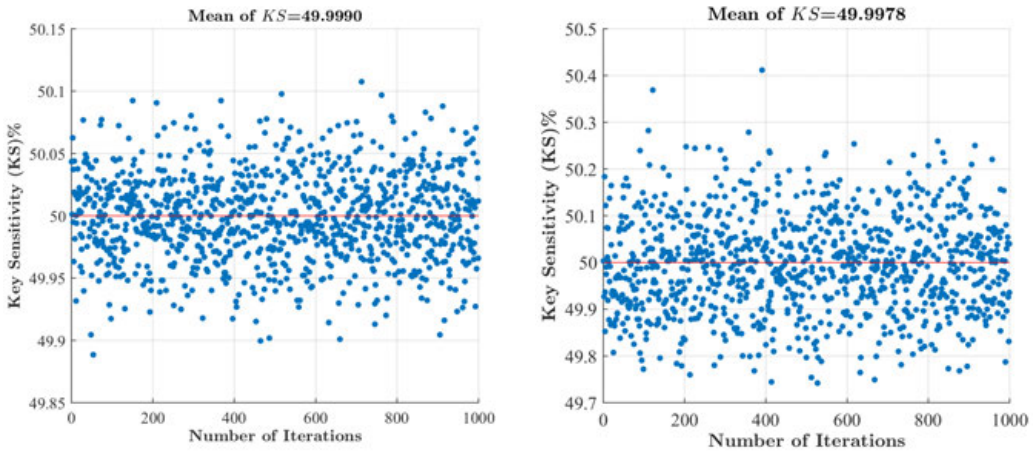

Fig. 5.14 Sensitivity tests for Lenna and text versus 1000 random different keys.

It is seen that the obtained values are always close to the optimal value (about 50% bits changes when 1 bit change in the key) for both input data as shown in Fig.5.14. This indicates that the proposed method ensures high sensitivity against any tiny change in the secret key. Similar results are obtained for the three video files used.

5.3.6 Visual Degradation for images

This test is specific for image that permits to quantify the visual degradation that is reached by employing a protection scheme. In fact, the degradation operated on the original image must be done in way that the visual content presented in the protected image must not be recognized. Two well known parameters are studied to measure the encryption visual quality which are Peak Signal-to-Noise Ratio (PSNR) [73] and Structural Similarity (SSIM) [169].

PSNR is derived from the Mean Squared Error (MSE), while MSE represents the cumulative squared error between two images. A low PSNR value [73] indicates that there is a high difference between the original image and the public and protected fragment.

Concerning SSIM [89], it is defined after the Human Visual System (HVS) has evolved so that we can extract the structural information from the scene. SSIM is in the interval [0,1] and a value of 0 means that there is no correlation between the original image and the public

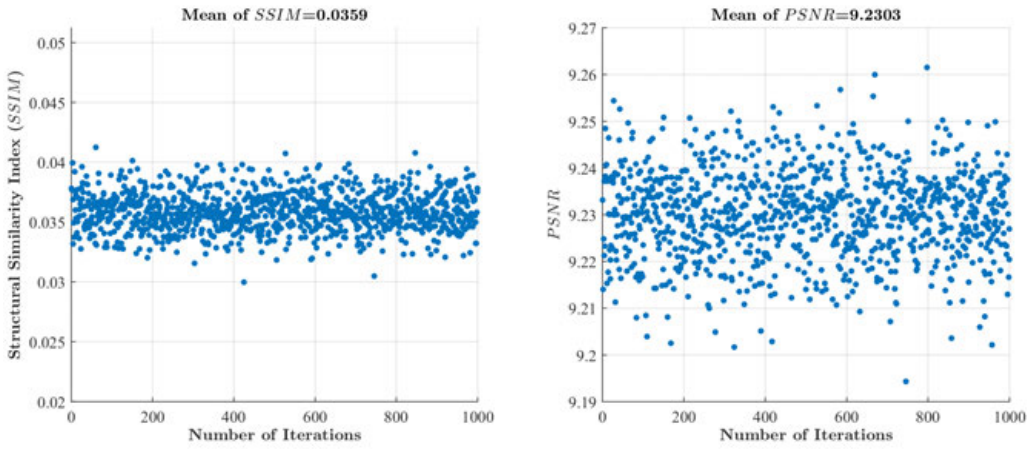

Fig. 5.15 *PSNR* and *SSIM* variation between original Lenna image and the corresponding public and protected fragment versus 1000 different keys.

and protected fragment, while a value close to 1 means that the two images are approximately the same. PSNR and SSIM are measured between the original Lenna image and its public and protected fragment for 1000 different keys and corresponding value distribution presented in Fig. 5.15, respectively. The mean PSNR value is 9.23 dB which validates that the proposed scheme provides a high difference in visual between the original image and its public and protected fragment. Also, the SSIM value did not exceed 0.036, which means that a high and hard visual distortion is obtained.

As a conclusion, the proposed scheme ensures a hard visual degradation. This means that no useful visual information or structure about the original image could be revealed from the protected and public fragments.

5.3.7 Propagation of errors

Indeed, an important criteria that should be ensured for any protection scheme is the error propagation while data is transmitted. The interference and noise in the transmission channel might cause errors. Bit error means that a substitution of '0' bit into '1' bit or vice versa. This error may propagate and lead to the destruction of decrypting data, which is a big challenge since a trade-off between avalanche effect and error propagation are shown in [101]. In this proposal, if a bit error takes place in sub-matrix of the public and protected fragment, the error will propagate randomly only in its corresponding sub matrix and will not affect its consecutive corresponding neighbour sub-matrix. Moreover, as we discussed before, in Fig. 5.4, the 1^{st} public and protected fragment can also be stored locally so when the communication channel is unreliable and transmission error occurs, the 2^{nd} public and

protected fragment are the only one that is affected. In this case, the defragmenting process is the XORing between the correct SHA-512 result of 1^{st} public and protected fragment and 2^{nd} public and protected fragment with errors. Thus, the decrypting 2^{nd} public and protected fragment will have 1 bit error if there is 1 bit error in the transmitted 2^{nd} public and protected fragment. As a result, we can conclude that in such communication channel, this design of dispersion is efficient to prevent the error propagation.

5.3.8 Cryptanalysis Discussion: Resistance against well-known types of attacks

In this subsection, typical published cryptanalytic cases are considered and a brief analysis of the proposed scheme against several cryptanalytic attacks is provided from a cryptanalysis viewpoint. The proposed method is considered to be public and the attacker has complete knowledge to all steps but no knowledge about the secret key.

The strength of the proposed scheme against attacks is based on the existing cipher systems we deployed.

For the private fragment, AES has key space that can be 2^{128}, 2^{192} or 2^{256}, which is sufficiently large to make the brute-force attack almost infeasible. Furthermore, differential and linear attacks would become ineffective. For the public and protected fragments, SHA-256 and SHA-512 guarantee the randomness. In fact, any change in any bit of the secret key causes a significant difference in the produced public and protected fragment as seen in Table 5.1. Hence, a key is used for every block (shown in Fig. 5.4) and as the difficulty of cipher-text-only attack is equal to one of the brute force attacks, it becomes impossible for a cipher-text-only attack to retrieve useful information from the public and protected fragment in our scheme.

For further cases like single plain-text failure and accidental key disclosure, Initialization Vector (IV) could be introduced to generate dynamic keys for each of the chunk. In such case, it is very difficult for an attacker to recover the dynamic secret key that is changed for every input chunk.

With regard to resisting the statistical attacks, the proposed approach achieves that the plain-text are changed in positions and values, which means that the confusion and diffusion properties are ensured in addition. An example is illustrated in Fig. 5.16, where a 8×8 matrix of the original Lenna image and its public and protected fragment are illustrated by values. This result demonstrates that all values are changed. Therefore, the randomness property is ensured and this consequently permits to prevent the reverse-attack algorithm.

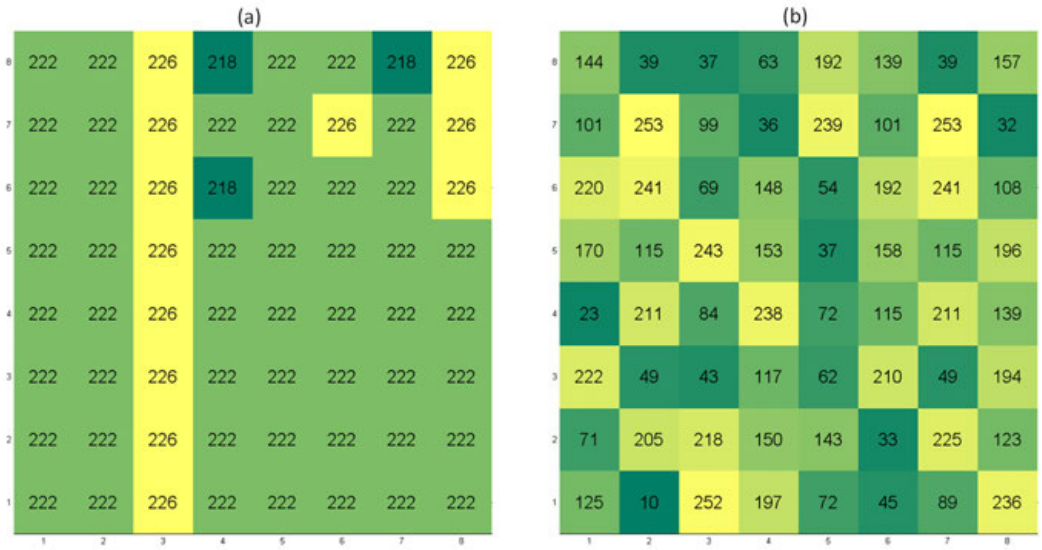

Fig. 5.16 (a) 8×8 cropped plain matrix with its corresponding gray scale matrix, (b) public and protected fragment of this matrix using the proposed scheme with its gray scale value.

More importantly, the spatial redundancy between adjacent elements of input plain data are removed and a high randomness degree of the whole fragment are proved. Different statistical tests such as the entropy analysis, probability density function, correlation tests are applied to validate the independence and uniformity property. Consequently, these results indicate that no useful information can be detected from the public and protected fragment. This validates the robustness of the proposed scheme and their high resistance to statistical attacks.

Moreover, key sensitivity analysis demonstrates the efficiency of the proposed scheme against related key attacks, while any change in any one bit of key provide a different (50%) public and protected fragment.

5.4 Benchmark with two computer architectures

In this section, we evaluate the performance of the whole protection process. As we are considering the allocation of the calculations on a PC platform, the hardware resource we have are a CPU and a GPGPU. However, the very different calculation capacities of GPGPU change the whole execution time of SE [107] [115]. So, the performance is evaluated in two typical use cases that are a laptop equipped with a low-end GPU and a desktop equipped with a high-end GPU.

Table 5.5 Performance evaluation for every calculation tasks of SE for two platforms.

	Input chunk size (byte)	1024×1024	2048×2048	3200×3200	4800×4800
Laptop Scenario	GPU time (DWT-2D)	1.39ms	4.87ms	12.6ms	24.1ms
	GPU time (SHA-256)	0.33ms	1.31ms	3.3ms	7.3ms
	GPU time (SHA-512)	1.45ms	5.8ms	14.2ms	31.8ms
	CPU time (AES-128)	0.29ms	1.14ms	3.06ms	6.67ms
desktop Scenario	GPU time (DWT-2D)	0.34ms	0.79ms	1.7ms	3.3ms
	GPU time (SHA-256)	0.05ms	0.13ms	0.29ms	0.63ms
	GPU time (SHA-512)	0.13ms	0.69ms	1.58ms	3.2ms
	CPU time (AES-128)	0.23ms	0.96ms	2.37ms	5.3ms

The key decision of the design is to distribute the calculation tasks between the GPU and the CPU. As pointed in Section 2.3.2, the DWT-2D, SHA-256 and SHA-512 can benefit from the GPU acceleration, so the design is based on the parallel execution of CPU with GPU while the GPU will take calculation tasks of DWT-2D, SHA-256 and SHA-512 in the process, CPU takes AES-128 for only private fragment. The initial plan for both low-end and high-end GPU cases is to keep the GPU busy and CPU would have time space for other tasks (Fig. 5.17).

For the laptop, there is an Intel I7-3630QM CPU and a Nvidia Nvs 5200M GPU. For the desktop, we have a CPU of Intel I7-4770K and a GPU of Nvidia Geforce gtx 780. In order to verify our initial plan and allocate the right calculation tasks to the right chip, we evaluate each of the tasks on laptop and desktop and results are shown in Table 5.5. For different size of input data chunk, the execution time of GPU for the second input data chunk can always overlap the execution time of CPU for the selected DWT-2D coefficients of the first input data chunk.

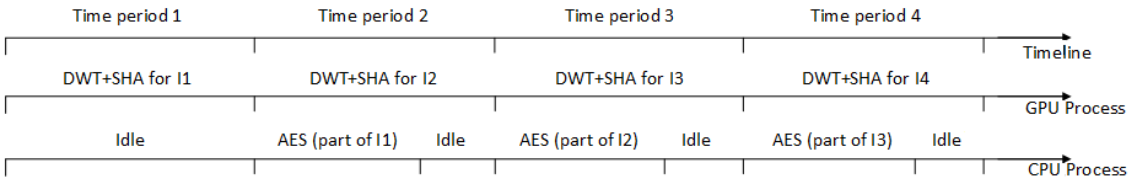

Fig. 5.17 Time overlapping architecture of the implementation.

From the two use cases we evaluated, the overlay design in Fig. 5.17 works. And the speed of the whole SE process relies on how fast the GPU can process its calculation tasks on input data as long as there are many chunks as input. That is to say, in these two scenarios, the time consumed by GPU is evaluated as the benchmark for our SE method. The calculation

speed of our scheme evaluated for this laptop scenario is about 360 MB/s and for this desktop scenario is about 2.8-3.2GB/s.

5.5 Discussion for benchmark

As shown in Table 3.1 in Chapter 3, the desktop GPU we used contains 2304 CUDA cores compared with the 96 CUDA cores on the laptop GPU. It is easy to conclude calculation speed of the desktop GPU is much faster than the laptop GPU which is a common scenario for different GPUs. As a consequence, Speed of the SE method is very different for the two PC scenarios as shown before. This very difference exists on the two typical hardware cases: low-end GPUs normally for laptops and high-end GPUs for desktops or gaming PCs.

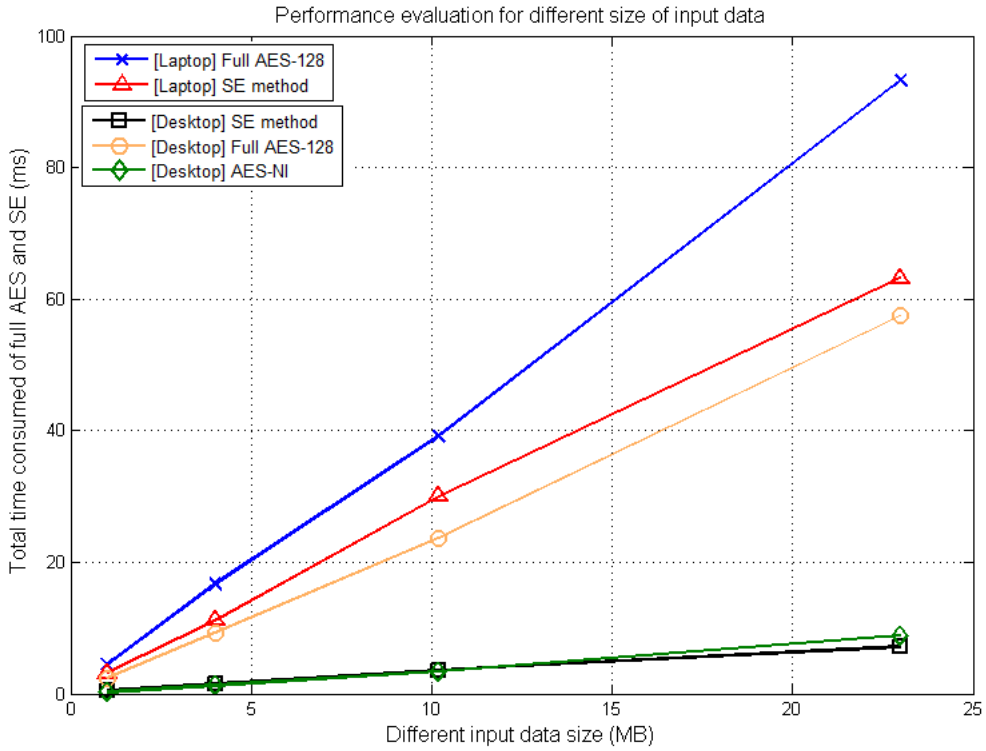

Fig. 5.18 Performance evaluations for SE compared with full AES on laptop and desktop scenarios.

In fact, as long as GPU architectures are rapidly evolving, the hardware configuration of a GPU may strongly influence software applications architectural choices necessary to derive the best possible implementation. This point could even invert the results of our evaluation since a large number of cores could very well favor the GPU calculation tasks that finally

change the overlay design. Also as pointed by [66], when a GPU calculation capacity is very high, bottleneck of the process is the memory transfer between the GPU memory and the host memory instead of calculation speed itself. This is mainly due to the limitation of transmission speed through the PCIE bus (Peripheral Component Interconnect Express [20]) between host memory and GPU memory. This problem can be avoided by arranging more calculation tasks on GPU instead of too much I/O usage or overlapping the transmission by execution time.

Here we presented the comparison of the SE method with the traditional CPU-only AES-128 speed ([37]) in Fig. 5.18. It is worth noticed that [17] pointed out that the CPU-only AES could also be very fast with the support of the New Instructions extension (NI) brought by Intel. This AES-NI could accelerate the AES on CPU for more than 5 times and achieve almost 3GB/s on a NI-enable CPU (shown in Fig. 5.18) which is almost the same speed as our method based on GPGPU. However, as pointed out in the Nvidia white paper [109], the Nvidia GeForce 1080 GPU (released in 2016) is already three times faster than the GPU used in this thesis (Nvidia GeForce 780, released in 2013), it is only fair to say the performance gain could be larger with employing the start-of-the-art GPGPU. Such rapid evolving in hardware is not seen in recent years' CPU manufacturing. In conclusion, our design on GPU could always achieve better performance than AES-NI on CPU with fair hardware.

5.6 Fragment transmission

This data protection method can be also used for secure data transmission and sharing between end-users. This design could generates three fragments for data sharing for each of the data chunk as shown in Fig.5.19. For the *private fragment*, the encryption algorithm used in this particular design is AES-128 (could be easily replaced by AES-NI with a NI-enabled CPU or any other encryption algorithms). This *private fragment* is the only fragment that is directly transmitted between end-users. The other two *protected and public fragments* are transmitted through the public cloud servers without leaking information. The storage space that the *private fragment* takes is 7.8% of the original data size, while the 1^{st} *and* 2^{nd} *protected and public fragments* take 24.2% and 93.8% of the original data storage space respectively.

Although the total data storage space usage is about 25% larger than the original one, the local storage space usage is only 7.8% which highly reduces the local storage usage and exploit the convenience brought by the Cloud servers with both efficiency and security.

Fig.5.20 gives an example for using this method for data sharing between end-users. The sender processes the fragmentation and protection before sending to the Clouds. The 1^{st} *and*

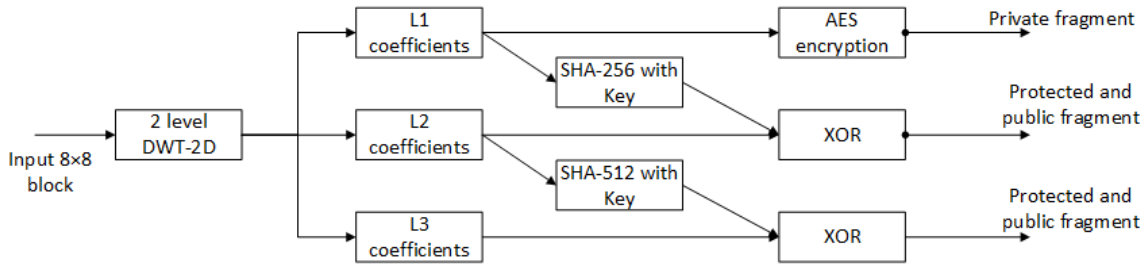

Fig. 5.19 Three fragments from one data chunk for further securing data sharing.

2^{nd} *protected and public fragments* will be sent to different Cloud servers and be available for any receiver to download at anytime. The *private fragment* will be sent through direct communication channel between senders and receivers.

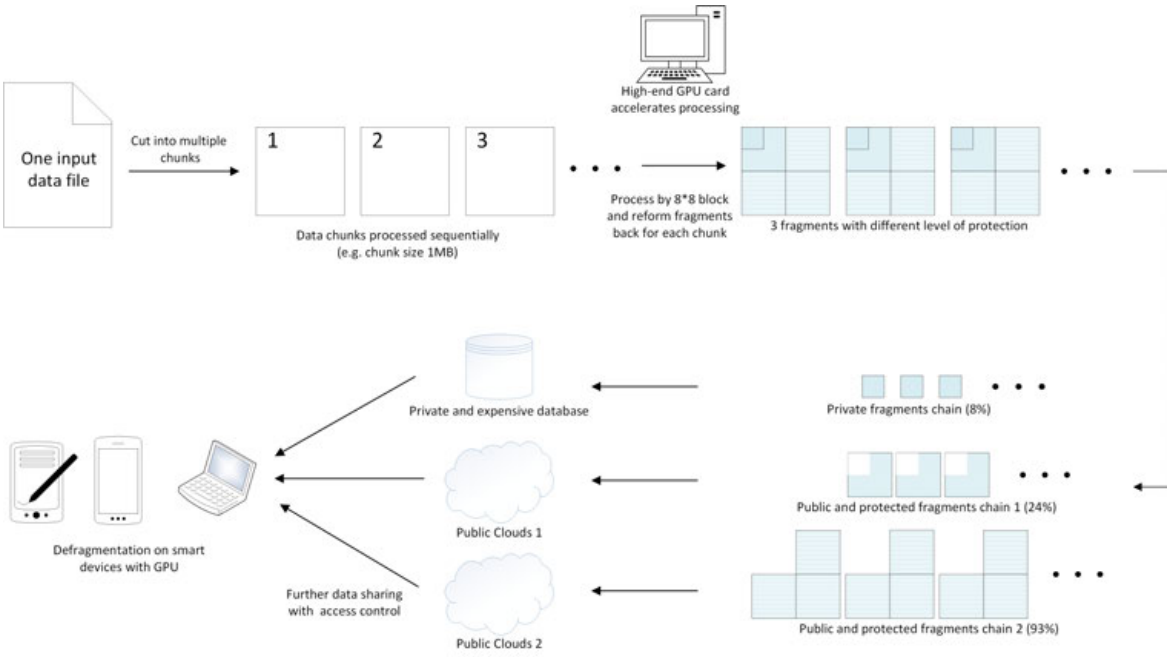

Fig. 5.20 Use case: secure data sharing between end-users through different Cloud servers based on fragmentation and dispersion.

The first advantage of this design is to largely reduce the local storage space usage while providing security and privacy for the end-user. This is specially useful in some use cases like when the end-user device is a mobile phone (local storage space is limited and expensive compared with the free large Cloud storage space). The second one is to efficiently process the fragmentation and protection solely on end-user's device which avoid any plain data transmission on insecure channel and could avoid using specific service provided by server end like BlackBerry Enterprise Server (BES) [25]. More importantly, as pointed out by [27]

and [185], DWT could be accelerated by mobile GPU which allows possible usage of this scheme in future when GPGPUs are largely deployed on smart phones.

Chapter 6

Conclusion and future work

In this thesis, a data protection scheme combining fragmentation, encryption and dispersion is presented based on improvement of selective encryption algorithms. In the past two decades, most SE algorithms, were initially dedicated to SE specific multimedia. They are based upon one of the steps for formatting compressing the content (transformation, encoding, and packeting).

From previous works, SE methods provides mainly more efficiency compared with traditional full encryption methods by protecting only a part of original data. However, this thesis points out that SE methods do not always provide efficiency considering the rapid evolution of both algorithms and hardware (pointed out in Chapter 3). Thus, an architecture according to existing different hardware configurations (the recent evolvement of hardware should be considered to fit in the frame and the scheme has the adaptivity for very different environments) is discussed including a flexible software architecture (the algorithms deployed could be easily replaced by the new ones while the main framework of the scheme remains the same).

In Chapter 4, two levels of Bitmap protection schemes are presented both using DCT 8×8 preprocessing and GPGPU acceleration. We defined a first level of lightweight protection with a very fast speed and a second level of strong protection with a good protection quality. For the second level of protection, many detailed designs are implemented for less information loss and avoiding recursive rounding error which improved the previous bitmap-related SE methods. Fragmentation is used in this scheme with an additional optimized memory allocation and transmission.

In Chapter 5, an agnostic SE architecture is presented based on lossless DWT 8×8 preprocessing. The initial motivation of this architecture is to solve the question of integrity for bitmap images. Then we realized that this method could deal with text format. And we

verified that in fact it is agnostic with regard to the format of the information to be protected at the difference of any SE method that we have been able to see in the current literature.

The proposed architecture employs the AES encryption algorithm to protect the private fragment that will be stored locally in the use case. It can be easily replaced by using other encryption algorithms like AES-NI instead. For the other fragments, SHA algorithms are used to produce a key-stream that will be employed to encrypt the public and protected fragment by mixing them. The SHA will guarantee the randomness of the key-streams generated even from the very similar neighbour 8×8 blocks which can provide the needed protection for the public and protected fragments.

More importantly, GPGPU is employed to reduce the overhead of applying the optimization DWT-2D operation, and sometimes both the AES and SHA operations. The architecture is flexible for different hardware configurations with the pure GPGPU experimentation and CPU with GPGPU overlay design. In order to validate that the proposed design can ensure the required goals, a benchmark was realized between the proposed experimentation and a full AES encryption for different kinds of data on two very different hardware platforms. And several experimental and theoretical security analysis were realized to prove the security, robustness and resistance against error propagation.

Therefore, the proposed solution can be considered as an agnostic selective encryption algorithm candidate that can be applied for most computer distributed systems in particular, we can use this method to store large amount of data in public clouds in a secure manner.

For future work, we propose considering to reconsider the design for redefining the important private fragment. According to recent work, the low frequency coefficients in transformations (like DWT 8×8 used in this thesis) are not necessarily more "important" than the high frequency coefficients. In fact, for agnostic fashion data protection schemes, a practical way to measure the importance of transformation coefficients is to calculate the influence of input values to the coefficients. For instance, some low frequency coefficients are related to only a small subset of input values (the change of rest input values will not lead to the change of these low frequency coefficients) while some high frequency coefficients can be related to more input values. This fact would give us a hint about how to define more "important" fragments by choosing those coefficients that are related to all input values ignoring how low or high frequencies are.

Regarding the implementation aspect, the non-general-purpose mobile GPU platforms should be experimented to fit the architecture of the proposed agnostic SE method to achieve both performance efficiency and energy saving purposes on today's smart phones. And, of course, more kinds of personal computer GPGPU platforms (such as multiple CPUs or GPGPUs platforms or newest generation hardware) should be experimented with deriving a

general solution for the allocation between CPUs and GPGPUs. As pointed out in former discussion, the evolution of hardware configuration never stops and sometimes the deployment of new hardware would totally change the software design.

At last, there are some future work regarding fragment dispersion and transmission with an environment based on user device and public and clouds. More standards like availability, data recovery should be taken into consideration for a more adaptable architecture.

Chapter 7

Résumé

7.1 Introduction

Au cours des deux dernières décennies, les données numériques ont augmenté en volume avec une vélocité sans précédent envahissant tous les domaines de l'activité humaine. En 2008, International Data Corporation (IDC) estimait à $2,25 \times 10^{21}$ le nombre de bits créés [12]. Ce montant dépasserait 6×10^{23} bits d'ici 2023. Plus important encore, les derniers progrès de la technologie de l'information et de la communication (TIC), incluant ordinateurs, téléphones intelligents ou tablettes, permettent désormais aux utilisateurs non professionnels de très facilement créer leur données et de les communiquer largement. Par exemple, de nos jours, 72 heures de vidéos sont téléchargées sur YouTube en moyenne chaque minute [103]. Les données générées, traitées, transmises et distribuées sont massives sur Internet et nécessitent d'être protégées avec des niveaux de protection variables.

Les machines multi-cœurs parallèles à grande échelle ainsi que les ordinateurs personnels de plus en plus efficaces et de cout de plus en plus abordables progressent continuellement et sont developpés et construits pour servir à acquérir, transmettre, stocker et calculer des données numériques. Une des avancées les plus remarquable a été de savoir assembler des serveurs pour construire un cluster informatique à très grande échelle pour le service de données massives à des couts étonnamment bas pour l'utilisateur. Le principal avantage du Cloud est d'offrir des services élastiques, tolérants aux pannes, avec des performances élevées à des coûts incomparablement réduits par rapport à une solution privée. De plus, cette technologie fournit à la demande des ressources de calcul et de stockage presque infinies pour les utilisateurs individuels et les entreprises en louant à distance des ressources matérielles (le plus souvent un nombre de processeurs par heure et un espace de stockage par jour). Par conséquent, les utilisateurs de cloud apprécient la variété des services de cloud (par exemple

les désormais classiques Data as a Service (Daas), Software as a Service (SaaS), Platform as a Service (PaaS), Infrastructure as a service (IaaS), etc.).

La tendance de ces dernières années consiste à externaliser le stockage et le traitement de l'information vers des services basés sur le cloud. En particulier, les services de stockage de données basés sur le cloud à destination des utilisateurs individuels gagnent en popularité. S'appuyant sur un grand espace de stockage gratuit et un canal de communication fiable, les fournisseurs de services basés sur le cloud comme Dropbox, Google Drive offrent aux utilisateurs individuels un espace de stockage quasi infini et à faible coût.

Cependant, cette situation soulève la question de confiance en des fournisseurs de services qui peuvent être "honnête mais curieux". En fait, de nombreux incidents de sécurité et de confidentialité sont observés dans les systèmes basés sur le Cloud. Certains de ces incidents sont répertoriés dans [188]:

• Steven Warshak arrête les perquisitions secrètes et les saisies répétées du gouvernement de son courrier électronique stocké en utilisant la loi fédérale sur les communications stockées (SCA) en juillet 2007.

• Un employé de Salesforce.com a été victime d'une attaque de phishing et a divulgué une liste de clients, ce qui a généré d'autres attaques de phishing ciblées en octobre 2007.

• Google Docs a détecté une faille qui partage par inadvertance les documents des utilisateurs en mars 2009.

• Epic.com a déposé une plainte officielle auprès de la FTC contre Google pour ses pratiques de confidentialité en mars 2009. EPIC a réussi une action contre Microsoft Passport.

• Yahoo a confirmé qu'au moins 500 millions de comptes d'utilisateurs ont été volés sur le réseau de l'entreprise fin 2014 suivant une attaque de 2013 sur 1 milliard de ses utilisateurs.

• Equifax a déclaré avoir perdu les données personnelles de 143 millions personnes début 2017.

La plupart de ces incidents sont dus à une exploitation malveillante d'erreurs humaines [129]. De plus, les fournisseurs de cloud eux-mêmes peuvent être "honnête mais curieux" et ont acces aux données stockées par leurs clients. En 2013, le programme de surveillance PRISM [54] a été exposé. Dans ce programme, la NSA a obtenu un accès direct aux systèmes de Google, Facebook, Apple et d'autres géants américains de l'Internet, ce qui rendait la confidentialité des données de chaque utilisateur vulnérable. Cela est dû au fait que les données transmises au cloud seront traitées par le Cloud lui-même. La situation pourrait être encore pire dans certains cas spécifiques comme le chiffrement d'externalisation montré dans [176] (le client doit externaliser des images protégées à d'autres utilisateurs via un canal non sécurisé mais n'a pas suffisamment de puissance de calcul ou d'énergie pour exécuter le

chiffrement). Ainsi, il devient de plus en plus important pour les utilisateurs de protéger leurs données personnelles (textes, images ou vidéos) non seulement de façon efficace mais surtout indépendamment du fournisseur de services de stockage. Une solution naturelle consiste à protéger les données en les chiffrant localement sur la machine d'un utilisateur final avant de les envoyer aux serveurs Cloud. Cela suffirait à rendre un premier niveau de protection indépendant du fournisseur de services.

Ainsi, dans ce travail, une hypothèse de base est que les fournisseurs de services Cloud ne peuvent pas être entièrement tenus responsables de la protection de données personnelles. Nous supposons qu'un logiciel «hon curieux» ou «malveillant» se trouve sur au moins un serveur Cloud et qu'il est capable d'observer toutes les données stockées dans le Cloud et qu'il incombe à l'utilisateur final de faire en sorte que sa machine locale soit digne de confiance.

Les systèmes de chiffrement comme les systèmes de chiffrement à clé symétrique standard (par exemple 3DES, ou son successeur AES, etc.) fonctionnent avec l'hypothèse que les données sont des séquences de symboles relativement indépendantes et identiquement distribuées (iid) et que les données doivent être décrypté avec précision. Cela ne s'applique pas de manière générale à tout format de données: on sait que les pixels de photos ou de video sont fortement corrélés avec leurs voisins et qu'il existe également une forte corrélation inter-image bien connue dans une trame video. Les redondances spatiales ou temporelles de ces données multimédia ne sont pas suffisamment exploitées par les méthodes de chiffrement traditionnelles, car ces dernières se sont essentiellement focalisées sur la protection de données textuelles. Par exemple, le besoin de précision n'est pas aussi critique pour des images de qualité moyenne: les utilisateurs peuvent tolérer un léger niveau de distorsion lors du déchiffrement d'une image avec une exigence modérée sur son rendu [80]. Un autre problème est que les méthodes de chiffrement traditionnelles ne suffisent pas à complètement protéger une image: par exemple, une image cryptée au moyen d'AES peut laisser percevoir une information sur la structure d'une image (voir Fig. 1 de [64]) .

D'autres méthodes de protection des données telles que le chiffrement sélectif (SE) ont été publiées au cours des dernières décennies. L'objectif est d'exploiter des redondances spéciales de données multimédia et de s'appuyer sur des algorithmes et transformations utilisés pour la compression d'images. Les différents SE publiés sont généralement dédiés à la protection d'images ou de vidéos où ils supportent la séparation automatique de l'image ou de la vidéo en deux fragments: un fragment reste «privé» contenant la plupart des informations pour que ce fragment soit suffisant pour comprendre l'image originale, un second fragment que nous appelons «public» et qui est censé contenir une quantité beaucoup plus petite d'information de sorte que ce fragment n'est pas exploitable. Ces deux fragments

sont protégés en utilisant différentes approches en fonction de leurs niveaux respectifs d'importance ou de confidentialité. L'état de l'art dans les méthodes de chiffrement sélectif montre que toutes ces méthodes proposent d'obtenir un fragment privé de petite taille comparé au contenu original [101] et dans certains cas de lui appliquer un chiffrement léger et rapide comparé à un chiffrement complet. Il en résulte un double avantage: on protège la donnée de façon très rapide et économique comparée à un stockage entièrement privé sensé être plus cher qu'un stockage sur Cloud. Ceci dit, cela soulève un premier problème consistant à déterminer le fragment privé optimal qui, d'une part, mérite une forte protection (sur support privé) et, d'autre part, est d'aussi petite taille que possible. Ensuite, nous sommes confrontés à un deuxième problème consistant à nous assurer que le faible niveau de protection que nous appliquons au fragment public empêchera bien toute fuite d'information.

Bien que les méthodes SE soient plus appropriées pour les données multimédia dans certains cas, il existe des limitations, par exemple, la plupart des méthodes SE sont spécifiquement liées au format des données (bitmap, jpeg) qu'elles traitent voire intégrée à une méthode de compression spécifique. Plus important encore, certaines données volumineuses transmises aujourd'hui ne sont pas compressées ou ne peuvent pas être compressées pour enregistrer des espaces de stockage comme une image de système d'exploitation. Il n'est pas efficace d'exploiter de nombreuses méthodes SE en fonction de nombreux formats de données multimédias différents. Ainsi, un défi surgit: est-il possible de concevoir une méthode SE efficace qui puisse généralement s'adapter à tout type de formats de données et garantir non seulement la sécurité mais aussi l'intégrité des données lors de leur déchiffrement?

7.2 Motivations

Comme indiqué précédemment, l'externalisation du stockage et du traitement des informations, les services basés sur le cloud pour le stockage de données ont gagné en popularité et peuvent aujourd'hui être considérés comme généralisés. Ils attirent des organisations ou des entreprises, en particulier les utilisateurs individuels qui ne veulent pas ou ne peuvent pas faire face au coût d'un nuage privé. Outre le facteur économique, les deux catégories de clients subordonnent leur choix d'un fournisseur de cloud adéquat à d'autres facteurs, en particulier la résilience, la sécurité et la confidentialité.

Renforcer la protection des données à l'aide d'une suite de fonctions devient de plus en plus important lorsque l'on considère des attaques continuelles et puissantes pour copier, espionner, modifier ou même détruire des informations. Même si la théorie des codes et la cryptologie progressent rapidement, le chiffrement doit être associé à d'autres techniques pour progresser avec cette question sans doute insoluble. C'est l'un des principes à la base

d'un certain nombre de projets comme le système Potshards [147]. De manièren parallèle la crypanalyse ainsi que la puissance de calcul des serveurs progressent également faisant qu'un niveau de chiffrement suffisant à moment donné paut ne pas le rester [106]. Dans [2], les auteurs ont montré comment compromettre les sites https avec un groupe de 512 bits; les auteurs ont même suggéré que le chiffrement à 1024 bits pourrait être cryptanalysé avec suffisamment de puissance de calcul. Enfin, il reste la difficile question de la gestion de la clé de chiffrement qui au fil du temps, peut être connue par trop de gens, volée ou perdue.

L'un des objectifs et des ambitions ultimes est de considérer la protection des données et la vie privée de bout en bout en combinant la fragmentation, le chiffrement et la dispersion [105, 104]. Cela signifie de dériver des schémas généraux et une architecture pour protéger les données pendant tout leur cycle de vie partout où ils vont dans un réseau de machines où ils sont traités, transmis et stockés. De plus, il s'agit d'offrir aux utilisateurs des choix parmi divers niveaux de confidentialité et de sécurité bien compris et rentables qui s'accompagneraient de niveaux prévisibles de performance en termes d'occupation de la mémoire, de consommation d'énergie et de temps de traitement. Afin de fournir une méthode pratique de protection des données pendant leur stockage, nous établirons une série d'hypothèses pour l'environnement matériel et logiciel dans lequel les utilisateurs finaux disposent d'un environnement personnel limité en ressources, comme les ordinateurs portables ou de desktop. De plus, le temps d'exécution doit être comparable aux algorithmes de chiffrement complets traditionnels. Pour vérifier ce point, nous devrons configurer un benchmark.

Usuellement, la fragmentation est largement utilisée à des fins de résilience. Dans [128], l'un des premiers résultats sur la fragmentation pour la tolérance aux pannes et la protection des données est trouvé. Dans [75], les auteurs abordent cette question en utilisant un algorithme de Reed Solomon basé sur la théorie des codes [130] pour éviter la simple duplication et gagner en consommation mémoire. En résumé, la fragmentation consiste à séparer les données à l'aide d'algorithmes plus ou moins complexes à des fins de résilience. Dans cet article, le concept de fragmentation est introduit afin de contribuer à la protection de données. De plus, nous séparons les données de telle manière qu'il soit possible de protéger les fragments différemment selon leur niveau de confidentialité ou de criticité. Ensuite, ces fragments doivent à leur tour être stockés dans différents emplacements physiques de manière plus ou moins sophistiquée afin d'augmenter le niveau de protection pour l'ensemble de l'information.

La fragmentation permet, par définition, de paralléliser transformations et chiffrements, ce qui permet de s'attendre à un gain d'efficacité important par rapport à un chiffrement

complet exécuté séquentiellement. La défragmentation pourrait alors suivre un modèle parallèle inverse.

Nous considérons un cas d'utilisation relativement simple: un utilisateur final (Alice) veut sauvegarder ses données multimédia dans un cloud public afin d'économiser de la mémoire dans son environnement privé à ressources limitées (un ordinateur desktop, un ordinateur portable ou même un smartphone), cependant, pour des raisons de confidentialité, elle hésite à mettre toutes ses données dans les mains d'un seul fournisseur de stockage. En d'autres termes, Alice désire utiliser une méthode ayant à la fois des performances raisonnables et permettent de stocker la majeure partie de ses données sur cloud tout en gardant une partie résiduelle sur son environnement privé à ressources limitées.

Nous présentons d'abord le travail relatif principalement à la notion de méthodes de chiffrement sélectif (SE pour Selective Encryption) conçues pour des contenus multimédias spécifiques. Le problème de performance et plusieurs limitations sont donnés pour illustrer la faiblesse de la plupart des méthodes SE. Puis nous présentons l'idée d'utiliser l'unité graphique à usage général (GPGPU) qui est originale pour les méthodes SE. Un GPGPU se comporte comme un accélérateur pour les méthodes particulièrement bien adaptées que nous avons conçues. Cependant, programmer sur GPGPU présente aujourd'hui un important problème de portabilité que nous allons discuter. Un premier cas de protection d'une image bitmap est considéré. Tous les détails de conception et de mise en œuvre sont donnés avec des évaluations de référence. Enfin, nous proposins une méthode plus sophistiquée pour adresser le besoin de traiter les données de manière agnostique en fonction de leur format. Pour chaque méthode, nous analysons en détail les problèmes de performances, de sécurité et d'intégrité et décrivons comment nos méthodes SE peuvent être utilisées pour stocker en toute sécurité des fragments importants de données dans des systèmes de stockage publics. Ensuite, nous concluons en évoquant des travaux futurs.

7.2.1 Evaluation de peerformance et définition d'un benchmark

Définir un benchmark est une opération critique car il permet de justifier un argument clé [121] pour développer des méthodes de protection sélective. Il y a très peu de travaux publiés qui étudient de manière approfondie et convaincante les performances des méthodes SE existantes [77]. Une raison principale est que certains travaux SE sont intégrés dans les algorithmes de compression ou d'encodage qui autorisent les auteurs à simplement ignorer les délais possibles causés par la première étape des méthodes SE puisqu'ils sont partagés avec les fonctions de compression. De plus, la plupart des méthodes SE ne sont pas comparées aux algorithmes de chiffrement traditionnels comme AES mis en œuvre avec du matériel ou des logiciels de pointe, ou ne tiennent pas compte de l'énorme progression des performances

causée par l'évolution constante du matériel. La nécessité de réaliser régulièrement un benchmark est ainsi renforcée par la progression rapide en particulier les architectures GPU et également avec les implémentations logicielles de méthodes de chiffrement complètes (par exemple, il y a une nette accélération de AES à AES-NI [17]). Ces changements d'architecture matérielle et d'algorithmes logiciels peuvent très bien changer le classement en treme de performance des différentes méthodes et finalement, changer la décision de l'utilisateur final. C'est pourquoi nous prêtons attention à la mise en œuvre de ces méthodes et les testons sur différents environnements matériels avec une implémentation adaptée (et par conséquent non portable). Par exemple, nous devons reconnaître que les performances d'une implémentation GPU ne sont accessibles qu'en considérant son architecture particulière comprenant son nombre de coeurs. En fait, une implémentation particulière pourrait atteindre les meilleures performances sur une plateforme donnée mais pas sur une autre. [37].

De plus, il est facile de supposer que le chiffrement d'une petite partie des données devrait être plus rapide que le chiffrement complet (de toute la donnée). Cependant, le gain en performance n'est pas si évident, car cette approche nécessite d'ajouter une phase de pré-traitement d'analyse et de division des données qui pourrait conduire à des performances globales moins bonnes que le chiffrement complet. Nous proposons de mesurer les performances de ces méthodes du point de vue de l'utilisateur final: du moment où il commence l'opération de protection jusqu'au moment où ses données sont protégées (de bout en bout) et ainsi de comparer la méthode avec un chiffrement complet (aujourd'hui, AES) - Bien sûr, ce benchmark doit utiliser un matériel similaire.

les performances sont un facteur clé pour déterminer si la méthode SE est pratique. Les changements possibles causés par l'évolution du matériel et l'optimisation logicielle doivent également être pris en compte et discutés, car ils peuvent modifier l'architecture globale. En résumé, nous montrons la possibilité d'utiliser les méthodes SE d'une manière pratique plutôt que de donner une solution ultime impossible à prédire tant les progrès des architectures de GPU sont importantes aujourd'hui.

7.2.2 Analyse de sécurité

La plupart des articles décrits dans [101] ou que nous avons abordés dans [104] s'intéressent principalement au niveau dégradation visuelle apportée par la méthode de protection. C'est une question légitime dans le cadre de la protection d'une image de qualité moyenne. Aussi analysons-nous cette possible dégradation pour le format bitmap dans une première méthode de protection. Cependant, pour des méthodes SE qui se voudraient agnostiques la restitution ne doit plus tolérer de distorstion par rapport aux données originales. La résistance aux attaques est bien évidemment un autre argument clé, même si un certain nombre d'auteurs

acceptent de présenter SE comme un compromis entre sécurité et performance et classent SE comme un processus de sécurité légère. Avec l'analyse de la dégradation visuelle s'ajoutent alors un nombre d'analyse destinées à monter qu'un fragment contient une information difficile à décrypter ainsi sont menées: une analyse statistique basée sur l'analyse de fréquence, une analyse de corrélation, une analyse d'entropie, une analyse différentielle et l'éventualité d'un effet avalanche est également analysé.

En fait, il y aura des fragments avec différents niveaux de sécurité et dispersés sur des emplacements différents. Pour le fragment le plus important, la méthode de protection est le cryptage complet traditionnel (peut être facilement remplacé par d'autres méthodes de protection) et le lieu de stockage est considéré comme sécurisé, de sorte que l'analyse de sécurité est omise. Les fragments qui sont transmis et stockés sur les serveurs Cloud sont la partie qui nécessite une analyse de sécurité.

Nous présentons les différernts résultats d'analyse de sécurité dans des tableaux pour des tests répétés plusieurs fois. Tant que différents formats de fichiers sont utilisés, certains critères tels que PSNR et SSIM juste pour les images ne sont pas utilisés pour d'autres formats de données tels des textes. Et certaines données multimédias compressées sont également utilisées pour le test, mais seulement avec une analyse statistique générale.

En résumé, tous les objectifs fondamentaux de l'analyse de sécurité sont de prouver quel que soit le format de données utilisé, les données après chiffrement doivent être aussi proches que possible des données aléatoires idéales. Et comme le chiffrement avec clé est utilisé pour la protection des données stockées localement, l'analyse de sensibilité de la clé est également nécessaire pour prouver la résistance aux attaques telles que l'attaque en texte brut.

7.3 Contexte de l'informatique parallèle

Les processeurs GPU ont été spécialement conçus et adaptés au rendu sur écran et à d'autres applications graphiques pour les données multimédia. Cette catégorie d'applications a su utiliser l'architecture dite SIMD (single-instruction-multiple-data) comme modèle d'exécution emprunté aux ordinateurs vectoriels [11] construits dans les années 1970.

Au cours de cette dernière décennie, motivé par les besoins des applications multimédias, en particulier l'industrie du jeu et les besoins d'accélération de certaines applications, le GPU a été développé avec des mises à jour rapides de matériels et des adaptations logicielles continuelles [115]. Aujourd'hui, presque tous les ordinateurs personnels sont équipés d'une GPGPU haute performance capable d'accélérer toute application de type vectoriel.

De nos jours, les GPU hautes performances sont courants non seulement sur les postes de travail professionnels, les serveurs ou les superordinateurs, mais aussi sur les smartphones avec bien sur des capacités adaptées.

7.3.1 Du GPU au GPGPU

Initialement pilotée par des besoins spécifiques pour les applications de visualisarion et de jeux, la capacité de calcul des GPU est principalement à fonction fixe. Depuis 2006, comme indiqué par [115], le GPU est devenu un puissant processeur programmable et l'évolution du GPU s'est concentrée sur les aspects programmables du GPU. La capacité de calcul est devenu de plus en plus diverse ouvrant des possibilités d'utilisation des GPU comme accélérateurs pour le calcul des tâches liées particulièrement au calcul vectoriel.

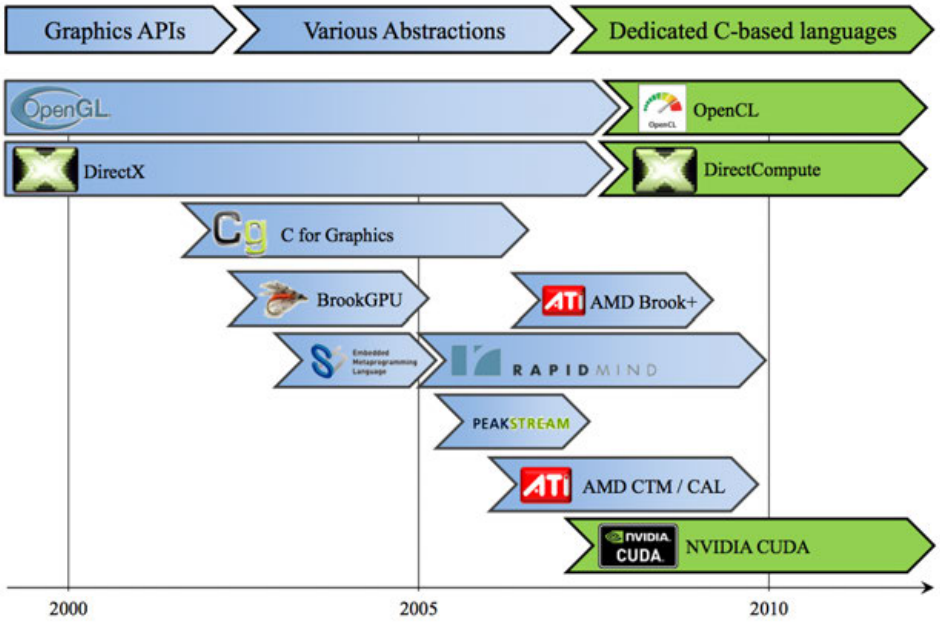

Fig. 7.1 Evolution des langages de programmation GPU. Initialement: depuis 2007 usage général CUDA, DirectCompute et OpenCL sont apparus. [19]

Dans les premiers temps de la programmation, des APIs spécifiques aux applications graphiques tels que OpenGL [172] ou DirectX [65] étaient utilisées pour effectuer des calculs. En 2003, certaines parties du pipeline de fonctions fixes des GPU sont devenues programmables avec la sortie du GPU NVIDIA GeForce 256 et C pour le langage graphique [49] (voir Fig. 7.1).

En 2006, les GPU ont commencé à prendre en charge un nombre arbitraire d'opérations directes et indirectes de la mémoire globale (texture), ce qui rend le calcul de précision

simple beaucoup plus facile à accélérer . Depuis lors, la conception des GPU se concentre de plus en plus sur les unités programmables dans les cœurs graphiques et au lieu d'être considérée comme un pipeline à fonction fixe, les GPU ont commencé à être décrits comme un moteur programmable supporté par un grand nombre d'unités à haute performance. .

En 2007, NVIDIA publie le premier langage de programmation pour GPU à usage général, (CUDA [110]). En outre, comme indiqué dans Fig. 7.1, deux autres outils de CUDA ont émergé: OpenCL (successeur d'OpenGL) et DirectCompute (successeur de DirectX).

Depuis, le développement de GPGPU est entré dans une nouvelle ère où la conception du matériel GPU est à des fins généralistes avec un modèle et une plate-forme parallèles donnant aux programmeurs un accès direct au jeu d'instructions virtuel GPU, aux éléments de calcul parallèles et aux opérations de mémoire arbitraires. Il est possible d'implémenter et d'optimiser des tâches de calcul complexes à très bas niveau sur GPU et les recherches récentes montrent que le gain de performance par rapport au CPU augmente très rapidement [19].

7.4 Chiffrement sélectif basé sur DCT pour les bitmaps

Dans cette section, les méthodes améliorées de chiffrement sélectif sont représentées en fonction de l'accélération DCT dûe à l'utilisation d'un GPGPU. Il y a deux niveaux de conception avec un but différent. Tout d'abord, la protection bitmap liée DCT est introduite. Il est souligné que des coefficients de DCT à haute fréquence pourraient être utilisés pour récupérer une partie du contenu. Ensuite, le problème de performance mentionné au chapitre 2 est résolu en utilisant GPGPU comme accélérateur matériel. Les deux niveaux de notre conception sont décrits avec beaucoup de détails pour garantir la perte mineure de qualité d'image. Ensuite, l'analyse de sécurité est présentée. Enfin, l'allocation de calcul pour l'accélération de la vitesse du processus est présentée pour intégrer les conceptions dans deux plates-formes matérielles différentes typiques.

7.4.1 Transformée DCT

La transformée en cosinus discrète (DCT) est proche de la transformée de Fourier, et a d'abord été proposée par [4]. Le but de DCT est d'effectuer une décorrélation du signal d'entrée et de présenter la sortie dans le domaine fréquentiel. Par rapport à la transformée de Fourier, qui représente un signal en tant que combinaison de sinus et de cosinus, DCT n'effectue que l'expansion en série cosinus.

DCT est largement utilisé dans de nombreux algorithmes de chiffrement sélectif ([28], [154], [165], [173], [74]). La raison pour laquelle DCT est utilisé dans de nombreuses méthodes SE est que DCT lui-même est largement utilisé dans les algorithmes de compression de contenu multimédia. Et DCT n'a que les coefficients cosinus qui lui permettent de faire correspondre des nombres réels à des nombres réels. Comparé à DCT, l'algorithme FFT a toujours des nombres complexes qui sont plus difficiles à stocker et à traiter. La deuxième raison est que la DCT est connue pour sa propriété de «compaction énergétique» très élevée, ce qui signifie que les coefficients de basse fréquence transformés sont très grands et que les coefficients de haute fréquence sont relativement très petits. En conséquence, ces résultats transformés peuvent être facilement compressés en utilisant la quantification pour ne conserver que quelques composants basse fréquence.

DCT a différentes versions décrites dans [79]. L'algorithme DCT le plus populaire est la variation symétrique bidimensionnelle de la transformée qui fonctionne sur des blocs 8×8 (DCT 8×8) et son inverse (iDCT 8×8). Ce DCT 8×8 est utilisé dans les routines de compression JPEG [164] et est devenu un standard important dans les algorithmes de transformation d'image et de vidéo et dans bien d'autres domaines. Le signal d'entrée bidimensionnel est divisé en l'ensemble des blocs 8×8 qui ne se chevauchent pas et le calcul pour un bloc bidimensionnel DCT 8×8 est défini comme suit:

$$C(u,v) = \alpha(u)\alpha(v) \sum_{x=0}^{7} \sum_{y=0}^{7} f(x,y) \cos\left[\frac{\pi(2x+1)u}{16}\right] \cos\left[\frac{\pi(2y+1)v}{16}\right] \tag{7.1}$$

L'inverse de DCT bidimensionnel 8×8 est défini comme:

$$f(x,y) = \sum_{u=0}^{7} \sum_{v=0}^{7} \alpha(u)\alpha(v)C(u,v) \cos\left[\frac{\pi(2x+1)u}{16}\right] \cos\left[\frac{\pi(2y+1)v}{16}\right] \tag{7.2}$$

où

$$\alpha(u) = \begin{cases} \sqrt{\frac{1}{8}}, u = 0 \\ \frac{1}{2}, u \neq 0 \end{cases} \tag{7.3}$$

Comme on peut le voir à partir de l'équation 4.1, en particulier, dans la DCT directe 8×8, la substitution de $u, v = 0$ donne:

$$C(0,0) = \alpha(0)\alpha(0) \sum_{0}^{7} \sum_{0}^{7} f(x,y) \tag{7.4}$$

qui est huit fois de la moyenne de 8×8 échantillon. En effet, cette valeur s'appelle le coefficient DC des résultats de transformation et les autres sont appelés les coefficients AC

qui sont indépendants de la valeur moyenne. Normalement, dans le cas de la compression d'image, le coefficient DC est d'une amplitude relativement grande alors que les termes AC deviennent de plus faible amplitude lorsqu'ils s'éloignent du coefficient DC. Cela signifie qu'en effectuant la DCT 8×8 sur l'image brute d'entrée, la représentation de l'image (les éléments principaux portés par une image) est concentrée dans les coefficients en haut à gauche de chacune des matrices 8×8 (c.-à-d. zone de basse fréquence), alors que les coefficients en bas à droite de la matrice de sortie contiennent des informations moins importantes comme les détails (zone de haute fréquence).

7.4.2 conception et implémentation

Différentes méthodes SE sont conçues pour différents objectifs de protection et d'utilisation. Ici, dans cette section, nous présentons deux modèles de SE basés sur DCT 8×8 pour les images bitmap: un premier niveau de protection lorsque la vitesse est prépondérante et qu'une forte dégration de la qualité visuelle d'image est adaptée aux exigences du cas d'utilisation, et puis un second niveau complexe de protection lorsqu'une protection plus globale de l'image est requise. D'une part, notre deuxième niveau de conception prouve qu'en chiffrant DC et quelques coefficients AC tout en protégeant le reste des coefficients AC en DCT 8×8 blocs peuvent atteindre un bon niveau de protection; d'autre part, notre travail montre que le modèle d'exécution parallèle aux données de GPU s'intègre bien avec l'étape de pré-traitement, DCT 8×8. Cette forme physique rendra GPU un gain de performance critique pour le chiffrement sélectif basé sur DCT 8×8 puisque c'est seulement grâce à une implémentation GPU que SE est plus efficace qu'un chiffrement complet. Nous soulignons également que l'allocation pour l'organisation des tâches de calcul peut changer en fonction de la configuration matérielle en fournissant des évaluations sur deux ordinateurs de carastéristiques différentes. Les résultats suivants ont été publiés dans [125] et [126]. Nous fournissons ici des cas de test supplémentaires et quelques détails supplémentaires par exemple sur la précision des calculs.

Protection de premier niveau

Au chapitre 2, nous avons défini l'étape de fragmentation pour étiqueter les données prétraitées avec différents niveaux d'importance. Ici, premièrement, les données d'entrée seront prétraitées en utilisant DCT 8×8. Ensuite, les résultats de la DCT 8×8 qui sont les coefficients de fréquence seront fragmentés en deux parties selon le rapport de sélection par rapport au niveau de déguisement visuel requis. Le système de chiffrement sera utilisé pour le fragment privé (Fragment 1 dans Fig. 7.2) et le public (Fragment 2 dans Fig. 7.2) est clair.

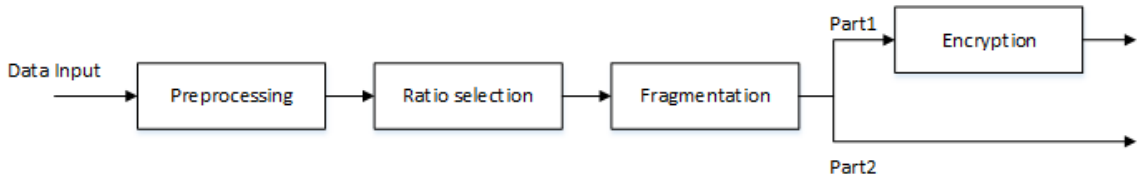

Fig. 7.2 Méthode de conception générale pour la protection de premier niveau où seul le fragment "part 1" (privé) est chiffré.

Bien que les informations visuelles ne puissent pas être totalement protégées et qu'elles présentent le risque que les coefficients puissent être quelque peu récupérés, cette méthode réduit considérablement le besoin de chiffrement complet des données et améliore les performances. L'étape de fragmentation possède un rapport de sélection effectué dans le domaine fréquentiel pour augmenter ou diminuer le fragment privé à chiffrer permettant à l'utilisateur d'augmenter ou de diminuer le niveau de protection souhaité. Le ratio de sélection peut être fixé par l'utilisateur, cependant, les coefficients [0,0], [0,1], [1,0], [2,0], [1,1], [0,2] du DCT 8×8 Le bloc cité par [80] constitue la sélection par défaut et est recommandé par expérience.

Cette méthode de protection effacera les caractères visuels les plus importants d'une image. Il est recommandé, par exemple, quand le but de l'utilisateur est de protéger son image contre un niveau d'attaque en sachant qui se trouve dans l'image. Plus généralement, ce premier niveau de protection est bon pour le chiffrement doux lorsque des performances élevées sont requises en même temps. Dans les sections suivantes, nous allons expliquer comment GPU est utilisé pour accélérer l'ensemble du processus et comment obtenir les meilleures performances possibles en exploitant au mieux l'architecture des différentes plates-formes matérielles.

Second niveau de protection

Comme indiqué précédemment, les coefficients de haute fréquence de DCT 8×8 peuvent parfois être utilisés pour révéler certaines informations sur l'image originale, en particulier certaines arêtes vives ou certains détails clairs. Pour certains cas d'utilisation comme la protection du contenu de l'image entière sans fuite d'information, une protection de niveau plus sévère est nécessaire pour protéger non seulement les coefficients de basse fréquence mais aussi les coefficients de haute fréquence. Afin de garantir que les performances pour l'ensemble du processus SE restent toujours meilleures que celles d'un chiffrement complet, une méthode de protection légère est utilisée pour protéger les coefficients haute fréquence

(voir Fig. 7.3, généralement, le chiffrement pour Part1 et protection de la lumière pour la partie 2).

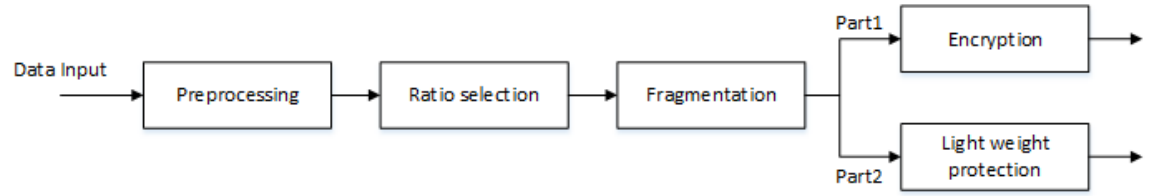

Fig. 7.3 Méthode de conception générale pour la protection de deuxième niveau où le fragment 2 est également protégé.

Une étape de dispersion est ajoutée pour séparer le stockage des deux parties de données protégées. Cette méthode de fragmentation utilise le fragment 1 pour construire une protection légère pour les coefficients à haute fréquence (fragment 2).

Fig. 7.4: l'étape de protection légère utilise la fonction SHA-512 [153] pour obtenir une chaîne unique de longueur fixe (512 bits) parmi les 6 sélectionnés coefficients (Fragment 1 dans Fig. 7.3). La fonction SHA-512 dispose d'une fonctionnalité qui peut générer deux chaînes de longueur fixe totalement différentes et imprévues même si un seul bit de la chaîne d'entrée est différent. De plus, selon [153], il n'est pas possible de récupérer les données d'entrée si seulement la chaîne de 512 bits en sortie est connue. Cette fonctionnalité garantira que la chaîne de 512 bits ne peut pas être utilisée pour faire des prédictions ou des reconstructions, même près de 8×8 Les blocs d'une image bitmap sont très similaires. Puisque le bloc que nous avons traité est 8×8, le DCT inverse (iDCT dans Fig. 7.4) résulte du reste des coefficients DCT (position DC remplie avec 1024 et coefficients AC restants avec zéros) pixels. Si nous stockons ces 64 pixels dans des entiers de 8 bits (Byte), la longueur totale est exactement de 512 bits. Ensuite, l'étape XOR peut protéger chaque bit pixel par pixel dans chaque bloc.

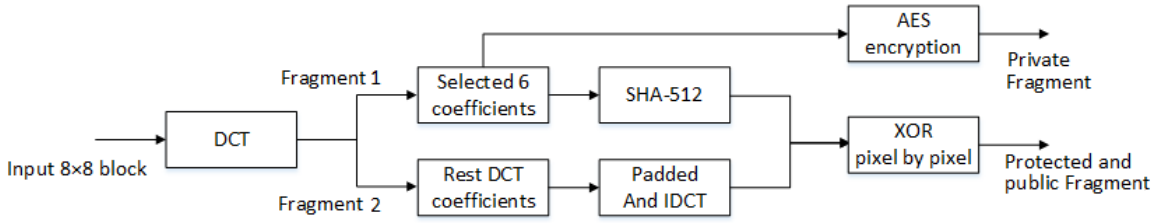

Fig. 7.4 Concevoir pour améliorer le niveau de protection.

7.4.3 Analyse de résultats

Comme indiqué par [116], on sait que de nombreux algorithmes de chiffrement ont été analysés avec succès par l'analyse statistique et plusieurs attaques statistiques. Dans la plupart des cas, la dégradation visuelle est utilisée pour évaluer la propriété de sécurité des méthodes SE pour les images. Pour tester la robustesse de notre méthode de chiffrement, nous effectuons une analyse statistique en donnant le PDF et les corrélations pour deux pixels adjacents dans la partie publique plus faiblement protégée.

Analyse de la fonction de densité de probabilité

Une fonction de densité de probabilité (PDF) de la représentation en octets d'image illustre comment les pixels d'une image sont distribués en représentant graphiquement le nombre de pixels du niveau d'intensité. Pour un cas d'image en échelle de gris, la Fig. 7.5 montre comment le PDF du fragment protégé et public de l'image est assez uniforme et significativement différent du PDF de l'image originale correspondante.

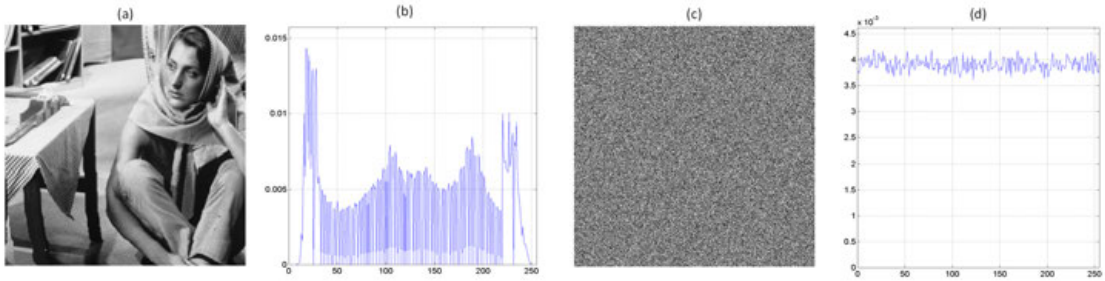

Fig. 7.5 L'image en échelle de gris ordinaire (a) et son PDF (b) par rapport au fragment protégé et public (c) et son PDF (d).

Analyse des coefficients

Une corrélation plus faible entre les données originales et cryptées est un facteur important qui permet de valider l'indépendance entre elles. Avoir un coefficient de corrélation uniformément réparti signifie que l'on obtient un haut degré de hasard. Selon [168], pour tester la corrélation entre deux pixels adjacents, les procédures suivantes sont effectuées. Tout d'abord, nous avons sélectionné de manière aléatoire 10 000 paires de deux pixels adjacents dans le sens horizontal, vertical et diagonal, puis calculez le coefficient de corrélation r_{xy} de chaque paire en utilisant:

$$r_{xy} = \frac{cov(x,y)}{\sqrt{D(x) \times D(y)}} \tag{7.5}$$

où

$$E(x) = \frac{1}{N} \times \sum_{i=1}^{N} x_i$$
$$D(x) = \frac{1}{N} \times \sum_{i=1}^{N} (x_i - E(x))^2$$
$$cov(x,y) = \frac{1}{N} \times \sum_{i=1}^{N} (x_i - E(x))(y_i - E(y))$$

x et y sont les valeurs des deux pixels adjacents dans l'image pour le cas de l'image en niveaux de gris.

Ensuite, les mêmes opérations sont effectuées le long des directions verticale et diagonale. Comme le montre la Fig. 7.6, les distributions de coefficients de corrélation des images chiffrées semblent uniformes par rapport à l'image simple originale. Dans une image bitmap au format RGB à trois couches, chaque pixel est stocké en utilisant 24 bits avec chaque 8 bits pour une couche de couleur. La protection va mélanger les distributions de coefficients de corrélation pour chacune des couches.

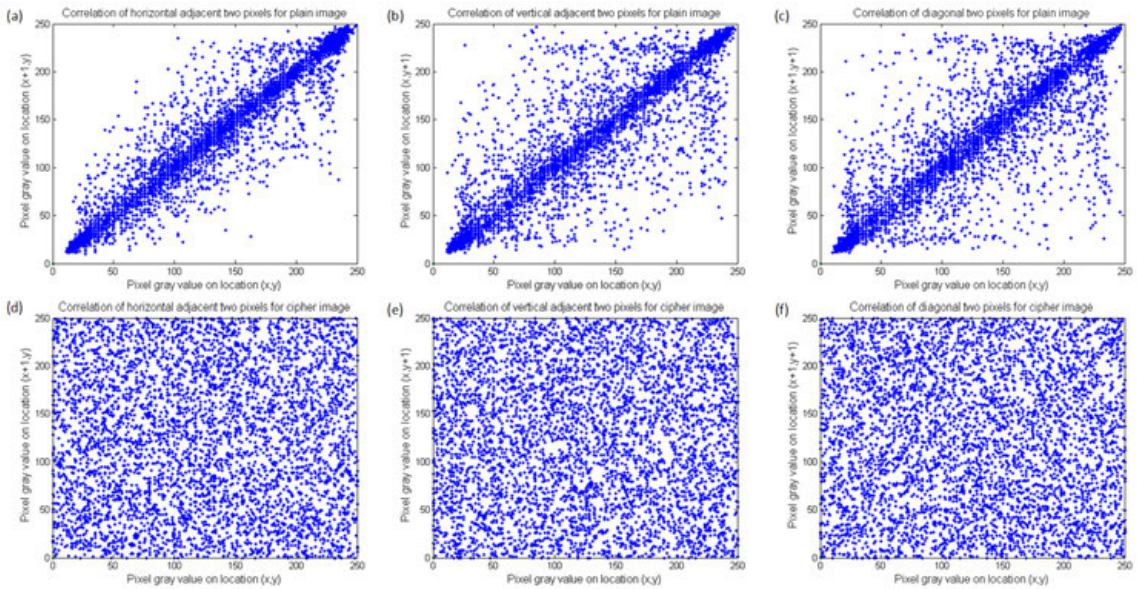

Fig. 7.6 Corrélation de pixels adjacents dans les directions horizontale, verticale et diagonale pour une image bitmap à échelle de gris.

7.4.4 Évaluations de référence

Dans cette section, nous discutons principalement de l'implémentation de l'allocation des tâches de calcul au GPU et au CPU et évaluons leurs performances. Ici, un GPU de jeu pour desktop (Nvidia GTX 780 équipé d'une CPU Intel I7-4770K) est utilisé pour tester l'allocation du calcul. Et seuls les résultats de référence pour le premier et deuxième niveau de protection sont affichés.

Selon [86], AES peut est calculé à plus de 50 Gbps sur un GPU Nvidia de desktop avec une implémentation CUDA (dans notre travail, elle peut atteindre presque 40 Gbps sur notre desktop comme le montre Table 7.1). Nous déplaçons tous les calculs SE incluant DCT et AES vers le GPU pour le premier niveau de SE. Cette conception utilise le GPU pour effectuer trois étapes en séquence pour chaque image d'entrée: DCT pour l'image originale, AES pour les coefficients sélectionnés et iDCT pour les coefficients restants. Dans la Table 7.1, nous listons l'évaluation pour un chiffrement complet sur CPU et GPU par rapport à SE sur GPU.

Table 7.1 Vitesse d'AES sur CPU et GPU, notre SE (protection de premier niveau) sur GPU.

Image size	1024×768	1600×1200	3240×2592	4800×4800
AES on desktop GPU	0.19 ms	0.46 ms	1.91 ms	5.46 ms
AES on desktop CPU	1.56 ms	3.8 ms	16.6 ms	45.5 ms
SE on desktop GPU	0.10 ms	0.21 ms	1.01 ms	2.76 ms

Nous pouvons voir que le SE que nous utilisons est toujours plus rapide que l'AES sur un processeur ou même sur un GPU. Ce résultat bénéficie de l'idée que tous les calculs de SE sont déplacés vers le GPU. Sur la base de ces observations, nous pouvons voir que l'utilisation d'un GPU comme accélérateur pour notre algorithme SE est toujours un meilleur choix par rapport à AES. La raison principale de cette situation est que, bien que l'AES puisse être accéléré par GPU, le calcul DCT 8×8 lui-même convient mieux qu'AES à l'architecture GPU. De manière plus détaillée, DCT 8×8 est optimisé par de nombreux travaux précédents que le calcul est adapté à l'architecture GPU Nvidia. Dans le même temps, la conception de l'algorithme AES utilisait des opérations logiques au niveau des bits, ce qui n'est pas aussi facile que la DCT à optimiser pour le GPU. Cette différence principale rend AES toujours plus lent que DCT sur la même plate-forme GPU. De plus, la méthode SE de la protection du premier et du second niveau ne génère qu'environ 13% des données originales pour effectuer l'opération AES, ce qui n'apporte en fait pas beaucoup de calcul.

Pour le second niveau de protection implementé sur desktop, la seule différence est comment allouer la tâche de calcul de hachage. Comme indiqué précédemment, selon

les tests basés sur les programmes de [146], les performances du SHA-512 sur GPU pour desktop, Nvidia GeForce GTX 780 est d'environ 136 MH/s (soit 136 millions de hachage par seconde). Nous devrions noter que pour chaque bloc 8×8, il y aura un calcul de hachage, donc nous pouvons évaluer le temps d'exécution pour SHA-512 comme dans la Table 7.2.

Table 7.2 Estimation de vitesse de SHA-512 d'une fois par bloc 8×8 sur GPU pour desktop.

Image size	1024×768	1600×1200	3240×2592	4800×4800
SHA-512 once per block	0.09 ms	0.22 ms	0.96 ms	2.65 ms

La vitesse est beaucoup plus rapide que SHA-512 sur l'implémentation basée sur CPU de [37]. Dans l'évaluation de la protection de second niveau, nous allouons également cette tâche de hachage au GPU. Au final, nous comparons la méthode de niveau fort de protection sur GPU avec AES sur GPU dans la Table 7.3.

Table 7.3 Evaluation d'AES sur GPU, notre SE (fort niveau de protection) sur GPU.

Image size	1024×768	1600×1200	3240×2592	4800×4800
AES on desktop CPU	1.56 ms	3.8 ms	16.6 ms	45.5 ms
AES on desktop GPU	0.19 ms	0.46 ms	1.91 ms	5.46 ms
SE level 2 on GPU	0.19 ms	0.43 ms	1.97 ms	5.41 ms

La Table 7.3 montre que le SE en mode de protection de second niveau sur GPU de desktop a les mêmes performances que AES-128 sur GPU. En résumé, l'allocation du calcul des tâches HASH et AES dépend toujours de la capacité de calcul du GPU alors que la tâche DCT peut toujours être allouée au GPU.

7.4.5 Discussion

Nous avons implémenté deux niveaux de protection des données avec des méthodes de chiffrement sélectif comprenant un prétraitement DCT 8×8 utilisant l'accélération GPU. Nous avons défini un premier niveau de protection léger, conçu principalement pour masquer la qualité de l'image. Ensuite, nous avons défini un second niveau de protection offrant un meilleur niveau de sécurité.

La séparation des données d'image en un fragment privé et un fragment public et protégé peut être utilisée pour résoudre efficacement le problème de protection efficace d'une grande quantité d'images bitmap utilisant des serveurs de stockage à distance comme un fournisseur de stockage en nuage. Nous séparons les données d'origine en plaçant le fragment privé important à stocker localement et en plaçant le fragment restant protégé sur un serveur distant.

Par exemple, dans un nuage avec la protection supplémentaire offerte par le fournisseur de cloud. Ce faisant, nous faisons le meilleur usage de la mémoire locale où nous stockons seulement environ 13% des données en fonction d'un nombre ajustable de coefficients sélectionnés pour constituer le fragment privé. Pour réaliser l'une ou l'autre des deux méthodes, nous avons raffiné l'architecture d'implémentation en utilisant le GPU et le CPU disponibles sur PC et atteignons un niveau de performance beaucoup plus rapide que AES sur CPU et comparable à AES basé sur GPU et jamais plus lent.

En résumé, notre travail montre clairement que le chiffrement sélectif peut devenir largement utilisé pour la protection d'image bitmap car il fournit un excellent temps de traitement, une perte minimale de contenu visuel, un bon niveau de protection en fragmentant bitmap en deux espace de stockage sans augmentation importante de la taille mémoire totale utilisée.

7.5 DWT pour la protection d'usage général

Dans les sections précédentes, DCT (Discrete Cosine Transform) a été utilisé pour prendre en charge la décision de fragmentation avant d'effectuer le chiffrement pour la protection d'image bitmap. Cependant, DCT ne peut pas garantir l'absence de perte totale due aux conversions entre entiers et nombres flottants, ce qui entraînera des erreurs d'arrondi (parfois même récursives). Ces erreurs d'arrondi peuvent être réduites en utilisant plus d'espace de stockage avec des conceptions plus détaillées mais ne peuvent pas être totalement évitées. C'est la raison pour laquelle DCT ne peut pas fournir le niveau d'intégrité requise pour traiter tout type de données.

La transformée discrète en ondelettes (DWT) [21] est parfois utilisée dans le chiffrement sélectif (voir travail précédent [63] [138] [121]), mais la plupart du temps, elle est utilisée comme compression standard. étape pour le formatage plutôt que comme étape de prétraitement pour la sélection dans des cas d'utilisation multimédia. Dans notre conception, DWT est utilisé comme une étape de prétraitement avant la fragmentation avec un filtre spécial Le Gall 5/3 [21] qui peut assurer l'intégrité des données et être efficace à la fois en termes de performances et d'utilisation de l'espace de stockage.

Les performances par comparaison au chiffrement complet sont constamment requises. La transformée utilisée dans l'étape de prétraitement de SE peut légitimement être retirée du cas-test lorsque SE et la compression sont intégrées et que la transformée est utilisée par les deux applications. Dans ces cas, SE effectue une protection légère dans le processus de compression ou de codage pour un format spécifique tel que MPEG4 [133] ou JPEG2000 [31]. Cependant, notre cas d'utilisation visant à traiter n'importe quel type de données devra

prendre en compte l'ensemble du processus en matière d'évaluation des performances car il devrait être capable de traiter tout format de données. Cela nous conduira à implémenter DWT sur un GPGPU pour bénéficier de son accélération [50].

7.5.1 DWT

DWT est une technique de traitement de signal pour extraire des informations principalement utilisées dans les standards de compression tels que JPEG2000 [31]. Il peut représenter des données par un ensemble de valeurs grossières et détaillées à différentes échelles. Naturellement, c'est une transformation unidimensionnelle. Mais, il peut également être utilisé comme une transformation bidimensionnelle appliquée dans les directions horizontale et verticale. Pour le cas de l'image, cette transformation DWT-2D générera quatre petites images dont chacune est un quart de l'image originale avec une transformation de niveau: une avec une basse résolution (LL), une avec une résolution verticale élevée et une basse résolution horizontale (HL), une avec une résolution verticale faible et une résolution horizontale élevée (LH), et une avec une haute résolution (HH). Ensuite, la transformée de second niveau ne sera effectuée que pour le premier quart (partie 'LL') du résultat du premier niveau qui est appelé décomposition dyadique comme indiqué dans la Fig. 7.7.

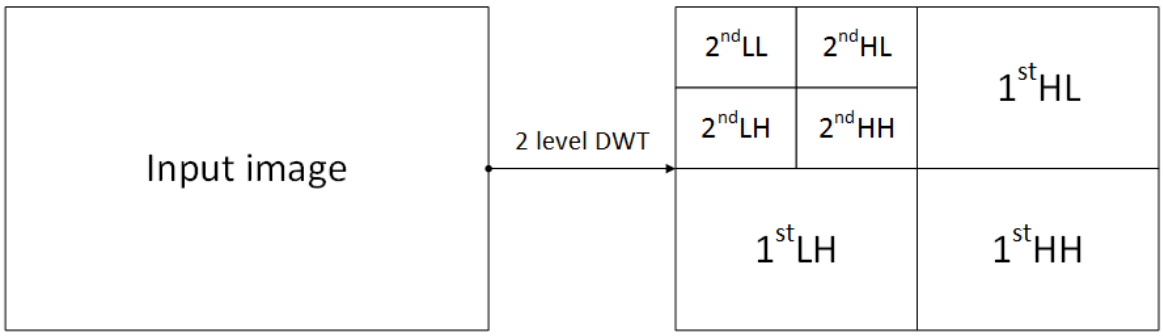

Fig. 7.7 Résultat 2D Transformée en ondelettes discrètes [31].

Pour effectuer la transformée DWT directe, une sous-bande unidimensionnelle est décomposée en un ensemble d'échantillons passe-bas et un ensemble d'échantillons passe-haut. Dans notre conception, le filtre "Le Gall 5/3 filter" par [21] est utilisé, donc aucune donnée ne sera perdue en raison de l'arrondissement numérique. Et le schéma de filtrage basé sur le levage [1] est utilisé pour mettre à jour les valeurs d'échantillons impairs avec une somme pondérée de valeurs d'échantillons pairs et mettre à jour un échantillon pair avec une somme pondérée de valeurs d'échantillons impairs. Le filtrage basé sur le levage pour le filtre d'analyse 5/3 est réalisé en utilisant des équations:

$$y(2n+1) = x_{ext}(2n+1) - \lfloor \frac{x_{ext}(2n) + x_{ext}(2n+2)}{2} \rfloor \tag{7.6}$$

$$y(2n) = x_{ext}(2n) - \lfloor \frac{y(2n-1) + y(2n+1) + 2}{4} \rfloor \tag{7.7}$$

où x_{ext} est le signal d'entrée étendu, y est le signal de sortie et $\lfloor a \rfloor$ indique le plus grand entier n'excédant pas a.

DWT peut être effectué à différents niveaux, nous avons choisi une transformée à deux niveaux comme illustré Fig. 7.7. Fig. 7.10, les coefficients sélectionnés pour construire le fragment privé sont 2^{nd} LL qui prend environ 1/16 de l'espace de stockage et comporte les éléments de base (informations grossières) de l'image originale. La raison du choix de deux niveaux pour DWT est motivée par des considérations de gestion mémoire: un seul niveau comportera toujours une partie basse fréquence (1/4 du résultat DWT-2D entier) à protéger de grande taille et trois niveaux ou plus rendent la plage de valeurs des coefficients de haute fréquence trop importante et vont gaspiller plus d'espace de stockage.

7.5.2 Accélération de DWT basée sur GPGPU

Des résultats récents [159] montrent de meilleures performances pour le calcul de DWT avec plus d'optimisation dans la gestion du problème des dépendances de blocs de données par plus d'étapes de transfert de mémoire. Et le résultat montre qu'une accélération d'un facteur 10 à 14 peut être atteinte par rapport à une implémentation de CPU utilisant des accélérations de niveau instruction (extensions MMX et SSE). En 2015, la mise en œuvre la plus rapide de DWT trouvée dans la littérature est proposée dans [43]. Dans ce chapitre, un schéma optimisé est implémenté avec le matériel de pointe (Nvidia GTX Titan GPU). Le DWT-2D avec filtre "Le Gall 5/3" pour une image 4096×4096 peut être fait en 0.467 ms.

Dans notre implémentation, le schéma de levage est utilisé et la méthode principale selon [159]. Comme nous ne nous concentrons pas sur la meilleure optimisation de l'implémentation de DWT-2D sur GPGPU, les évaluations de performances sont basées uniquement sur le matériel dont nous disposons.

7.5.3 Conception de SE basée sur DWT

Pour traiter des données de grande taille, nous avons proposé dans [127] de les découper en plusieurs matrice 2D de même taille (par exemple vu comme un bloc 512×512 ou 1024×1024 octet qui est choisi pour s'adapter à la transformation ultérieure ou à l'architecture de la plate-forme matérielle) comme indiqué Fig. 7.8. Ensuite, chaque bloc (D_i) va au processus

SE pour générer trois fragments qui sont le fragment privé D_iA, le premier fragment public et protégé D_iB, et le second fragment public et protégé D_iC. Ensuite, les fragments D_iA vont dans la zone de confiance comme une machine locale sous le contrôle de l'utilisateur et les fragments D_iB, D_iC peuvent être transmis à une zone de stockage publique telle qu'un clooud sans crainte d'une attaque puisque D_iB, D_iC sont censés comporter peu d'informations et de plus, être protégés.

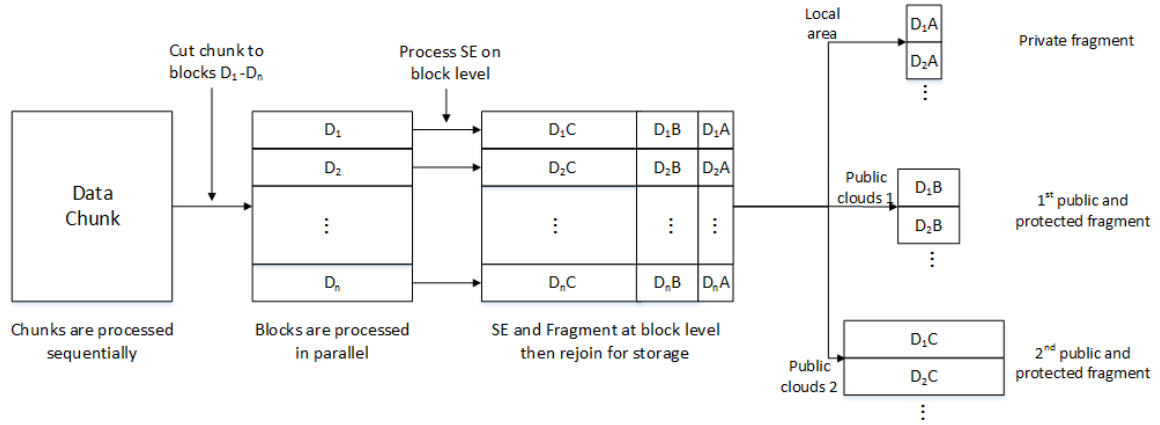

Fig. 7.8 SE Méthode générale de traitement d'une grande quantité de données.

L'idée principale est de considérer chaque bloc D_i comme une matrice et d'être traité comme telle par le processus SE. C'est-à-dire que n'importe quel type de données peut être vu comme une matrice en considérant chaque octet de données comme un pixel pour former une image en échelle de gris bitmap. Ensuite, chaque "image" D_i est simplement traitée en utilisant la méthode SE un bloc à la fois avec la taille de bloc 8×8 montrée Fig. 7.10. La taille de bloc choisie peut être modifiée en fonction de la taille des données d'origine. Cette étape de pavage est utilisée pour obtenir un bon ajustement avec l'architecture GPGPU.

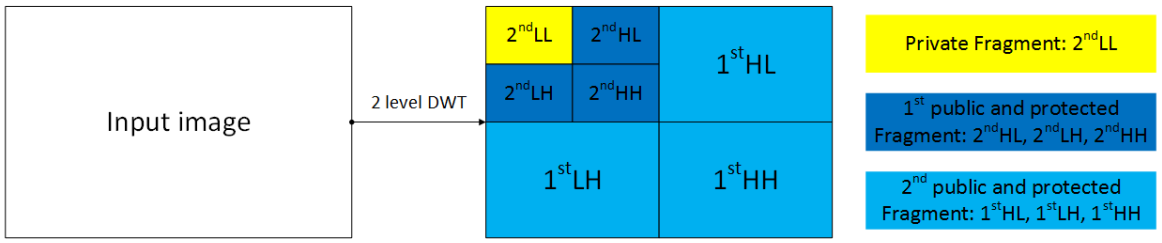

Fig. 7.9 DWT-2D et processus de fragmentation pour le bloc unique 8×8.

Le fragment privé est utilisé pour générer une séquence de 256 bits en utilisant SHA-256 [153] ce qui garantit une séquence binaire très différente générée même lorsque les coefficients correspondants des autres fragments privés dans les blocs voisins sont très

similaires. Cette séquence de bits est utilisée pour protéger le premier fragment public (constitués par les coefficients restants du second niveau DWT montrés Fig. 7.9) en effectuant une opération XOR. Ensuite, le premier fragment public et protégé sera lui-même utilisé pour générer une séquence de bits de longueur 512 en utilisant SHA-512 [153] pour protéger le second fragment public et protégé (le reste des coefficients DWT-2D) en effectuant une opération XOR.

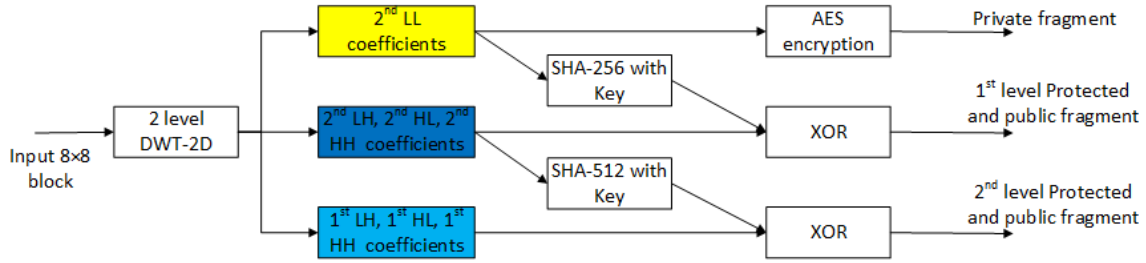

Fig. 7.10 SE processus pour le bloc unique 8×8.

La protection des «fragments protégés et publics» fournis par une opération XOR est basée sur le caractère aléatoire garanti par les opérations de hachage. Par exemple, dans le cas d'un bitmap, tant qu'il y a des redondances, les coefficients peuvent être très similaires, en particulier entre les blocs voisins. Cependant, les opérations SHA-256 et SHA-512 engendreront des séquences de bits totalement différentes même s'il n'y a qu'un seul bit différent dans les entrées (provenant du second niveau de DWT). Ce caractère aléatoire sera ajouté aux deux 'fragments protégés et publics' par XORing permettant ainsi de mieux les protéger. Pour d'autres formats de fichiers en entrée, cette méthode a un effet bénéfique similaire. Une analyse de sécurité plus poussée est menée section suivante.

7.5.4 Analyse de sécurité

Un algorithme de chiffrement sécurisé doit résister à plusieurs types d'attaques classiques [111, 29]. Dans cette section, différents tests de sécurité sur le schéma proposé sont effectués pour établir son niveau de sécurité.

L'hypothèse de base est que le fragment de données privé sélectionné est sécurisé en utilisant AES-128. Il est également facile de remplacer AES-128 par d'autres algorithmes de chiffrement. La propriété de sécurité de ce fragment privé n'est donc pas analysée ici.

Les fragments publics et protégés qui sont stockés dans un espace de stockage public (cloud) dans notre cas d'utilisation sont analysés en terme de niveau de sécurité: on vérifie s'ils atteignent de bonnes performances cryptographiques. Fig.7.10, afin de simplifier la présentation, on ne considerara que les coefficients constituant la second fragment public

et protégé. Cependant, d'après notre travail, les propriétés de sécurité des coefficients du premier fragment public et protégé sont très similaires à celles que nous analysons ici.

Les mesures d'analyse sur le bloc de données original et le fragment public et protégé utilisé sont les suivantes:

1. *Analyse d'uniformité* est donnée en calculant la fonction de densité de probabilité (PDF);

2. *Analyse d'entropie d'information* est donnée en calculant l'entropie;

3. *Analyse de corrélation* est donnée en calculant les coefficients de corrélation;

4. *Difference analysis* est de tester la différence dans le niveau de bits et aussi l'information mutuelle normalisée (NMI);

5. *Analyse de sensibilité* est donnée en calculant la sensibilité lors de la saisie de texte brut et de changement de clé;

6. *Analyse de dégradation visuelle* ne concerne que les bitmaps en calculant le rapport signal-bruit maximal (PSNR) et la similarité structurelle (SSIM);

7. *La propagation des erreurs* est également discutée.

7.5.5 Benchmark avec deux architectures logicielles

Dans cette section, nous évaluons la performance de l'ensemble du processus de protection. Comme nous considérons l'allocation des calculs sur une plate-forme PC, la ressource matérielle dont nous disposons est un processeur et un GPGPU. Cependant, les capacités de calcul très différentes de GPGPU modifient le temps d'exécution de SE [107] [115]. Ainsi, la performance est évaluée dans deux cas d'utilisation: un ordinateur portable équipé d'un GPU bas de gamme et un ordinateur desktop équipé d'un GPU haut de gamme.

Table 7.4 Évaluation des performances pour toutes les tâches de calcul de SE pour deux plates-formes.

	Input chunk size (byte)	1024×1024	2048×2048	3200×3200	4800×4800
Laptop Scenario	GPU time (DWT-2D)	1.39ms	4.87ms	12.6ms	24.1ms
	GPU time (SHA-256)	0.33ms	1.31ms	3.3ms	7.3ms
	GPU time (SHA-512)	1.45ms	5.8ms	14.2ms	31.8ms
	CPU time (AES-128)	0.29ms	1.14ms	3.06ms	6.67ms
desktop Scenario	GPU time (DWT-2D)	0.34ms	0.79ms	1.7ms	3.3ms
	GPU time (SHA-256)	0.05ms	0.13ms	0.29ms	0.63ms
	GPU time (SHA-512)	0.13ms	0.69ms	1.58ms	3.2ms
	CPU time (AES-128)	0.23ms	0.96ms	2.37ms	5.3ms

La décision la plus délicate de la conception logicielle est de répartir les tâches de calcul entre le GPU et le CPU. Comme indiqué dans la section 2.3.2, les DWT-2D, SHA-256

et SHA-512 peuvent bénéficier de l'accélération GPU, donc la conception est basée sur l'utilisation parallèle du CPU et du GPU. Tandis que le GPU va se voir assigné des tâches de calcul de DWT- 2D, SHA-256 et SHA-512, le CPU lui se chargera du calcul d'AES-128 pour seulement les coefficients de niveau 1. Le plan initial pour les cas de GPU bas et haut de gamme est de garder le GPU le plus occupé possible et le CPU aura des tranches de temps libre qui pourront être utilisées pour d'autres tâches (Fig. 7.11).

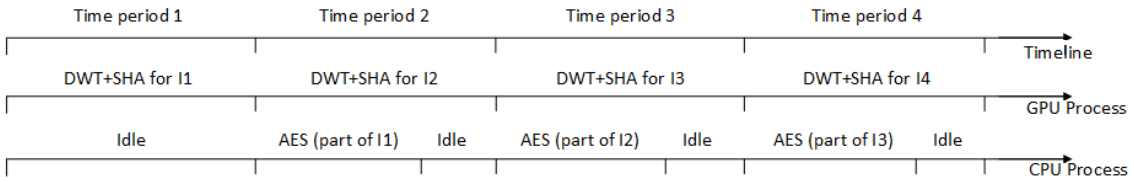

Fig. 7.11 Architecture de chevauchement temporel de l'implémentation.

L'ordinateur portable possède un processeur Intel I7-3630QM et un GPU Nvidia Nvs 5200M. Le desktop lui, possède un processeur Intel I7-4770K et un GPU de Nvidia Geforce gtx 780. Afin de vérifier notre plan initial et d'allouer chaque tâche de calcul au processeur le mieux adapté, nous évaluons chacune des tâches sur ordinateur portable et desktop. Les résultats sont affichés Table 7.4. Pour une taille de bloc de données d'entrée de taille différente, le temps d'exécution du GPU pour le deuxième bloc de données d'entrée peut toujours chevaucher le temps d'exécution du CPU pour les coefficients DWT-2D sélectionnés du premier bloc de données d'entrée; on réalise ainsi une sorte d'architecture pipeline.

7.5.6 Discussions sur le benchmark

Le GPU du desktop que nous avons utilisé contient 2304 cœurs CUDA par rapport aux 96 cœurs CUDA sur le GPU d'ordinateur portable. Il est facile de conclure que la vitesse de calcul du GPU de desktop est beaucoup plus rapide que le GPU d'un ordinateur portable. En conséquence, la méthode SE aura une architecture logicielle qui diffèrera avec la catégorie de GPU disponible ce qui pose un dilemme de portabilité connue par ailleurs pour les applications sur GPU.

En fait, tant que les architectures GPU évoluent au rythme actuel, la configuration matérielle d'un GPU peut fortement influencer les choix architecturaux des applications logicielles nécessaires pour établir la meilleure implémentation possible. Ce point pourrait même inverser les résultats de notre évaluation car un grand nombre de cœurs pourrait très bien favoriser les tâches de calcul du GPU qui modifient finalement le design de superposition. Aussi, comme indiqué par [66], quand une capacité de calcul GPU est très élevée, le goulot

d'étranglement du processus est le transfert de mémoire entre la mémoire GPU et la mémoire hôte au lieu de la vitesse de calcul elle-même. Ceci est principalement dû à la limitation de la vitesse de transmission via le bus PCIE (Peripheral Component Interconnect Express [20]) entre la mémoire hôte et la mémoire GPU. Ce problème peut être évité en organisant plus de tâches de calcul sur le GPU au lieu d'utiliser trop d'I/O ou en superposant la transmission par le temps d'exécution.

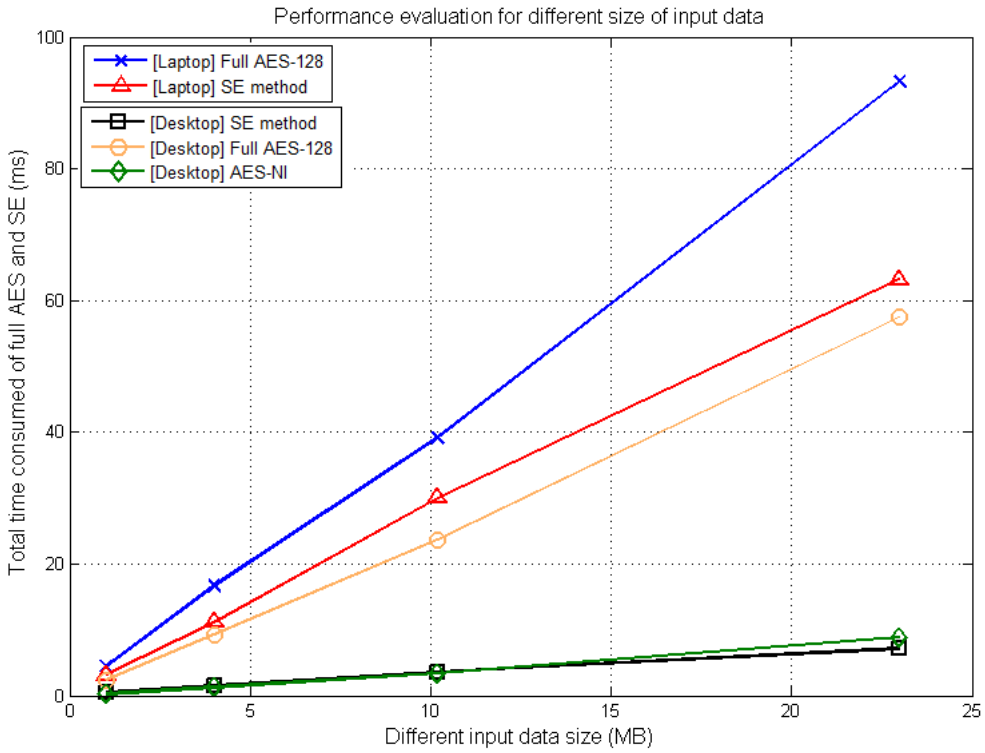

Fig. 7.12 Évaluations de performance pour SE par rapport à AES complet sur des scénarios d'ordinateurs portables et de desktop.

Fig. 7.12, nous avons présenté la comparaison de la méthode SE avec AES-128 sur CPU ainsi que AES-NI ([37]).

Il convient de noter que [17] a souligné qu'AES sur monoprocesseur pouvait également être très rapide avec le support de l'extension New Instructions (NI) apportée par Intel. Cet AES-NI pourrait accélérer l'AES sur CPU plus de 5 fois et atteindre presque 3GB/s sur un CPU NI-enable (montré Fig. 7.12) qui est presque la même vitesse que notre méthode basée sur GPGPU. Cependant, comme le souligne le livre blanc de Nvidia, le GPU Nvidia GeForce 1080 (sorti en 2016) est déjà trois fois plus rapide que le GPU utilisé dans cette thèse (Nvidia GeForce 780, sorti en 2013), il est juste de dire que le gain de performance pourrait être plus

important avec l'utilisation de GPGPU à la pointe de la technologie. Cette évolution rapide du matériel n'est pas visible dans la fabrication des processeurs de ces dernières années. En conclusion, notre conception sur GPU pourrait toujours atteindre de meilleures performances que AES-NI sur CPU avec un matériel comparable.

7.5.7 Transmission de fragments

Notre méthode de protection des données peut également être utilisée pour sécuriser la transmission et le partage de données entre utilisateurs finaux. Ce design pourrait engendrer trois fragments pour le partage de données pour chacun des segments de données comme indiqué Fig.7.13. Pour le *fragment privé*, l'algorithme de chiffrement utilisé reste AES-128 (qui comme indiqué précédemment pourrait être facilement remplacé par AES-NI avec un processeur NI ou tout autre algorithme de chiffrement). Ce *fragment privé* est le seul fragment directement transmis entre utilisateurs finaux. Les deux autres textit fragments protégés et publics sont transmis via les serveurs cloud publics sans fuite d'informations. L'espace de stockage que le *fragment privé* prend est 7.8% de la taille des données d'origine, alors que les deux autres fragments prennent respectivement 24.2% et 93,8% de l'espace de stockage de données d'origine.

Bien que l'utilisation totale de l'espace de stockage soit d'environ 25% supérieure à celle d'origine, l'utilisation de l'espace de stockage local est seulement de 7,8%, ce qui réduit considérablement l'utilisation du stockage local qui est sensé être plus couteux que l'espace public et optimise l'efficacité et la sécurité de notre méthode.

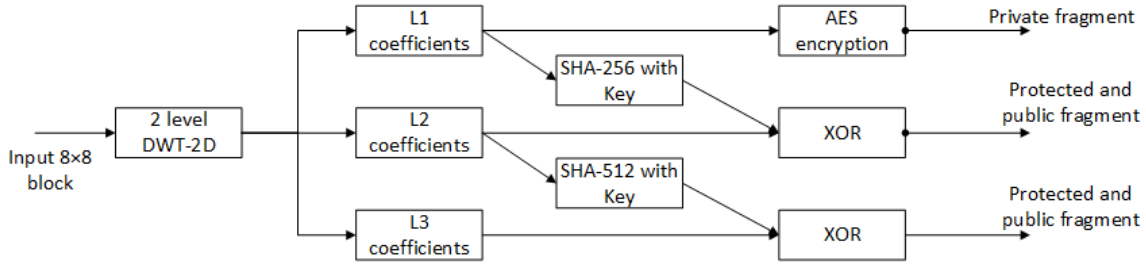

Fig. 7.13 Trois fragments d'un bloc de données pour sécuriser davantage le partage de données.

La Fig.7.14 donne un exemple d'utilisation de cette méthode pour le partage de données entre utilisateurs finaux. L'expéditeur effectue les routines de fragmentation et de protection avant de disperser les fragments sur Clouds. Les fragments protégés et publics seront envoyés à différents serveurs Cloud et pourront être téléchargés n'importe quand. Le *fragment privé* sera envoyé via un canal de communication direct entre expéditeurs et destinataires.

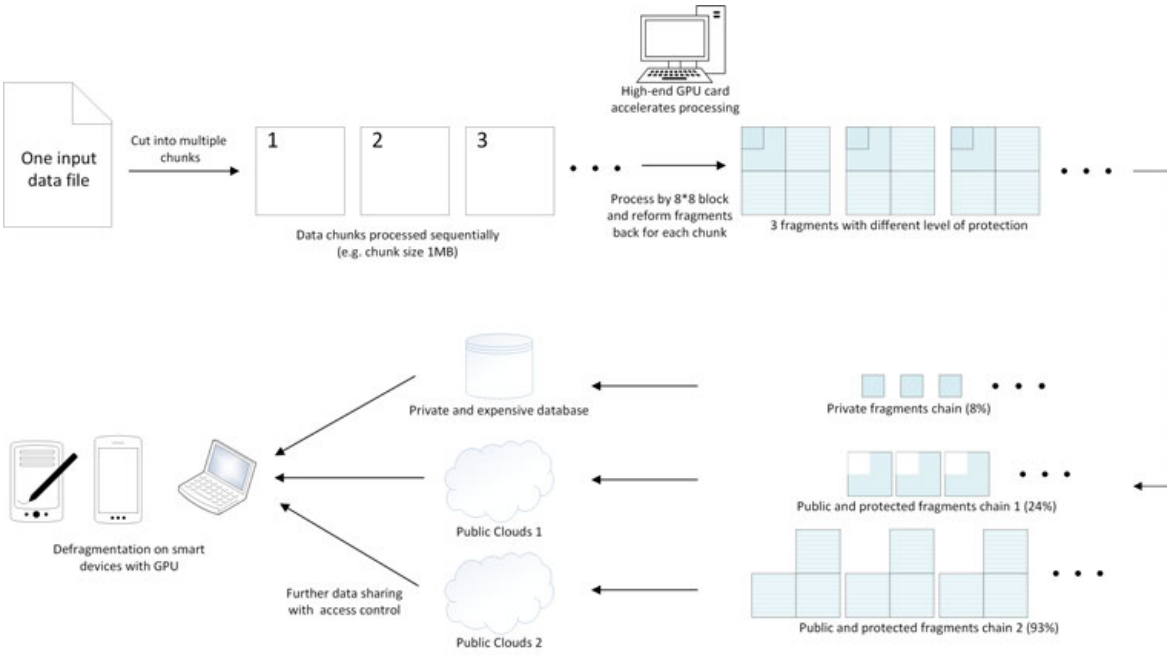

Fig. 7.14 Cas d'utilisation: sécuriser le partage de données entre utilisateurs finaux via différents serveurs Cloud en fonction de la fragmentation et de la dispersion.

Le premier avantage de cette conception est de réduire considérablement l'utilisation de l'espace de stockage local tout en assurant la sécurité et la confidentialité pour l'utilisateur final. Ceci est particulièrement utile dans certains cas d'utilisation, par exemple lorsque le périphérique de l'utilisateur final est un téléphone mobile (l'espace de stockage local est relativement limité et coûteux surtout par rapport à l'espace de stockage d'un cloud public de grande capacité et gratuit).

Le second avantage consiste à traiter efficacement fragmentation et protection sur le dispositif de l'utilisateur final afin d'éviter toute transmission de données en clair sur un canal non sécurisé et afin d'éviter d'utiliser un service spécifique fourni par le serveur comme BlackBerry Enterprise Server (BES) [25]. Plus important encore, comme le soulignent [27] et [185], DWT pourrait être accéléré par le GPU mobile, ce qui permet une utilisation future de ce schéma lorsque les GPGPUs sont largement déployés sur les téléphones portables intelligents.

7.6 Conclusion

Dans ce travail, un schéma de protection des données combinant fragmentation, chiffrement et dispersion a été présenté sur la base de l'amélioration des algorithmes de chiffrement

sélectif. Au cours des deux dernières décennies, la plupart des algorithmes SE ont été initialement dédiés au multimédia spécifique SE. Ils sont basés sur l'une des étapes de formatage de la compression du contenu (transformation, codage et conditionnement).

Dans les travaux antérieurs que nous avons étudiés, les méthodes SE fournissent principalement plus d'efficacité en terme de temps d'exécution par rapport aux méthodes traditionnelles de chiffrement complet en protégeant seulement une partie des données originales. Cependant, notre étude souligne que les méthodes SE ne fournissent pas toujours une efficacité optimale compte tenu de l'évolution rapide des algorithmes et du matériel. Ainsi, une architecture selon différentes configurations matérielles existantes (l'évolution du matériel devrait être prise en compte comme s'insérant dans ce cadre; le schéma devrait également s'averer adaptable pour des environnements très différents) est discutée y compris une architecture logicielle flexible (les algorithmes déployés pourraient être facilement remplaçables alors que le cadre principal reste inchangé).

Deux niveaux de schémas de protection Bitmap ont été présentés à la fois en utilisant le prétraitement DCT 8×8 et l'accélération GPGPU. Nous avons défini un premier niveau de protection légère avec des temps d'exécution très rapides et un second niveau de protection avec de meilleures qualités de protection. Pour le second niveau de protection, de nombreuses conceptions détaillées sont mises en œuvre pour réduire la perte d'informations et éviter les erreurs d'arrondi récursives qui améliorent les méthodes SE précédentes liées au bitmap. La fragmentation est utilisée dans ce schéma avec une allocation mémoire optimisées.

En section 6, une architecture SE agnostique en termes de format de données est présentée sur la base d'un prétraitement sans perte de DWT 8×8. La motivation initiale de cette architecture est de résoudre la question de restitution intégrale des images bitmap (intégrité) après déchiffrement. Ensuite, nous avons réalisé que cette méthode pourrait traiter tout format de données, en particulier du texte. Et nous avons vérifié qu'en fait il est agnostique en ce qui concerne le format de l'information à protéger à la différence de toute méthode SE que nous avons pu voir dans la littérature actuelle.

L'architecture proposée utilise l'algorithme de chiffrement AES pour protéger le fragment privé qui sera stocké localement. Il peut être facilement remplacé en utilisant d'autres algorithmes de chiffrement tel que AES-NI. Pour les autres fragments, les algorithmes de hachage SHA sont utilisés pour produire un flux de clé qui sera utilisé pour chiffrer le fragment public et protégé en les mélangeant. SHA garantira le caractère aléatoire des flux de clé générés même par les blocs voisins très similaires 8×8 qui peuvent fournir la protection nécessaire pour le public et les fragments protégés.

Plus important encore, le processeur graphique est utilisé pour réduire les couts additionnels en terme de temps d'exécution dû à l'opération d'optimisation DWT-2D, et parfois à la

fois les opérations AES et SHA. L'architecture est flexible pouvant s'adapter à différentes configurations matérielles avec l'expérimentation pure GPGPU et CPU avec la conception de superposition GPGPU. Un benchmark a été réalisé entre l'expérimentation proposée et AES appliquée sur toute la donnée pour différents formats de données sur deux plates-formes matérielles très différentes. Et plusieurs analyses de sécurité expérimentales et théoriques ont été réalisées pour établir le niveau de sécurité atteint, la robustesse et la résistance à la propagation d'erreurs.

Par conséquent, la solution proposée peut être considérée comme un algorithme de chiffrement sélectif agnostique qui peut être appliqué à la plupart des systèmes distribués. Nous pouvons utiliser cette méthode pour stocker une grande quantité de données dans des nuages publics de manière sécurisée.

Le meilleur choix pour définir le fragment privé reste une question ouverte. Selon des travaux récents, les coefficients de basse fréquence dans les transformations (comme DWT 8×8 utilisés dans cette thèse) ne sont pas nécessairement plus "importants" que les coefficients de haute fréquence. En fait, pour les schémas agnostiques de protection des données de mode, un moyen pratique de mesurer l'importance des coefficients de transformation consiste à calculer l'influence des valeurs d'entrée sur les coefficients. Par exemple, certains coefficients de basse fréquence ne sont liés qu'à un petit sous-ensemble de valeurs d'entrée (la modification des valeurs d'entrée de repos n'entraînera pas le changement de ces coefficients de basse fréquence) tandis que certains coefficients de haute fréquence peuvent être liés à Ce fait nous donnerait un indice sur la façon de définir plus de fragments "importants" en choisissant les coefficients qui sont liés au plus grand nombre de valeurs d'entrée en ignorant basses ou hautes fréquences.

En ce qui concerne la mise en œuvre logicielle, les plates-formes de GPU pour mobiles non polyvalentes devraient être expérimentées pour s'adapter à l'architecture de la méthode SE agnostique proposée pour atteindre à la fois l'efficacité et les économies d'énergie sur les smartphones actuels. Et, bien sûr, plusieurs types de plates-formes GPGPU d'ordinateurs personnels (comme les plates-formes multi-processeurs ou GPGPU ou le matériel de dernière génération) devraient être expérimentés pour déduire une solution générale pour l'allocation entre CPU et GPGPU. Comme indiqué dans les discussions précédentes, l'évolution du matériel ne s'arrête pas et bien entendu, le déploiement de nouveau matériel d'architecture inatendue pourrait de nouveau changer totalement notre architecture logicielle.

Enfin, nous envisageons des travaux futurs concernant la dispersion et la transmission des fragments avec un environnement basé sur le dispositif utilisateur et des clouds publics. D'autres besoins telles que la disponibilité, la récupération de données devraient être pris en compte pour une architecture encore plus flexible et plus adaptable.

References

[1] Acharya, T. and Chakrabarti, C. (2006). A survey on lifting-based discrete wavelet transform architectures. *Journal of VLSI signal processing systems for signal, image and video technology*, 42(3):321–339.

[2] Adrian, D., Bhargavan, K., Durumeric, Z., Gaudry, P., Green, M., Halderman, J. A., Heninger, N., Springall, D., Thomé, E., Valenta, L., et al. (2015). Imperfect forward secrecy: How diffie-hellman fails in practice. In *Proceedings of the 22nd ACM SIGSAC Conference on Computer and Communications Security*, pages 5–17. ACM.

[3] Aggarwal, G., Bawa, M., Ganesan, P., Garcia-Molina, H., Kenthapadi, K., Motwani, R., Srivastava, U., Thomas, D., and Xu, Y. (2005). Two can keep a secret: A distributed architecture for secure database services. *CIDR 2005*.

[4] Ahmed, N., Natarajan, T., and Rao, K. R. (1974). Discrete cosine transform. *IEEE transactions on Computers*, 100(1):90–93.

[5] Akenine-Moller, T. and Strom, J. (2008). Graphics processing units for handhelds. *Proceedings of the IEEE*, 96(5):779–789.

[6] Amigó, J., Kocarev, L., and Szczepanski, J. (2007). Theory and practice of chaotic cryptography. *Physics Letters A*, 366(3):211–216.

[7] AnandTech (2014). The iphone 6 review: A8's cpu: What comes after cyclone?

[8] Anderson, R. (2008). *Security engineering*. John Wiley & Sons.

[9] Asanovic, K., Bodik, R., Catanzaro, B. C., Gebis, J. J., Husbands, P., Keutzer, K., Patterson, D. A., Plishker, W. L., Shalf, J., Williams, S. W., et al. (2006). The landscape of parallel computing research: A view from berkeley. Technical report, Technical Report UCB/EECS-2006-183, EECS Department, University of California, Berkeley.

[10] Association, J. S. S. T. et al. (2012). Jedec standard: Ddr4 sdram. *JESD79-4, Sep*.

[11] Bailey, D. H. (1987). Vector computer memory bank contention. *IEEE Transactions on Computers*, 100(3):293–298.

[12] Berman, F. (2008). Got data?: a guide to data preservation in the information age. *Communications of the ACM*, 51(12):50–56.

[13] Bertoni, G., Zaccaria, V., Breveglieri, L., Monchiero, M., and Palermo, G. (2005). Aes power attack based on induced cache miss and countermeasure. In *International Conference on Information Technology: Coding and Computing (ITCC'05)-Volume II*, volume 1, pages 586–591. IEEE.

[14] Bhatnagar, G. and Wu, Q. J. (2012). Selective image encryption based on pixels of interest and singular value decomposition. *Digital signal processing*, 22(4):648–663.

[15] Bixby, R. E. (2002). Solving real-world linear programs: A decade and more of progress. *Operations research*, 50(1):3–15.

[16] Blythe, D. (2006). The direct3d 10 system. *ACM Trans. Graph.*, 25(3):724–734.

[17] Bogdanov, A., Lauridsen, M. M., and Tischhauser, E. (2015). Comb to pipeline: Fast software encryption revisited. In *International Workshop on Fast Software Encryption*, pages 150–171. Springer.

[18] Brakerski, Z. and Vaikuntanathan, V. (2014). Efficient fully homomorphic encryption from (standard) lwe. *SIAM Journal on Computing*, 43(2):831–871.

[19] Brodtkorb, A. R., Hagen, T. R., Schulz, C., and Hasle, G. (2013). Gpu computing in discrete optimization. part i: Introduction to the gpu. *EURO journal on transportation and logistics*, 2(1-2):129–157.

[20] Budruk, R., Anderson, D., and Shanley, T. (2004). *PCI express system architecture*. Addison-Wesley Professional.

[21] Burrus, C. S., Gopinath, R. A., and Guo, H. (1997). Introduction to wavelets and wavelet transforms: a primer.

[22] Cao, X., Moore, C., O'Neill, M., O'Sullivan, E., and Hanley, N. (2013). Accelerating fully homomorphic encryption over the integers with super-size hardware multiplier and modular reduction. *IACR Cryptology ePrint Archive*, 2013:616.

[23] Casazza, J. (2009). Intel core i7-800 processor series and the intel core i5-700 processor series based on intel microarchitecture (nehalem). *White paper, Intel Corp*.

[24] Chen, L. and Zhao, D. (2005). Optical image encryption based on fractional wavelet transform. *Optics Communications*, 254(4):361–367.

[25] Chen, Y.-F., Huang, H., Jana, R., Jim, T., John, S., Jora, S., Muthumanickam, R., and Wei, B. (2002). Enterprise mobile server platform. US Patent App. 10/165,887.

[26] Cheng, H. and Li, X. (2000). Partial encryption of compressed images and videos. *IEEE Transactions on signal processing*, 48(8):2439–2451.

[27] Cheng, K.-T. and Wang, Y.-C. (2011). Using mobile gpu for general-purpose computing–a case study of face recognition on smartphones. In *VLSI Design, Automation and Test (VLSI-DAT), 2011 International Symposium on*, pages 1–4. IEEE.

[28] Chiaraluce, F., Ciccarelli, L., Gambi, E., Pierleoni, P., and Reginelli, M. (2002). A new chaotic algorithm for video encryption. *IEEE Transactions on Consumer Electronics*, 48(4):838–844.

[29] Cho, J.-S., Yeo, S.-S., and Kim, S. K. (2011). Securing against brute-force attack: A hash-based rfid mutual authentication protocol using a secret value. *Computer Communications*, 34(3):391–397.

[30] Chou, C.-H., Liu, P., Wu, T., Chien, Y., and Zhao, Y. (2014). Implementation of parallel computing fast algorithm on mobile gpu. In *Unifying Electrical Engineering and Electronics Engineering*, pages 1275–1281. Springer.

[31] Christopoulos, C., Skodras, A., and Ebrahimi, T. (2000). The jpeg2000 still image coding system: an overview. *IEEE transactions on consumer electronics*, 46(4):1103–1127.

[32] Clauset, A. (2011). A brief primer on probability distributions. *Santa Fe Institute. http://tuvalu. santafe. edu/˜ aaronc/courses/7000/csci7000-001_2011_L0. pdf*.

[33] Coppersmith, D. (1994). The data encryption standard (des) and its strength against attacks. *IBM journal of research and development*, 38(3):243–250.

[34] Coron, J.-S., Mandal, A., Naccache, D., and Tibouchi, M. (2011). Fully homomorphic encryption over the integers with shorter public keys. In *Annual Cryptology Conference*, pages 487–504. Springer.

[35] Coron, J.-S., Naccache, D., and Tibouchi, M. (2012). Public key compression and modulus switching for fully homomorphic encryption over the integers. In *Annual International Conference on the Theory and Applications of Cryptographic Techniques*, pages 446–464. Springer.

[36] Daemen, J. and Rijmen, V. (1999). Aes proposal: Rijndael.

[37] Dai, W. (2007). Crypto++ library.

[38] Dai, W., Doröz, Y., and Sunar, B. (2014). Accelerating ntru based homomorphic encryption using gpus. In *High Performance Extreme Computing Conference (HPEC), 2014 IEEE*, pages 1–6. IEEE.

[39] Doröz, Y., Hu, Y., and Sunar, B. (2014). Homomorphic aes evaluation using ntru. *IACR Cryptology ePrint Archive*, 2014:39.

[40] Doröz, Y., Öztürk, E., Savaş, E., and Sunar, B. (2015a). Accelerating ltv based homomorphic encryption in reconfigurable hardware. In *International Workshop on Cryptographic Hardware and Embedded Systems*, pages 185–204. Springer.

[41] Doröz, Y., Öztürk, E., and Sunar, B. (2013). Evaluating the hardware performance of a million-bit multiplier. In *Digital System Design (DSD), 2013 Euromicro Conference on*, pages 955–962. IEEE.

[42] Doröz, Y., Öztürk, E., and Sunar, B. (2015b). Accelerating fully homomorphic encryption in hardware. *IEEE Transactions on Computers*, 64(6):1509–1521.

[43] Enfedaque, P., Auli-Llinas, F., and Moure, J. C. (2015). Implementation of the dwt in a gpu through a register-based strategy. *IEEE Transactions on Parallel and Distributed Systems*, 26(12):3394–3406.

[44] Engel, D., Stütz, T., and Uhl, A. (2007). Format-compliant jpeg2000 encryption with combined packet header and packet body protection. In *Proceedings of the 9th workshop on Multimedia & security*, pages 87–96. ACM.

[45] Engel, W. F. (2002). *Direct3d Shaderx: Vertex and Pixel Shader Tips and Tricks with Cdrom*. Wordware Publishing Inc.

[46] Engel, W. F. et al. (2004). *ShaderX2: Shader Programming Tips & Tricks with DirectX 9*. Citeseer.

[47] Fang, B., Shen, G., Li, S., and Chen, H. (2005). Techniques for efficient dct/idct implementation on generic gpu. In *2005 IEEE International Symposium on Circuits and Systems*, pages 1126–1129. IEEE.

[48] Fawaz, Z., Noura, H., and Mostefaoui, A. (2016). An efficient and secure cipher scheme for images confidentiality preservation. *Signal Processing: Image Communication*, 42:90–108.

[49] Fernando, R. and Kilgard, M. J. (2003). *The Cg Tutorial: The definitive guide to programmable real-time graphics*. Addison-Wesley Longman Publishing Co., Inc.

[50] Franco, J., Bernabé, G., Fernández, J., and Acacio, M. E. (2009). A parallel implementation of the 2d wavelet transform using cuda. In *Parallel, Distributed and Network-based Processing, 2009 17th Euromicro International Conference on*, pages 111–118. IEEE.

[51] Fray, J.-M., Deswarte, Y., and Powell, D. (1986). Intrusion-tolerance using fine-grain fragmentation-scattering. In *Security and Privacy, 1986 IEEE Symposium on*, pages 194–194. IEEE.

[52] Frigo, M. and Johnson, S. G. (2005). The design and implementation of fftw3. *Proceedings of the IEEE*, 93(2):216–231.

[53] Garcia, A. and Shen, H.-W. (2005). Gpu-based 3d wavelet reconstruction with tileboarding. *The Visual Computer*, 21(8):755–763.

[54] Gellman, B. and Poitras, L. (2013). Us, british intelligence mining data from nine us internet companies in broad secret program. *The Washington Post*, 6.

[55] Gentry, C. (2009). *A fully homomorphic encryption scheme*. PhD thesis, Stanford University.

[56] Gentry, C. and Halevi, S. (2011). Implementing gentry's fully-homomorphic encryption scheme. In *Annual International Conference on the Theory and Applications of Cryptographic Techniques*, pages 129–148. Springer.

[57] Gentry, C., Halevi, S., and Smart, N. P. (2012a). Better bootstrapping in fully homomorphic encryption. In *International Workshop on Public Key Cryptography*, pages 1–16. Springer.

[58] Gentry, C., Halevi, S., and Smart, N. P. (2012b). Fully homomorphic encryption with polylog overhead. In *Annual International Conference on the Theory and Applications of Cryptographic Techniques*, pages 465–482. Springer.

[59] Gentry, C., Halevi, S., and Smart, N. P. (2012c). Homomorphic evaluation of the aes circuit. In *Advances in Cryptology–CRYPTO 2012*, pages 850–867. Springer.

[60] Gervasi, O., Russo, D., and Vella, F. (2010). The aes implantation based on opencl for multi/many core architecture. In *Computational Science and Its Applications (ICCSA), 2010 International Conference on*, pages 129–134. IEEE.

[61] Gillman, D. W., Mohtashemi, M., and Rivest, R. L. (1996). On breaking a huffman code. *IEEE Transactions on Information theory*, 42(3):972–976.

[62] Giraud, C. (2004). Dfa on aes. In *International Conference on Advanced Encryption Standard*, pages 27–41. Springer.

[63] Gonçalves, D. d. O. and Costa, D. G. (2015). A survey of image security in wireless sensor networks. *Journal of Imaging*, 1(1):4–30.

[64] Grangetto, M., Magli, E., and Olmo, G. (2006). Multimedia selective encryption by means of randomized arithmetic coding. *IEEE Transactions on Multimedia*, 8(5):905–917.

[65] Gray, K. (2003). *Microsoft DirectX 9 programmable graphics pipeline*. Microsoft Press.

[66] Gregg, C. and Hazelwood, K. (2011). Where is the data? why you cannot debate cpu vs. gpu performance without the answer. In *Performance Analysis of Systems and Software (ISPASS), 2011 IEEE International Symposium on*, pages 134–144. IEEE.

[67] Guan, Z.-H., Huang, F., and Guan, W. (2005). Chaos-based image encryption algorithm. *Physics Letters A*, 346(1):153–157.

[68] HEATProject (2015). H2020: Homomorphic encryption applications and technology. *https://heat-project.eu/*.

[69] Hopf, M. and Ertl, T. (2000). Hardware accelerated wavelet transformations. In *Data Visualization 2000*, pages 93–103. Springer.

[70] http://boingboing.net/2009/03/22/jpeg-compression 600.html (2009). Jpeg compression 600 times over.

[71] http://www.anandtech.com/show/7003/the-haswell-review-intel-core-i74770k-i54560k tested/5 (2014). The haswell review.

[72] http://www.top500.org (2011). Top 500 supercomputer sites.

[73] Huynh-Thu, Q. and Ghanbari, M. (2008). Scope of validity of psnr in image/video quality assessment. *Electronics letters*, 44(13):800–801.

[74] Kankanhalli, M. S. and Guan, T. T. (2002). Compressed-domain scrambler/descrambler for digital video. *IEEE Transactions on Consumer Electronics*, 48(2):356–365.

[75] Kapusta, K., Memmi, G., and Noura, H. (2016). Poster: A keyless efficient algorithm for data protection by means of fragmentation. In *Proceedings of the 2016 ACM SIGSAC Conference on Computer and Communications Security*, pages 1745–1747. ACM.

[76] Kapusta, K., Memmi, G., and Noura, H. (2017). Secure and resilient scheme for data protection in unattended wireless sensor networks. In *1st Cyber Security in Networking Conference*. IEEE.

[77] Khashan, O. A., Zin, A. M., and Sundararajan, E. A. (2014). Performance study of selective encryption in comparison to full encryption for still visual images. *Journal of Zhejiang University SCIENCE C*, 15(6):435–444.

[78] Kirk, D. et al. (2007). Nvidia cuda software and gpu parallel computing architecture. In *ISMM*, volume 7, pages 103–104.

[79] Kresch, R. and Merhav, N. (1999). Fast dct domain filtering using the dct and the dst. *IEEE transactions on Image Processing*, 8(6):821–833.

[80] Krikor, L., Baba, S., Arif, T., and Shaaban, Z. (2009). Image encryption using dct and stream cipher. *European Journal of Scientific Research*, 32(1):47–57.

[81] Kulkarni, N. S., Raman, B., and Gupta, I. (2009). Multimedia encryption: a brief overview. In *Recent advances in multimedia signal processing and communications*, pages 417–449. Springer.

[82] Le Gall, D. (1991). Mpeg: A video compression standard for multimedia applications. *Communications of the ACM*, 34(4):46–58.

[83] Lei, S.-M. and Sun, M.-T. (1991). An entropy coding system for digital hdtv applications. *IEEE transactions on circuits and systems for video technology*, 1(1):147–155.

[84] Li, C. and Lo, K.-T. (2011). Optimal quantitative cryptanalysis of permutation-only multimedia ciphers against plaintext attacks. *Signal processing*, 91(4):949–954.

[85] Li, J. and Lei, S. (1999). An embedded still image coder with rate-distortion optimization. *IEEE Transactions on Image Processing*, 8(7):913–924.

[86] Li, Q., Zhong, C., Zhao, K., Mei, X., and Chu, X. (2012). Implementation and analysis of aes encryption on gpu. In *High Performance Computing and Communication & 2012 IEEE 9th International Conference on Embedded Software and Systems (HPCC-ICESS), 2012 IEEE 14th International Conference on*, pages 843–848. IEEE.

[87] Li, S., Karrenbauer, A., Saupe, D., and Kuo, C.-C. J. (2011). Recovering missing coefficients in dct-transformed images. In *2011 18th IEEE International Conference on Image Processing*, pages 1537–1540. IEEE.

[88] Li, S., Li, C., Chen, G., Bourbakis, N. G., and Lo, K.-T. (2008). A general quantitative cryptanalysis of permutation-only multimedia ciphers against plaintext attacks. *Signal Processing: Image Communication*, 23(3):212–223.

[89] Li, S. and Zheng, X. (2002). Cryptanalysis of a chaotic image encryption method. In *Circuits and Systems, 2002. ISCAS 2002. IEEE International Symposium on*, volume 2, pages II–708. IEEE.

[90] Liu, H. and Wang, X. (2010). Color image encryption based on one-time keys and robust chaotic maps. *Computers & Mathematics with Applications*, 59(10):3320–3327.

[91] Livny, M., Basney, J., Raman, R., and Tannenbaum, T. (1997). Mechanisms for high throughput computing. *SPEEDUP journal*, 11(1):36–40.

[92] Lookabaugh, T. (2004). Selective encryption, information theory and compression. In *Signals, Systems and Computers, 2004. Conference Record of the Thirty-Eighth Asilomar Conference on*, volume 1, pages 373–376. IEEE.

[93] Lookabaugh, T. D., Sicker, D. C., Keaton, D. M., Guo, W. Y., and Vedula, I. (2003). Security analysis of selectively encrypted mpeg-2 streams. In *ITCom 2003*, pages 10–21. International Society for Optics and Photonics.

[94] López-Alt, A., Tromer, E., and Vaikuntanathan, V. (2012). On-the-fly multiparty computation on the cloud via multikey fully homomorphic encryption. In *Proceedings of the forty-fourth annual ACM symposium on Theory of computing*, pages 1219–1234. ACM.

[95] Lyubashevsky, V., Peikert, C., and Regev, O. (2013). On ideal lattices and learning with errors over rings. *Journal of the ACM (JACM)*, 60(6):43.

[96] Macedonia, M. (2003). The gpu enters computing's mainstream. *Computer*, 36(10):106–108.

[97] Mallat, S. G. (1989). A theory for multiresolution signal decomposition: the wavelet representation. *IEEE transactions on pattern analysis and machine intelligence*, 11(7):674–693.

[98] Markas, T. and Reif, J. (1992). Quad tree structures for image compression applications. *Information Processing & Management*, 28(6):707–721.

[99] Martin, K., Lukac, R., and Plataniotis, K. N. (2005). Efficient encryption of wavelet-based coded color images. *Pattern Recognition*, 38(7):1111–1115.

[100] Massoudi, A., Lefebvre, F., De Vleeschouwer, C., and Devaux, F.-O. (2008a). Secure and low cost selective encryption for jpeg2000. In *Multimedia, 2008. ISM 2008. Tenth IEEE International Symposium on*, pages 31–38. IEEE.

[101] Massoudi, A., Lefebvre, F., De Vleeschouwer, C., Macq, B., and Quisquater, J.-J. (2008b). Overview on selective encryption of image and video: challenges and perspectives. *EURASIP Journal on Information Security*, 2008(1):1.

[102] Matela, J. (2009). Gpu-based dwt acceleration for jpeg2000. In *Annual Doctoral Workshop on Mathematical and Engineering Methods in Computer Science*, pages 136–143.

[103] Mayer-Schönberger, V. and Cukier, K. (2013). *Big data: A revolution that will transform how we live, work, and think*. Houghton Mifflin Harcourt.

[104] Memmi, G., Kapusta, K., Lambein, P., and Qiu, H. (2015a). Data protection: Combining fragmentation, encryption, and dispersion, a final report. *ITEA CAP project, arXiv preprint arXiv:1512.02951*.

[105] Memmi, G., Kapusta, K., and Qiu, H. (2015b). Data protection: Combining fragmentation, encryption, and dispersion. In *Cyber Security of Smart Cities, Industrial Control System and Communications (SSIC), 2015 International Conference on*, pages 1–9. IEEE.

[106] Memmi, G. and Rambaud, M. (2017). Note sur la cryptanalyse de diffie-hellman. In *International Conference on Software and Systems Engineering and their Applications*. Génie Logiciel 120.

[107] Mittal, S. and Vetter, J. S. (2015). A survey of methods for analyzing and improving gpu energy efficiency. *ACM Computing Surveys (CSUR)*, 47(2):19.

[108] Norouzi, B., Seyedzadeh, S. M., Mirzakuchaki, S., and Mosavi, M. R. (2014). A novel image encryption based on hash function with only two-round diffusion process. *Multimedia systems*, 20(1):45–64.

[109] NVIDIA (2016). White paper: Nvidia geforce gtx 1080.

[110] Nvidia, C. (2007). Compute unified device architecture programming guide.

[111] Nyberg, K. and Knudsen, L. R. (1995). Provable security against a differential attack. *Journal of Cryptology*, 8(1):27–37.

[112] Obukhov, A. and Kharlamov, A. (2008). Discrete cosine transform for 8x8 blocks with cuda. *NVIDIA white paper*.

[113] Ors, S. B., Gurkaynak, F., Oswald, E., and Preneel, B. (2004). Power-analysis attack on an asic aes implementation. In *Information Technology: Coding and Computing, 2004. Proceedings. ITCC 2004. International Conference on*, volume 2, pages 546–552. IEEE.

[114] Owens, J. (2007). Gpu architecture overview. In *SIGGRAPH Courses*, page 2.

[115] Owens, J. D., Houston, M., Luebke, D., Green, S., Stone, J. E., and Phillips, J. C. (2008). Gpu computing. *Proceedings of the IEEE*, 96(5):879–899.

[116] Pareek, N. K., Patidar, V., and Sud, K. K. (2006). Image encryption using chaotic logistic map. *Image and Vision Computing*, 24(9):926–934.

[117] Patel, P., Wong, J., Tatikonda, M., and Marczewski, J. (2009). Jpeg compression algorithm using cuda. *Department of Computer Engineering, University of Toronto, Course Project for ECE*, 1724.

[118] Pennebaker, W. B. and Mitchell, J. L. (1992). *JPEG: Still image data compression standard*. Springer Science & Business Media.

[119] Pennebaker, W. B., Mitchell, J. L., Langdon, G., and Arps, R. B. (1988). An overview of the basic principles of the q-coder adaptive binary arithmetic coder. *IBM Journal of research and development*, 32(6):717–726.

[120] Piret, G. and Quisquater, J.-J. (2003). A differential fault attack technique against spn structures, with application to the aes and khazad. In *International Workshop on Cryptographic Hardware and Embedded Systems*, pages 77–88. Springer.

[121] Pommer, A. and Uhl, A. (2003). Selective encryption of wavelet-packet encoded image data: efficiency and security. *Multimedia Systems*, 9(3):279–287.

[122] PRISM (2013). https://en.wikipedia.org/wiki/prism_(surveillance_program).

[123] Puech, W. and Rodrigues, J. M. (2005). Crypto-compression of medical images by selective encryption of dct. In *Signal Processing Conference, 2005 13th European*, pages 1–4. IEEE.

[124] Qiao, L., Nahrstedt, K., and Tam, M.-C. (1997). Is mpeg encryption by using random list instead of zigzag order secure? In *Consumer Electronics, 1997. ISCE'97., Proceedings of 1997 IEEE International Symposium on*, pages 226–229. IEEE.

[125] Qiu, H. and Memmi, G. (2014). Fast selective encryption method for bitmaps based on gpu acceleration. In *Multimedia (ISM), 2014 IEEE International Symposium on*, pages 155–158. IEEE.

[126] Qiu, H. and Memmi, G. (2015). Fast selective encryption methods for bitmap images. *International Journal of Multimedia Data Engineering and Management (IJMDEM)*, 6(3):51–69.

[127] Qiu, H., Memmi, G., and Noura, H. (2017). An efficient secure storage scheme based on information fragmentation. In *Cyber Security and Cloud Computing (CSCloud), 2017 IEEE 4th International Conference on*, pages 108–113. IEEE.

[128] Rabin, M. O. (1989). Efficient dispersal of information for security, load balancing, and fault tolerance. *Journal of the ACM (JACM)*, 36(2):335–348.

[129] Rambaud, M. and Memmi, G. (2017). Note sur la cryptanalyse de diffie-hellman. *Génie Logiciel*, 120.

[130] Reed, I. S. and Solomon, G. (1960). Polynomial codes over certain finite fields. *Journal of the society for industrial and applied mathematics*, 8(2):300–304.

[131] Regev, O. (2009). On lattices, learning with errors, random linear codes, and cryptography. *Journal of the ACM (JACM)*, 56(6):34.

[132] Rhouma, R. and Belghith, S. (2008). Cryptanalysis of a new image encryption algorithm based on hyper-chaos. *Physics Letters A*, 372(38):5973–5978.

[133] Richardson, I. E. (2004). *H. 264 and MPEG-4 video compression: video coding for next-generation multimedia*. John Wiley & Sons.

[134] Rijmen, V. and Daemen, J. (2001). Advanced encryption standard. *Proceedings of Federal Information Processing Standards Publications, National Institute of Standards and Technology*, pages 19–22.

[135] Rivest, R. L., Adleman, L., and Dertouzos, M. L. (1978a). On data banks and privacy homomorphisms. *Foundations of secure computation*, 4(11):169–180.

[136] Rivest, R. L., Shamir, A., and Adleman, L. (1978b). A method for obtaining digital signatures and public-key cryptosystems. *Communications of the ACM*, 21(2):120–126.

[137] Rohloff, K. and Cousins, D. B. (2014). A scalable implementation of fully homomorphic encryption built on ntru. In *International Conference on Financial Cryptography and Data Security*, pages 221–234. Springer.

[138] Sadourny, Y. and Conan, V. (2003). A proposal for supporting selective encryption in jpsec. *IEEE Transactions on Consumer Electronics*, 49(4):846–849.

[139] Sandmel, J. (2014). Working with metal - overview.

[140] Schaller, R. R. (1997). Moore's law: past, present and future. *IEEE spectrum*, 34(6):52–59.

[141] Schramm, K., Leander, G., Felke, P., and Paar, C. (2004). A collision-attack on aes. In *International Workshop on Cryptographic Hardware and Embedded Systems*, pages 163–175. Springer.

[142] Shannon, C. E. (1949). Communication theory of secrecy systems. *Bell system technical journal*, 28(4):656–715.

[143] Shi, C. and Bhargava, B. (1998). A fast mpeg video encryption algorithm. In *Proceedings of the sixth ACM international conference on Multimedia*, pages 81–88. ACM.

[144] Shi, C., Wang, S.-Y., and Bhargava, B. (1999). Mpeg video encryption in real-time using secret key cryptography. In *in Proc. Int. Conf. Parallel and Distributed Processing Techniques and Applications*. Citeseer.

[145] Stehlé, D. and Steinfeld, R. (2011). Making ntru as secure as worst-case problems over ideal lattices. In *Annual International Conference on the Theory and Applications of Cryptographic Techniques*, pages 27–47. Springer.

[146] Steube, J. (2013). oclhashcat-plus-advanced password recovery.

[147] Storer, M. W., Greenan, K. M., Miller, E. L., and Voruganti, K. (2009). Potshards—a secure, recoverable, long-term archival storage system. *ACM Transactions on Storage (TOS)*, 5(2):5.

[148] Stutz, T. and Uhl, A. (2006). On format-compliant iterative encryption of jpeg2000. In *Eighth IEEE International Symposium on Multimedia (ISM'06)*, pages 985–990. IEEE.

[149] Sweldens, W. (1998). The lifting scheme: A construction of second generation wavelets. *SIAM journal on mathematical analysis*, 29(2):511–546.

[150] Taneja, N., Raman, B., and Gupta, I. (2011). Selective image encryption in fractional wavelet domain. *AEU-International Journal of Electronics and Communications*, 65(4):338–344.

[151] Tang, L. (1997). Methods for encrypting and decrypting mpeg video data efficiently. In *Proceedings of the fourth ACM international conference on Multimedia*, pages 219–229. ACM.

[152] Taubman, D. and Marcellin, M. (2012). *JPEG2000 Image Compression Fundamentals, Standards and Practice: Image Compression Fundamentals, Standards and Practice*, volume 642. Springer Science & Business Media.

[153] Toolkit, N. C. (2006). Secure hashing. *http:csrc.nist.gov/encryption/tkhash.html*.

[154] Tosun, A. S. and Feng, W.-C. (2000). Efficient multi-layer coding and encryption of mpeg video streams. In *Multimedia and Expo, 2000. ICME 2000. 2000 IEEE International Conference on*, volume 1, pages 119–122. IEEE.

[155] Tran, N.-P., Lee, M., Hong, S., and Lee, S.-J. (2011). Parallel execution of aes-ctr algorithm using extended block size. In *Computational Science and Engineering (CSE), 2011 IEEE 14th International Conference on*, pages 191–198. IEEE.

[156] Tveit, A., Morland, T., and Røst, T. B. (2016). Deeplearningkit-an gpu optimized deep learning framework for apple's ios, os x and tvos developed in metal and swift. *arXiv preprint arXiv:1605.04614*.

[157] Uehara, T. and Safavi-Naini, R. (2000). Chosen dct coefficients attack on mpeg encryption schemes. In *Proceedings of IEEE Pacific Rim Conference on Multimedia*, pages 316–319.

[158] Uehara, T., Safavi-Naini, R., and Ogunbona, P. (2006). Recovering dc coefficients in block-based dct. *IEEE Transactions on Image Processing*, 15(11):3592–3596.

[159] van der Laan, W. J., Jalba, A. C., and Roerdink, J. B. (2011). Accelerating wavelet lifting on graphics hardware using cuda. *IEEE Transactions on Parallel and Distributed Systems*, 22(1):132–146.

[160] Van Dijk, M., Gentry, C., Halevi, S., and Vaikuntanathan, V. (2010). Fully homomorphic encryption over the integers. In *Annual International Conference on the Theory and Applications of Cryptographic Techniques*, pages 24–43. Springer.

[161] Veyrat-Charvillon, N. and Standaert, F.-X. (2009). Mutual information analysis: how, when and why? In *Cryptographic Hardware and Embedded Systems-CHES 2009*, pages 429–443. Springer.

[162] Viola, P. and Jones, M. (2001). Rapid object detection using a boosted cascade of simple features. In *Computer Vision and Pattern Recognition, 2001. CVPR 2001. Proceedings of the 2001 IEEE Computer Society Conference on*, volume 1, pages I–511. IEEE.

[163] Wall, D. W. (1991). *Limits of instruction-level parallelism*, volume 19. ACM.

[164] Wallace, G. K. (1992). The jpeg still picture compression standard. *IEEE transactions on consumer electronics*, 38(1):xviii–xxxiv.

[165] Wang, C., Yu, H.-B., and Zheng, M. (2003). A dct-based mpeg-2 transparent scrambling algorithm. *IEEE Transactions on Consumer Electronics*, 49(4):1208–1213.

[166] Wang, W., Hu, Y., Chen, L., Huang, X., and Sunar, B. (2012). Accelerating fully homomorphic encryption using gpu. In *High Performance Extreme Computing (HPEC), 2012 IEEE Conference on*, pages 1–5. IEEE.

[167] Wang, W. and Huang, X. (2013). Fpga implementation of a large-number multiplier for fully homomorphic encryption. In *2013 IEEE International Symposium on Circuits and Systems (ISCAS2013)*, pages 2589–2592. IEEE.

[168] Wang, Y., Wong, K.-W., Liao, X., and Chen, G. (2011). A new chaos-based fast image encryption algorithm. *Applied soft computing*, 11(1):514–522.

[169] Wang, Z., Bovik, A. C., Sheikh, H. R., and Simoncelli, E. P. (2004). Image quality assessment: from error visibility to structural similarity. *Image Processing, IEEE Transactions on*, 13(4):600–612.

[170] Webster, A. and Tavares, S. E. (1985). On the design of s-boxes. In *Conference on the Theory and Application of Cryptographic Techniques*, pages 523–534. Springer.

[171] Wikipedia (2015). Fhe. *https://en.wikipedia.org/wiki/Homomorphic_encryption*.

[172] Woo, M., Neider, J., Davis, T., and Shreiner, D. (1999). *OpenGL programming guide: the official guide to learning OpenGL, version 1.2*. Addison-Wesley Longman Publishing Co., Inc.

[173] Wu, C.-P. and Kuo, C.-C. J. (2001a). Efficient multimedia encryption via entropy codec design. In *Photonics West 2001-Electronic Imaging*, pages 128–138. International Society for Optics and Photonics.

[174] Wu, C.-P. and Kuo, C.-C. J. (2001b). Fast encryption methods for audiovisual data confidentiality. In *Information Technologies 2000*, pages 284–295. International Society for Optics and Photonics.

[175] Wu, Y. and Deng, R. H. (2004). Compliant encryption of jpeg2000 codestreams. In *Image Processing, 2004. ICIP'04. 2004 International Conference on*, volume 5, pages 3439–3442. IEEE.

[176] Xiang, T., Hu, J., and Sun, J. (2015). Outsourcing chaotic selective image encryption to the cloud with steganography. *Digital Signal Processing*, 43:28–37.

[177] Xiang, T., Yu, C., and Chen, F. (2014). Secure mq coder: An efficient way to protect jpeg 2000 images in wireless multimedia sensor networks. *Signal Processing: Image Communication*, 29(9):1015–1027.

[178] Yagisawa, M. (2015). Fully homomorphic encryption without bootstrapping. *IACR Cryptology ePrint Archive*, 2015:474.

[179] Yen, J.-C. and Guo, J.-I. (1999). A new mpeg encryption system and its vlsi architecture. In *IEEE workshop on signal processing systems, Taipei, Taiwan*, pages 430–437.

[180] Yuen, C.-H. and Wong, K.-W. (2011). A chaos-based joint image compression and encryption scheme using dct and sha-1. *Applied Soft Computing*, 11(8):5092–5098.

[181] Zeng, W. and Lei, S. (2003). Efficient frequency domain selective scrambling of digital video. *IEEE Transactions on Multimedia*, 5(1):118–129.

[182] Zhang, G. and Liu, Q. (2011). A novel image encryption method based on total shuffling scheme. *Optics Communications*, 284(12):2775–2780.

[183] Zhang, Y., Xiao, D., Wen, W., and Liu, H. (2013a). Vulnerability to chosen-plaintext attack of a general optical encryption model with the architecture of scrambling-then-double random phase encoding. *Optics letters*, 38(21):4506–4509.

[184] Zhang, Y., Xiao, D., Wen, W., and Tian, Y. (2013b). Edge-based lightweight image encryption using chaos-based reversible hidden transform and multiple-order discrete fractional cosine transform. *Optics & Laser Technology*, 54:1–6.

[185] Zhao, D. (2015). Fast filter bank convolution for three-dimensional wavelet transform by shared memory on mobile gpu computing. *The Journal of Supercomputing*, 71(9):3440–3455.

[186] Zhao, X.-y., Cheng, G., Zhang, D., Wang, X.-h., and Dong, G.-c. (2004). Decryption of pure-position permutation algorithms. *Journal of Zhejiang University SCIENCE*, 5(7):803–809.

[187] Zhou, J., Liang, Z., Chen, Y., and Au, O. C. (2007). Security analysis of multimedia encryption schemes based on multiple huffman table. *IEEE Signal Processing Letters*, 14(3):201–204.

[188] Zhou, M., Zhang, R., Xie, W., Qian, W., and Zhou, A. (2010). Security and privacy in cloud computing: A survey. In *Semantics Knowledge and Grid (SKG), 2010 Sixth International Conference on*, pages 105–112. IEEE.